DISSERTATION

CHARACTERIZATION OF MOSQUITO DENSONUCLEOSIS VIRUS NON-STRUCTURAL PROTEIN NS2

Submitted by

Yevgeniy "Eugene" Azarkh

Department of Microbiology, Immunology, and Pathology

In partial fulfillment of the requirements

For the Degree of Doctor of Philosophy

Colorado State University

Fort Collins, Colorado

Summer 2008

COLORADO STATE UNIVERSITY

July 9, 2008

WE HEREBY RECOMMEND THAT THE DISSERTATION PREPARED UNDER OUR SUPERVISION BY YEVGENIY "EUGENE" AZARKH ENTITLED CHARACTERIZATION OF MOSQUITO DENSONUCLEOSIS VIRUS NON-STRUCTURAL PROTEIN NS2 BE ACCEPTED AS FULFILLING IN PART REQUIREMENTS FOR THE DEGREE OF DOCTOR OF PHILOSOPHY.

Committee on Graduate Work

Carol D Blair
Dr. Carol Blair

RoxAnn Karkhoff-Schweizer
Dr. RoxAnn Karkhoff-Schweizer

Kenneth E Olson
Dr. Kenneth Olson

Dr. Olve Peersen

Jonathan Carlson
Dr. Jonathan Carlson, Adviser

Carol D Blair
Dr. Carol Blair, Interim Department Head

ABSTRACT OF DISSERTATION

CHARACTERIZATION OF MOSQUITO DENSONUCLEOSIS VIRUS

NON-STRUCTURAL PROTEIN NS2

Mosquito densonucleosis viruses (or mosquito densoviruses) are insect parvoviruses that present practical interest as potential bio-insecticides and theoretical interest as a distinct parvoviral group with unique properties. Non-structural protein NS2 of the mosquito densonucleosis viruses is poorly characterized and bears no sequence similarity to NS2 proteins of other parvoviruses. It was hypothesized that mosquito densovirus NS2 is required for efficient viral propagation in cell cultures and during mosquito host infections, and that direct interactions between NS2 and other viral constituents are likely to play a role in NS2-mediated stages of viral life cycle.

Mutagenesis studies, promoter activity assays, and various imaging techniques were used to test this hypothesis and to characterize NS2 protein. Additionally, attempts were made to over-express this protein in a prokaryotic system and to characterize the recombinant NS2 protein *in vitro*.

It was found that NS2 mutations resulted in different phenotypes depending on the type of mutation, the route of infection initiation, and possibly on the cell type. Where abnormal phenotype was observed, decrease in efficiency of the viral DNA

synthesis appeared to be a primary defect. The early stages of viral life cycle appeared to be more sensitive to NS2 mutations.

Imaging studies revealed that NS2 is targeted to the nucleus where it co-localizes and interacts with non-structural protein NS1. Nuclear localization of NS2 does not depend on other viral proteins, but requires intact carboxy-terminus of NS2.

A truncated version of NS2 protein was expressed in a prokaryotic system and tested for its ability to bind DNA. While NS2-DNA interactions have been observed, their specificity could not be determined conclusively. The assays used to study these interactions were complicated by the protein's propensity to form aggregates *in vitro*. It is possible that NS1-NS2 interactions documented *in vivo* are required for correct folding and physiological activity of NS2. This conclusion is supported by the sequence analysis of the protein's carboxy-terminus.

Further studies of mosquito densonucleosis virus non-structural protein NS2 are needed. These studies will broaden our understanding of mosquito densoviruses, which is especially important in the context of using these viruses as bio-insecticidal agents.

Yevgeniy "Eugene" Azarkh
Department of Microbiology, Immunology, and Pathology
Colorado State University
Fort Collins, CO 80523
Summer 2008

ACKNOWLEDGEMENTS

As the five years of my graduate research work are about to culminate in defending this dissertation, I would like to recognize the people who made it possible, the people who were there for me and helped me in every possible way. This work would not be possible without them.

- Dr. Jonathan Carlson, my adviser, who has guided me through all these years of research and encouraged me to think independently and to make important research-related decisions
- My graduate committee members, Drs. Carol Blair, RoxAnn Karkhoff-Schweizer, Kenneth Olson, and Olve Peersen, who, together with Dr. Carlson, supervised my work and provided me with valuable feedback
- Dr. Boris Afanasiev who has been my mentor when I first came to Dr. Carlson's lab, and who taught me about mosquito densoviruses and techniques to study them
- My colleagues (current and former) from the Carlson research group: John Betz, Jared Bodecker, Davina Carter, Jennifer Chinniquy, Mark Flipse, Petra Gest, David Grzenia, Dr. Supanee Hirunkanokpun, Diana Ir, Dr. Dan Konet, Laura Mitrescu, Joe Piper, Erin Robinson, Dr. Rachel Specht, Dr. Erica Suchman, Dr. Cicely Washington, Dr. Svetlana Zakharova

- Dr. Alan Schenkel, Dr. Mercedes Gonzalez-Juarrero, and Eric Lee, who helped me figure out and perform FRET assays
- Grace Campagnola, who helped me with protein purification techniques
- My family – wife Vicki, our daughters Katherine and Margarita, and our parents (those who are with us, and those who are gone). Nothing would happen without my family, without their patience, trust, and support.
- This country, which became my second homeland in 1994, and which made me believe in myself again

The research work described in this dissertation was supported by NIH grant R01 A1147139 and by a grant from the Foundation for the National Institutes of Health through the Grand Challenges in Global Health initiative.

The Table of Contents

The Table of Figures

The Table of Tables

The List of Abbreviations

AAV	Adeno-associated virus
***Ae*DNV**	*Aedes aegypti* densovirus
ANS2	NS2 from *Ae*DNV
APAR	Autonomous parvovirus-associated replication bodies (also see SAAB)
***A*PeDNV**	*Aedes albopictus* C6/36 cell culture densovirus (Peruvian strain)
***Av*GFP**	See GFP
***Bm*DNV**	*Bombyx mori* densovirus
BWB	Binding and wash buffer (Promega)
C6/36DNV	C6/36 cell culture densovirus
CFP	(Enhanced) cyan fluorescent protein (also see eCFP)
CPE	Cytopathic effect
CPV	Canine parvovirus
Cryo-TEM	Cryogenic transmission electron microscopy
DAPI	4',6-diamidino-2-phenylindole
DNA	Deoxyribonucleic acid
eCFP	Enhanced cyan fluorescent protein (also see CFP)
eYFP	Enhanced yellow fluorescent protein (also see YFP)
FITC	Fluorescein isothiocyanate
FPLV	Feline panleukopenia virus
FRET	Fluorescence (or Förster) resonance energy transfer
GFP	Green fluorescent protein (in this work, abbreviation GFP refers to unmodified protein from *Aequorea victoria*, also known as *Av*GFP)

***Gm*DNV**	*Galleria mellonella* densovirus
GST	Glutathione-S-transferase
GUS	β-glucuronidase
***He*DNV**	*Haemagogus equinus* densovirus
I.I.	Instability index
IFA	Immuno-fluorescence assay
IPTG	Isopropyl β-D-1-thiogalactopyranoside
IRES	Internal ribosome entry site
LUT	Lookup table (ImageJ)
mRNA	Messenger RNA
MVM	Minute virus of mice
MW	Molecular weight
NES	Nuclear export signal
NLS	Nuclear localization signal
NPC	Nuclear pore complex
NS1	Non-structural protein 1 (and the gene that codes for this protein)
NS2	Non-structural protein 2 (and the gene that codes for this protein)
NS3	Non-structural protein 3 (in the case of *Gm*DNV, also the gene that codes for this protein)
ORF	Open reading frame
P(NS)	Non-structural gene promoter
P(VP)	Structural gene promoter
PAGE	Polyacrylamide gel electrophoresis
PBR	Putative NS2-binding region of mosquito densovirus DNA
PBS	Phosphate-buffered saline
PCNA	Proliferating cell nuclear antigen
PCR	Polymerase chain reaction

***Pf*DNV**	*Periplaneta fuliginosa* densovirus
pH	Potential of hydrogen
pI	Isoelectric point
PMSF	Phenylmethylsulphonyl fluoride
PNS2	NS2 from *A*PeDNV
qPCR	Quantitative polymerase chain reaction`
RF	Replicative form
RNA	Ribonucleic acid
SAAB	Smn1-associated autonomous parvovirus-associated replication bodies (Smn1-associated APAR)
SDS	Sodium dodecyl sulfate
SSC	Sodium chloride/sodium citrate buffer
trANS2	Truncated NS2 from *Ae*DNV
tRNA	Transfer RNA
trPNS2	Truncated NS2 from *A*PeDNV
VP	Viral (structural) protein gene
VP1	Viral (structural) protein 1
VP2	Viral (structural) protein 2
YFP	(Enhanced) yellow fluorescent protein (also see eYFP)
β-Gal	β-galactosidase

Chapter 1. Literature review

Section 1-1. Introduction

Mosquito densonucleosis viruses comprise a group of closely related viral species in the genus *Brevidensovirus*, subfamily *Densovirinae*, family *Parvoviridae* (ICTV Database, 2006). The prototype member of the group, *Aedes aegypti* densovirus (*Ae*DNV) was isolated in 1972 from a laboratory mosquito colony maintained at Kiev State University, Ukraine (Lebedeva et al., 1973). The disease caused by theses viruses affected all stages of mosquito development, although the first manifestations were typically observed during late larval stages (instars III or IV). The symptoms in larvae included motor dysfunction, deformities, and death. Those diseased individuals that lived on to become imago displayed a weak phenotype with decreased fecundity. On the histological level, the most characteristic sign of the disease was the appearance of infected nuclei that could be seen even in unstained preparations due to the large size and dense texture, hence the disease name densonucleosis (Buchatsky, 1989). Since then, several other mosquito densoviruses have been isolated. These viruses were found to be similar to *Ae*DNV and to each other in many aspects, which warranted their placement within the same genus *Brevidensovirus* (Table 1).

In addition to mosquito densoviruses, genus *Brevidensovirus* now includes *Penaeus stylirostris* densovirus (*Pst*DNV) better known as Infectious Hypodermal and

Name	Original source of isolation	First report published in	GenBank reference
*Ae*DNV	Laboratory colony of *Aedes aegypti* mosquitoes	Lebedeva et al., 1973	M37899
*Aal*DNV	*Aedes albopictus* C6/36 cell culture	Jousset et al., 1993	NC_004285
*He*DNV	*Haemagogus equinus* GML-HE-12 cell culture	O'Neill et al., 1995	AY605055
*Ta*DNV	*Toxorhynchites amboinensis* TRA-284 cell culture	O'Neill et al., 1995	N/A
*A*ThDNV	Laboratory colony of *Aedes albopictus* mosquitoes	Kittayapong et al., 1999	N/A (numerous small fragments of viral mutants only)
*A*PeDNV	*Aedes albopictus* C6/36 cell culture	Ledermann et al., 2004	AY310877
C6/36DNV	*Aedes albopictus* C6/36 cell culture	Chen et al, 2004	AY095351
*Ts*DNV	Laboratory colony of *Toxorhynchites splendens* mosquitoes	Pattanakitsakul et al., 2007	AF395903 (partial sequence only)
*Cpp*DNV*	Wild-caught *Culex pipiens ssp. pallens* mosquitoes	Zhai et al., 2008	EF579756 through EF579771 (multiple strains, CDS only)
*Ag*DNV	*Anopheles gambiae* cell culture	Rasgon, 2007	N/A

Table 1. Mosquito densonucleosis viruses (genus *Brevidensovirus*).

(*) Not to be confused with *Cp*DNV (genus Densovirus) discovered by Jousset et al. (2000) and placed into genus *Densovirus* based on the genomic organization similarities and serological cross-reactivity with *Junonia coenia* densovirus.

Hematopoietic Necrosis Virus of penaeid shrimp (IHHNV). This virus was isolated by Bonami et al (1990), and it was shown to be similar enough to the mosquito densoviruses be included in *Brevidensovirus* genus (Hiroko et al, 2000).

Naturally, the ability of most mosquito densoviruses to reduce mosquito populations and to impair their fitness and fecundity made this group of viruses into attractive candidates for the new-generation biological insecticides. The efforts to generate such an insecticide culminated in creation of Viroden, a viral biological control agent with *Ae*DNV as an active ingredient. Preliminary studies demonstrated that Viroden was effective against all ontogenic stages of haematophagous mosquitoes from *Aedes, Culex,* and *Culiseta* genera, yet safe for the non-target animal species (Buchatsky et al., 1987). These data were corroborated by detailed specificity and pathogenicity studies (reviewed in Buchatsky et al., 1997). According to these studies, *Ae*DNV failed to infect or to otherwise cause any adverse reaction in the number of non-target invertebrate (non-bloodsucking mosquitoes, domestic fly, honey bee, silkworm, crustaceans, worms, etc.) and vertebrate (fish, chickens, mice, rats, rabbits) hosts as well as in several vertebrate cell lines. The limited field trials conducted in 1985-1986 in several regions of the former USSR generated encouraging results (Buchatsky et al., 1988); however, most of the work on preparation Viroden ceased with the collapse of the Soviet Union in 1991. Today, this work continues in our labs, where different aspects of mosquito densovirus pathogenicity, transmission, and ecology are investigated in detail (see Carlson et al., 2006 for review).

Another promising application for mosquito brevidensoviruses is their potential use as transducing vectors. The genes delivered with high specificity to the narrow range of haematophagous mosquitoes and expressed inside of their cells could interfere with the life cycle of arboviruses transmitted by these mosquitoes or with the mosquito hosts

themselves. Both pathogenic and non-pathogenic members of mosquito brevidensovirus group could be used for this purpose. One of the possibilities is to use the two-component transduction system consisting of a recombinant mosquito densovirus in which the structural gene VP is replaced with a gene of interest and a wild-type densovirus that provides the structural proteins to package both types of viral genomes. This possibility was successfully demonstrated by Afanasiev et al. (1999), who used wild-type *Ae*DNV to provide packaging for transducing virus with the VP gene largely replaced with GFP fused in-frame to the non-structural gene NS1. Both NS1 and GFP domains of the resulting fusion protein remained functional, and the entire transducing system successfully propagated and spread through the body of the infected mosquito. An even more intriguing possibility is to clone the gene of interest into the non-coding region of the viral genome downstream from the viral poly-adenylation site. Such transducing vector does not require a helper virus, and the only significant drawback is that the size of transducing gene is limited to just few hundreds of bases by the packaging constraints. Konet et al. (2007) demonstrated that this limited space could be efficiently used to deliver and express a short hairpin RNA, which can in turn induce RNA interference and silence a gene of interest (which in this case was firefly luciferase).

While studying the viruses from the perspective of their usefulness or practical importance can be both exciting and rewarding, one should never ignore the value of basic scientific research. Mosquito densonucleosis viruses represent a distinct group within the viral world with many unique characteristics that set them apart even from other insect parvoviruses, not to mention more distantly related viral groups. Therefore,

studying these viruses could result in unpredicted and fascinating discoveries that would enrich our knowledge about the viruses in particular and life in general. This is why I chose to focus on molecular biology of mosquito densoviruses and, more narrowly, on the role of non-structural protein NS2 in the viral life cycle.

In the following sections of this chapter, I will present a review of what is currently known about brevidensoviral molecular biology and the properties of NS2 proteins. Unfortunately, there are significant gaps in our knowledge about densoviruses when compared to their mammalian cousins. While some aspects of mosquito densovirus biology (such as expression of viral genes) have been studied extensively, very little is known about the earliest (attachment, penetration, and uncoating) and the latest (packaging and release) stages of the viral life cycle. When covering these stages, I will present information on mammalian parvoviruses, such as canine parvovirus (CPV), minute virus of mice (MVM), and others. By doing so, I do not imply that mammalian and insect parvoviruses are similar in these aspects, although it is possibly the case. Only further research of densoviruses can bring certainty into our understanding of all facets of densoviral biology.

Section 1-2. Life cycle of mosquito densoviruses and other members of family Parvoviridae

1-2-1. Virus particles

Initial characterization of *Ae*DNV capsids (reviewed in Buchatsky et al., 1997) indicated that they were on average 21 nm in diameter, although atypical particles as small as 18 nm or as large as 26 nm have also been observed. The virions were

determined to have sedimentation coefficient of 98 S and buoyant density in CsCl of 1.39 g/cm^3. Some particles were filled with genomes, while others were hollow (Figure 1).

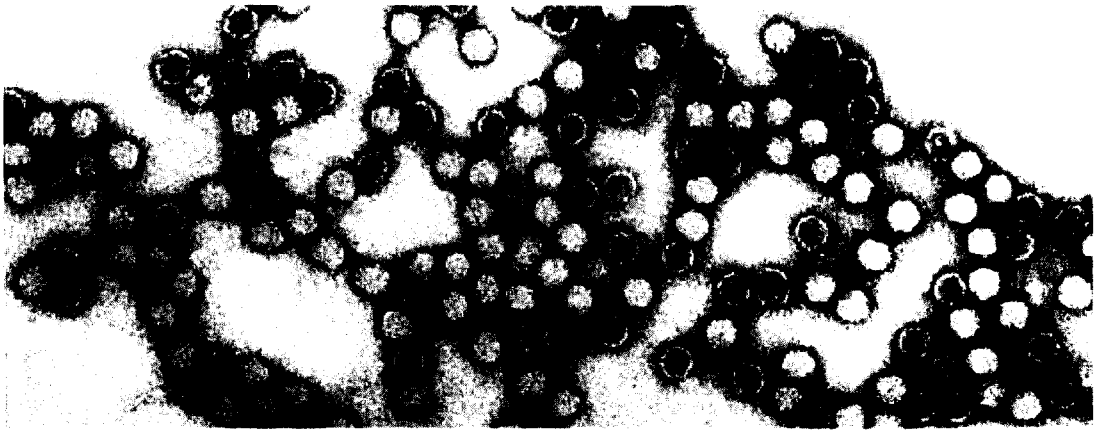

Figure 1. Electron micrograph of *Ae*DNV virus particles stained with 1% uranyl acetate (from Carlson et al., 2006)

The viral genomes were found to be represented by linear DNA molecules. Electron microscopy studies revealed that most DNA molecules were 1.5 μ in length, which corresponds to MW = 1.4 MDa. These data correlate well with genome sequencing data obtained by Afanasiev et al. (1991). A number of biochemical studies conducted in the course of initial characterization of *Ae*DNV viral particles indicated that the viral genomes were largely single-stranded, but the double-stranded regions were also present. For example, no appreciable hyperchromic effect could be observed when viral genomes were heated in 0.1x SSC, which indicated that the genomes were mostly single-stranded. Melting in higher ionic strength (1x SSC) resulted in some hyperchromic effect (up to 20%), but increase in hyperchromicity was gradual, consistent with the presence of some double-stranded regions within otherwise single-stranded DNA molecules. Consistent with biochemical data, the genomic termini appeared coiled under electron

microscopy – a common trait for all parvoviral DNA genomes resulting from the formation of terminal secondary structures. Afanasiev et al. (1991) demonstrated that about 85% of all genomes packaged inside *Ae*DNV virions had negative-sense polarity.

In addition to the full-length genomes, some dimeric (3 μ) and incomplete (0.8-1.2 μ) genomes were seen on the electron microphotograms, but this observation should be interpreted with caution. As noted by Afanasiev et al. (1994), the limited size of the capsid interior restricts the size of genetic material that could be packaged. While attempting to package various β-galactosidase fusion constructs, these authors noticed that the packaging efficiency decreased as the length of recombinant genomes exceeded that of *Ae*DNV by as little as 8%, and no packaging at all could be observed for a construct with 60% genome length excess. It is, therefore, unlikely for the dimeric genomes described by Buchatsky et al. (1997) to have come from the virions; rather, they should be viewed as free replicative forms (RF) contained in the nuclei of infected cells and contaminating the virus particle preparations.

Further studies of mosquito densovirus virions, conducted in our lab and elsewhere, indicate that brevidensoviral capsids share many common traits with other members of *Parvoviridae* family. As reviewed in Hueffer and Parrish (2003), parvoviral capsids are characterized by small size and T=1 icosahedral symmetry. The 60 nearly-identical copies of structural protein VP represent one major and one to three minor species. The capsid surface is characterized by raised regions at the fivefold symmetry axes surrounded by canyons, protrusions near the threefold axes, and depressions (dimples) along the twofold axes. The data obtained in our lab (Afanasiev et al., 1991)

suggest that the capsids of mosquito densoviruses are composed of major structural protein VP1 (41 kDa) and minor structural protein VP2 (39 kDa), with the latter thought to be a proteolytic cleavage product of the former. Our Chinese colleagues employed cryo-TEM and X-ray crystallography techniques to reconstruct brevidensoviral capsids at 1.2-nm resolution (Cheng et al., 2007). As a source of capsids, they used C6/36DNV, a brevidensovirus closely related to *Ae*DNV with 87.7% amino-acid homology in the VP gene. These authors identified all the major parvoviral capsid features discussed above within the reconstructed C6/36DNV capsid. Additionally, they discovered that the brevidensoviral capsids bore closer resemblance to human parvovirus B19 (genus *Erythrovirus*) than to densoviruses *Gm*DNV and *Pf*DNV (genera *Densovirus* and *Pefudensovirus*, respectively). The authors further speculated that mosquito densoviruses may have arisen from B19-like mammalian parvoviruses, and not from other insect parvoviruses. This hypothesis is both intriguing and plausible, but it has yet to be proven.

1-2-2. Attachment, penetration, and uncoating

To date, very little is known about attachment, penetration, and uncoating of mosquito densoviruses. While some educated guesses can be made by comparing these viruses with other members of *Parvoviridae* family, this strategy can be misleading, especially when attempting to characterize viral attachment to the host cell. Interactions that occur between the viral capsids and the host cell receptors and other possible attachment molecules can differ significantly even among related viral species, as these interactions largely define the host range and tissue specificity of a given virus. As reviewed in Vihinen-Ranta et al. (2004), heparin sulfate, sialic acid, platelet-derived

growth factor, globoside, and many other molecules can act as receptors and co-receptors for various parvoviruses. It is certain, however, that all parvoviruses enter their host cells through receptior-mediated endocytosis. In case of canine parvovirus (CPV), and presumably other parvoviruses, intake of the virus is clathrin-mediated, and it requires endosomal acidification, as both NH_4Cl and Bafilomycin A1 treatments resulted in the loss of CPV infectivity (Parker and Parrish, 2000).

Eventually, whole intact CPV capsids enter the nucleus through the nuclear pore complexes (NPC), which has been demonstrated by staining with whole-capsid antibodies (Vihinen-Ranta et al., 2000). Again, this property has only been verified for CPV, but is presumed to be true for other parvoviruses. Since the capsids are too large to freely diffuse through NPC, their transport must occur through an active energy-consuming process. Most commonly, such transport is associated with Ran-GTP hydrolysis and carried out by the group of proteins called importins (Lange et al., 2007), which recognize nuclear localization signals (NLS) within the translocated proteins. Afanasiev et al. (1994) proposed that in mosquito densovirus VP proteins the role of NLS is played by sequence KRKR located in the protein's amino-terminus. Indeed, β-galactosidase and GFP domains fused to the N-terminus of VP protein localized to the nucleus as long as the putative NLS sequence was preserved (Afanasiev et al., 1994; Afanasiev et al., 1999). It is not known whether this NLS is only used to transport nascent VP proteins for assembly and packaging in the nucleus, or it is also active in virion transport into the nucleus following the viral infection.

One of the many mysteries that surround mosquito densovirus life cycle is the absence of phospholipase A_2 (PLA_2) domain in their capsids. This domain was found in all parvoviral genera except *Brevidensovirus*. It was shown to be highly conserved, and necessary for infectivity (Zádori et al., 2001). The mutations that interfered with PLA_2 activity did not affect early cytoplasmic trafficking of the capsids, but resulted in their accumulation in the late endosomes/lysosomes in the perinuclear compartments and prevented further transport of viral genomes into the nucleus. Obviously, mosquito densovirus DNA reaches the nucleus despite the fact that the capsids of these viruses lack PLA_2 activity. This means that brevidensoviruses employ mechanisms of escape from late endosome/lysosome that are principally different from those used by the rest of parvoviruses.

Comparative analysis of GenBank data reveals that the "structural" right ORF is significantly (by about 1000 nt) shorter in brevidensoviruses than in any other parvoviral taxon (for example, see genome sequences for brevidensoviruses *Ae*DNV [M37899] and IHHNV [NC_002190], and compare with iteravirus *Bm*DNV [NC_003346], parvovirus MVM [NC_001510], erythrovirus B19 [NC_000883], or amdovirus AMDV [NC_001662]). This observation suggests that the PLA_2 was lost as a result of a large deletion, and not through a series of nucleotide substitutions. In addition to eliminating PLA_2 domain, this deletion reduced the genome size from 5 kb typical for the parvoviruses to 4 kb (hence the genus name *Brevidensovirus* – brevis = short [lat.]). The capsomer size also became reduced nearly by half, which probably contributed to the

reduction in average capsid size (from 26 nm quoted by Hueffer and Parrish [2003] to 21 nm).

Uncoating of mosquito densoviruses is another stage of viral life cycle that should be interpreted with caution. According to Vihinen-Ranta et al. (2004), the possibility of DNA externalization without complete capsid disassembly has been shown for MVM, CPV, and AAV2. These viruses do not completely internalize their genomes during the packaging, leaving 20-30 nucleotides exposed and covalently attached to NS1 protein at the 5'-terminus of genomic DNA. During uncoating step, the genome is thought to pass through the channel at a 5-fold symmetry axis of the capsid. However, the structure of C6/36DNV capsid indicates that, unlike most parvoviruses, brevidensoviral capsids have no channels (Cheng et al., 2007), and the existence of exposed genomic terminus has yet to be demonstrated for brevidensoviruses. Also, Cotmore and Tattersall (1989) demonstrated that enzymatic removal of the exposed nucleotides and NS1 from MVM virions did not result in any decrease in infectivity, which makes their required participation in uncoating unlikely.

An alternative mechanism of uncoating was proposed for B-19 parvovirus by Ros et al. (2006). These authors found that incubating B-19 virions at temperatures above 60° C or at pH between 5 and 6.5 results in rapid externalization of genomic DNA without capsid disassembly. However, the former treatment is not physiologically relevant, and the latter treatment, while mimicking physiologic conditions of late endosome acidification, is not likely to apply to brevidensoviruses. According to Buchatsky et al. (1989), capsids of *Ae*DNV are extremely stable, and the viruses do not become

inactivated after prolonged treatments in a broad pH range of 4 to 11. It is possible that brevidensoviral capsid stability is affected by VP1→ VP2 proteolytic cleavage, but there are no data currently available to support this hypothesis.

1-2-3. Genome organization and gene expression strategies

The genome of *Ae*DNV was sequenced and characterized by Afanasiev et al. (1991). Other mosquito densoviruses were sequenced as indicated inTable 1, and while their genomes differ from *Ae*DNV in minor details, they all share the same basic features. Some of these features are common for all insect parvoviruses, while others are similar to those seen in the members of genus *Parvovirus* (Table 2).

Virus	Taxonomy	Origin	Genome size (nt)	Termini	Gene orientation	Large active ORFs	Reference
*Ae*DNV	Denso: Brevi	Insect	4012	Mostly unique	Mono	Left Middle Right	Afanasiev et al., 1991
*Bm*DNV	Denso: Itera	Insect	5077	ITR	Mono	Left Middle Right	Li et al., 2001
*Gm*DNV	Denso: Denso	Insect	6039	Large ITR	Ambi	Left-1 Left-2 Middle Minus	Tijssen et al., 2003
AAV-3	Parvo: Dependo	Mamm	4726	ITR	Mono	Left Right	Muramatsu et al., 1996
B-19	Parvo: Erythro	Mamm	5112	ITR	Mono	Left Right	Shade et al., 1986
MVM	Parvo: Parvo	Mamm	5081	Unique	Mono	Left Right	Astell et al., 1983

Table 2. Genomic features of selected parvoviruses.

Denso: – subfamily *Densovirinae*; Parvo: – subfamily *Parvovirinae*; Brevi – genus *Brevidensovirus*; Itera – genus *Iteravirus*; Denso – genus *Densovirus*; Dependo – genus *Dependovirus*; Erythro – genus *Erythrovirus*; Parvo – genus *Parvovirus*. Mamm – mammalian; ITR – inverted terminal repeat; Mono – monosense; Ambi – ambisense.

The genomes of mosquito densoviruses are about 4000 bases long, which makes them the smallest genomes among all parvoviruses. They are represented by single-stranded DNA molecules with imperfect terminal palindromes that fold into T-shaped secondary structures. In some cases, other terminal conformations are possible. For example, the right terminus of *A*PeDNV could potentially fold into a simple hairpin in addition to "classical" T-shaped structure (Afanasiev et al., unpublished data). Unlike other insect parvoviruses whose terminal sequences are represented by inverted terminal repeats (ITRs), the sequences of brevidensoviral genomic termini are mostly unique, with complementarity observed only for short stretches of cross-arm sequences.

Similarly to other parvoviral taxa (except for the genus *Densovirus*), the genomes of mosquito densoviruses have all genes encoded on the same strand of the double-stranded intracellular replicative form of viral DNA (RF). By convention, this strand is designated as positive-sense, while the complementary strand is designated as negative-sense. Although the negative-sense genomes are predominantly packaged by mosquito densoviruses (Afanasiev et al., 1991), the positive-sense orientation is used to designate the termini (left and right) and ORFs (left, middle, and right).

Initially, 4 ORFs were identified based on *Ae*DNV sequence analysis (Afanasiev et al., 2001). One of them, located on the negative-sense strand, is now thought to be inactive, as it lacks any identifiable promoter and poly-adenylation sequences associated with it. No protein expression was observed when β-galactosidase gene was fused to the minus ORF (Afanasiev et al., 1994). In other mosquito densoviruses, this ORF is broken

into several smaller frames by stop codons. However, the remaining 3 ORFs are present in all brevidensoviruses, and with some variations in other insect parvoviruses (see Figure 2 for *Ae*DNV ORF locations and protein expression strategy). The left ORF is the largest, and it codes for non-structural protein NS1. The other two ORFs (middle and right) are smaller, and they are shifted relative to the left ORF (+1 and -1, respectively). The middle ORF is completely embedded in the left ORF, while the end of the left ORF overlaps with the beginning of the right ORF. The middle ORF codes for non-structural protein NS2 – a primary object of my research, and the right ORF codes for structural proteins VP1 and VP2. The presence of a relatively large ORF that is completely embedded in an even larger ORF is a feature found in all members of *Densovirinae* family, but not in mammalian parvoviruses (see Table 2 for examples and references).

Based on *Ae*DNV sequence, three putative promoters and two poly-adenylation sites have been identified (Afanasiev et al., 1991), but only two of the promoters were determined to drive protein expression (Afanasiev et al., 1994), and only one poly-adenylation site appears to be used under natural conditions (Ward et al., 2001; also see Figure 2). The non-structural gene promoter P(NS) drives expression of non-structural proteins NS1 and NS2. Its TATA box starts at base 264, and the initiator (Inr) site of the transcript is currently unknown. The only transcript that can be detected on the northern blot by hybridizing with NS-specific probes is approximately 3.5 kb-long, which indicates that transcription is not terminated until the second of the two predicted poly-adenylation sites is reached (Ward et al., 2001). This site is located downstream from the end of the right ORF. If the first out of the two predicted poly-adenylation sites were

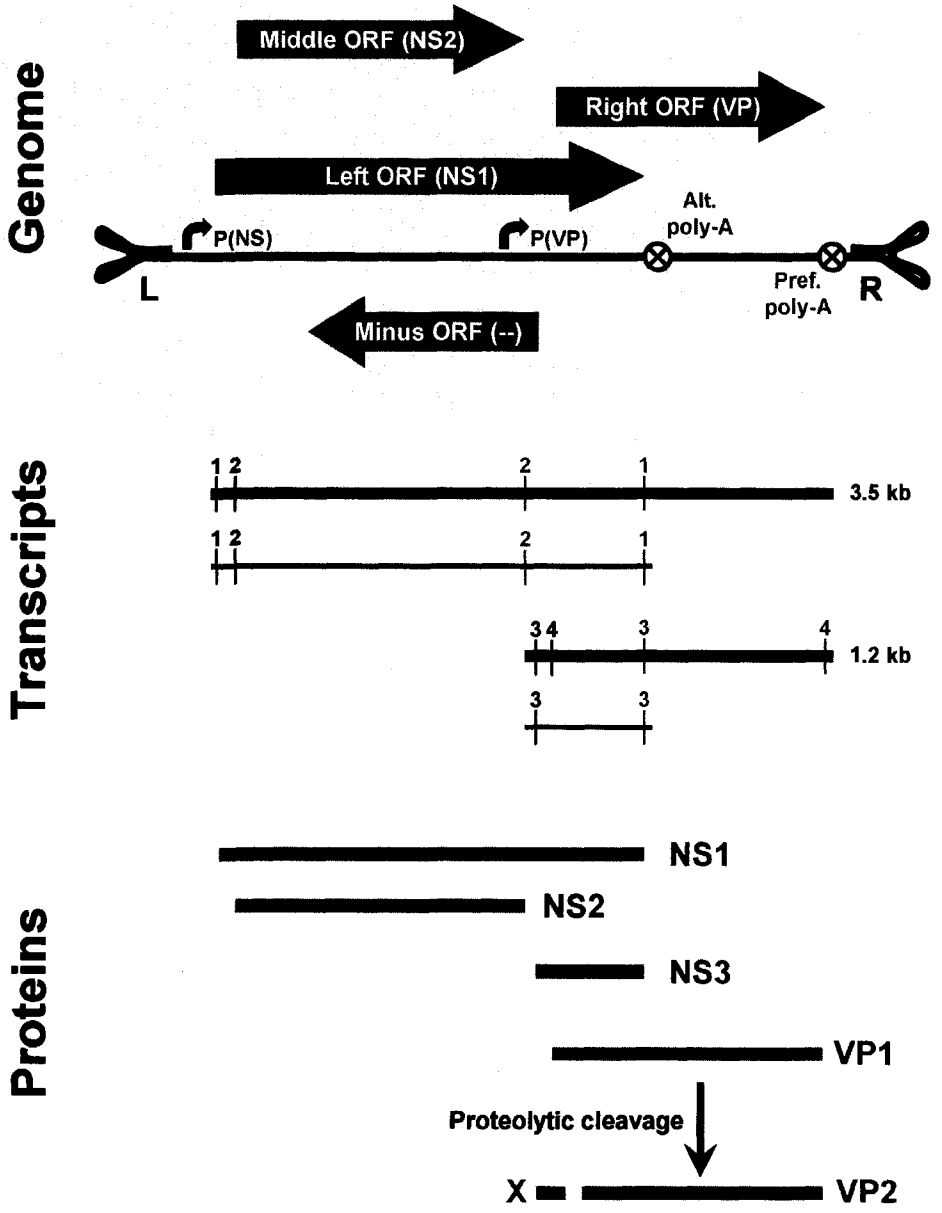

Figure 2. Genomic organization and gene expression strategy of *Ae*DNV.

GENOME: L and R – left and right termini; P(NS) and P(VP) – non-structural and structural gene promoters; alt. and pref. poly-A – alternative and preferred poly-adenylation sites. TRANSCRIPTS: Thick lines – 3.5-kb and 1.2-kb transcripts detectable by northern blot analysis; thin lines – hypothetical minor transcript species. Numbered markers denote initiator (black) and terminator (red) codons for translation of NS1 (1), NS2 (2), NS3 (3), and VP1 (4) protein. PROTEINS: X – an amino-terminal fragment cleaved from VP1 during the formation of VP2, likely degraded after being cleaved off.

efficiently used by the virus, the northern blot should reveal a smaller band of about 2.5 kb. It is important to note, however, that pUCA-INV construct used in trans-activation experiments (Afanasiev et al., 1994; Ward et al, 2001) successfully expresses the non-structural proteins despite the fact that its preferred poly-adenylation site is in the wrong orientation. The only reasonable explanation for successful protein expression by pUCA-INV is that the alternative poly-adenylation site is used by this construct.

The β-glucuronidase (GUS) reporter gene was expressed successfully when fused to both the first and second ATG of the NS-transcript (the start codons in the left and the middle ORFs, respectively), but not to the subsequent ATG sequences (Kimmick et al., 1998). A region downstream from the first ATG was found to be critical for successful expression. This region of transcript was predicted to form a stem-loop structure. A 3-base deletion (positions 328-330) that altered predicted secondary structure of the transcript without introducing a frameshift resulted in decreased expression in both frames (20-fold decrease of expression from the first ATG and 3-fold decrease in expression from the second ATG). However, RNase protection assays did not reveal any difference in the level of the transcripts between the wild type fusions and the deletion mutants, so the secondary structure must be important in regulation of translation rather than transcription.

When the messenger RNA is translated in a cap-dependent manner (which is the case for the majority of eukaryotic transcripts), the translation usually starts at the first AUG codon. However, translation of NS-transcript could be initiated at either of the first two AUG codons located 73 bases apart. This phenomenon in principle could be

explained by alternative splicing, cap-independent translation, or leaky ribosome scanning.

Mammalian parvoviruses are known to use alternative splicing to produce multiple proteins from a single primary transcript. For example, in MVM, alternative splicing of the long primary transcript synthesized under control of P4 promoter results in 4 secondary transcripts that are translated into non-structural protein NS1 and 3 isoforms of NS2 (Cotmore and Tattersall, 1990). Alternative splicing is also used by an insect parvovirus *Gm*DNV to remove the entire NS3 sequence, which allows translation of its NS1 and NS2 proteins (Tijssen et al., 1987). In the case of mosquito densoviruses, alternative splicing could be used to remove the first AUG codon in some of the transcripts, so that the translation would initiate at the second AUG. There is no direct evidence against this hypothesis, as the two secondary transcripts would be difficult to distinguish on the northern blots. However, Kimmick et al. (1998) found no consensus splice signals within *Ae*DNV sequence. Also, the secondary structure found to be required for efficient translation in both frames would likely be removed from the transcript and would not have the effect on the middle ORF translation should alternative splicing take place.

Cap-independent translation is more widespread than previously thought, and it is used to translate various viral and host cell transcripts (Hellen and Sarnow, 2001). In this process, the initiating 40S ribosomal subunit bypasses the 5'-cap (if one is present) and loads onto an internal ribosome entry site (IRES). The translation then begins at the first AUG codon encountered downstream from the IRES. While exact composition of IRES

varies from one transcript to another, it is universally characterized by extensive secondary structure. According to Kimmick et al., no such structures were predicted between the two AUG codons. If the essential secondary structure described above were part of IRES, its elimination would cause dramatic effect on the middle ORF expression, but little or no effect on expression of the right ORF, contrary to the actual experimental results.

The leaky scanning occurs when the first AUG codon is not in the optimal sequence context. According to Kozak (1989), initiation of translation at the first AUG depends on the surrounding sequence. Translation initiation is the most efficient when this sequence matches the consensus RCCAUGG (R = purine; initiator AUG underlined). The presence of R^{-3} and G^{+4} are the most important, and they have a cumulative effect on efficiency of translation initiation. If the context of the first AUG is suboptimal, the 40S ribosomal subunit is likely to bypass it and continue scanning until an AUG codon in a better context is found, at which point the 60S subunit joins in, and the message is translated. In NS-transcript of *Ae*DNV, the context sequences are GUGAUGA and AGCAUGA for the first and second AUG, respectively. Therefore, both codons are in a suboptimal context (no G in +4 position), but the second AUG codon's context is somewhat better (both A^{-3} and C^{-1} match the consensus). It is then possible that the translation of NS-transcript could initiate from the first AUG in some instances and from the second AUG in others. Currently, this appears to be the most likely model for NS1/NS2 translation strategy.

The structural gene promoter P(VP) is located in the right half of *Ae*DNV genome. It drives expression of VP gene resulting in synthesis of VP1 and VP2 proteins. VP1 protein is a major species, and it is a full-length translational product. The minor VP2 protein is thought to be generated post-translationally by proteolytic cleavage of VP1 at a conserved site predicted by Afanasiev et al. (1991). The TATA box of P(VP) promoter starts at the position 2372. The older name for this promoter, P61, referred to another putative TATA box that was located at 61 map units (starting at position 2449). Primer extension assays conducted by Ward et al. (2001) mapped the transcription initiator to C^{2402}, which makes the promoter's location at 61 m.u. impossible. Site-directed mutagenesis studies conducted by these authors demonstrated that the TATA box is dispensable, but Inr sequence context (TCAGTC) is absolutely required for P(VP)-driven gene expression. The length of the VP transcript is about 1.2 kb. On the northern blots, the VP-transcript is recognized by VP-specific but not NS-specific probes, while NS-transcript is recognized by both.

As noted by the authors, the VP-transcript contains the end of the left ORF in addition to the entire right ORF. Interestingly, the first AUG codon belongs to the left ORF, and not to the right one. The Kozak context sequences are CAUAUGG and ATCAUGG for the first and the second AUG, respectively. The second AUG is a near-perfect match to the consensus, so it should be strongly favored, which indeed is the case. The first AUG is in a suboptimal context, but it has a G at +4 position, so it could still occasionally serve as a translation initiator codon. The resulting polypeptide should be identical to the last 80 carboxy-terminal residues of NS1 protein. Some evidence for this

polypeptide's existence has been presented by Erin Robinson who tentatively named this polypeptide NS3 (unpublished data). However, investigation of NS3 is still at the very preliminary stage.

The effects of non-structural proteins on P(NS) and P(VP) activity have been studied extensively in our lab (Afanasiev et al., 1994; Kimmick et al., 1998; Ward et al., 2001), and the results invariably led to conclusion that the non-structural proteins trans-activate both promoters. The magnitude of trans-activation depended on the presence of intact genomic termini. Only slight (less than 2-fold) increase in promoter activity was observed when the reporter construct lacked both termini. This effect increased significantly in the presence of either right or left terminus, and the maximum trans-activation (about 40-fold increase) was reached when both termini were retained. In the latter case, this increase in the magnitude of trans-activation could be explained by DNA replication, which increases the number of templates for transcription. However, the constructs with a single terminus cannot replicate. Therefore, there must additional mechanisms involved that regulate promoter activity in the terminus-dependent manner. It was assumed that the non-structural protein involved in trans-activation of the viral promoters was NS1, as it was the case with MVM (Doerig et al., 1988; Hanson and Rhode, 1991) and other mammalian parvoviruses. Afanasiev et al. (1994) demonstrated that NS2 alone had no effect on the activity of *Ae*DNV promoters. However, every time NS1 was expressed in these experiments, it was co-expressed with NS2. This issue is further addressed in Section 2-3 of the following chapter.

1-2-4. DNA replication, packaging of genomes, and viral shedding

The details of mosquito densovirus DNA replication remain unknown. However, several important DNA replication features that set parvoviruses apart from the rest of the viral world appear to be universal throughout the *Parvoviridae* family. Therefore, these features are assumed to apply to brevidensoviruses as well.

Replication of parvoviral DNA strictly depends on their host cell cycle (Tattersall, 1972). Unlike papovaviruses, which can force resting cells into S-phase, parvovirus replication does not start unless the host cell enters S-phase on its own (Clemens and Pintel, 1988). While the G1-phase cell extracts do not normally support replication of MVM DNA, addition of recombinant cyclin A/cdk triggers replication, and this effect is concentration-dependent (Bashir et al., 2000). Cyclin A complexed with its cyclin-dependent kinase cdk is required for induction and maintenance of the S-phase. According to the authors, cyclin E/cdk2, which is also involved in S-phase but peaks earlier in the cell cycle, had no effect on MVM DNA replication. Importantly, the presence of proliferation cell nuclear antigen (PCNA) was absolutely required for replication to occur. PCNA is a known co-factor of elongation polymerase δ, so the authors concluded that this polymerase, and not the initiation polymerase-primase α is responsible for parvoviral replication. In principle, polymerase ε, another highly processive PCNA-dependent elongation polymerase could also be involved, but it is currently thought to elongate the lagging strand (Johnson and O'Donnell, 2005). Since there is no evidence for lagging strand synthesis at any point in parvoviral replication, involvement of polymerase ε is not very likely. Either way, the self-priming

unidirectional replication model of parvoviral DNA replication described next suggests that the host cell must provide the machinery for elongation, but not for initiation.

While a number of models have been proposed to explain replication behavior of specific parvoviruses (reviewed in Chen et al., 1989), the cornerstone of them all is the concept of rolling hairpin transfer. This concept was first proposed by Cavalier-Smith (1974) as a theoretical solution for telomere shortening problem. As it turned out a decade later, this solution was incorrect because the telomeres of linear eukaryotic chromosomes are rebuilt by the action of telomerases, and not by ordinary DNA replication (Greider and Blackburn, 1985). However, this model appeared to explain parvoviral replication very well, so it was rapidly accepted by parvovirologists (Tattersall, 1976). Some details of the rolling hairpin model are described next (also see Figure 3).

As previously discussed, the termini of parvoviral genomes contain imperfect palindrome sequences that can fold into hairpin structures of variable complexity. At the 3' end of the genome, these structures can prime elongation reactions thus eliminating the need for RNA primer synthesis and solving the telomere shortening problem. DNA synthesis then proceeds until the 5'-end of the template strand is reached, resulting in a double-stranded DNA molecule covalently closed at one end, but open at another. Since the open ends contain the hairpin sequences, these hairpins can be reformed after the open ends partially melt, resulting in so-called "rabbit ears" structure. The 3'-end of this structure can then initiate another round of DNA synthesis, which in theory can proceed indefinitely, resulting in concatamers of genomes in alternating back-to-back and tail-to-

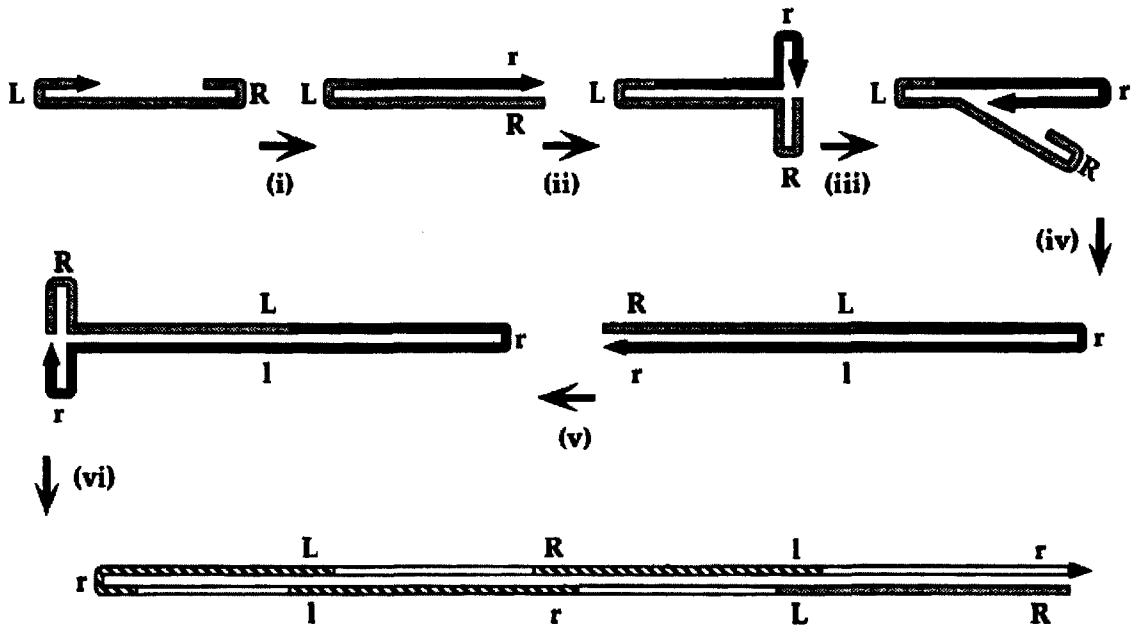

Figure 3. Rolling hairpin replication (from Cotmore and Tattersall, 1995).

L and R – left and right termini. Capital and small case letters denote flip and flop hairpin sequences, respectively.

tail arrangements. In parvovirus replication, these concatamers are resolved (sometimes even before they could form) by a site-specific nickase. The nickase makes a single-stranded cut just upstream from the 3'-hairpin "turn-around" sequence, which becomes extended as it serves as a template for the parental 3'-hairpin repair. This effectively results in the transfer of the parental 3'-hairpin to the 5'-end of the progeny genome with simultaneous inversion of the original hairpin sequences at the 3'-end of the parental genome. Inversion of the 3'-hairpin results in an almost identical structure that differs from the original hairpin only at several nucleotides that are not included in terminal palindromes. These nearly identical structures are arbitrarily designated as "flip" and "flop." The designation is important because the flip-flop transitions do not always

coincide with the synthesis of positive- or negative-sense genomes. This is because the 5'-hairpin is merely transferred from the 3'-end of parental DNA, and not synthesized complementary to the template like the rest of the progeny molecule.

As it is apparent from the model, at least two enzymes are needed in addition to DNA polymerase to enable parvoviral replication – a site-specific nickase to resolve the junction between the monomer genomic units and a helicase to melt secondary structures in the process of replication. In parvoviruses, both enzymatic activities are carried out by the same multifunctional non-structural protein NS1 (Cotmore and Tattersall, 1995). MVM NS1 binds to specific sequences upstream from the terminal hairpins, nicks them, binds to the 5'-end of the nick, and usually remains attached to DNA throughout the end of viral cycle (Gunther and Tattersall, 1988; Cotmore and Tattersall, 1989). The subset of monomeric replicative form DNA (mRF) that was found by Gunther and Tattersall (1988) to be free of NS1 was most likely composed of covalently closed molecules that formed in the absence of NS1 shortly after uncoating. Under these conditions, DNA polymerase extends the 3'-end of single-stranded genomes until the 5'-end is encountered, and the resulting nick is probably closed by an unidentified host cell ligase (Cotmore and Tattersall, 1995). In addition to its role in viral DNA replication, MVM NS1 trans-activates both viral promoters (Doerig et al., 1988; Hanson and Rhode, 1991) while trans-inactivating some cellular promoters and causing cytotoxicity (Legendre and Rommelaere, 1992). It is also thought to participate in packaging and viral egress from infected cells (Cotmore and Tattersall, 1989). Homologues of this protein are found in all parvoviruses, although not all NS1 domains are equally conserved.

Afanasiev et al. (1991) determined that *Ae*DNV NS1 contains a 150-residue region highly conserved in all parvoviruses. Within this sequence, the authors identified a motif that matches an NTP-binding consensus sequence. This is in accordance with MVM data, where ATPase activity of NS1 has been confirmed, found to be required for NS1 functioning, and thought to be a trigger for NS1 oligomerization *in vivo* (Nuesch and Tattersall, 1993). Surprisingly, the rest of *Ae*DNV NS1 showed little similarity to other parvoviral NS1 proteins. It is possible that the variable regions of NS1 are responsible for the interactions with other viral and host cell proteins, and consequently they could be very different in the viruses that infect unrelated host species.

According to Cotmore and Tattersall (1995), packaging of parvoviral genomes depends on the presence of preformed capsids and ongoing DNA replication. However, the details of this process remain unclear. It was previously thought that MVM genomes are sequestered into preformed capsids as they are being displaced by elongating DNA strand. More recent data indicate that displaced single-stranded genome units accumulate before the onset of packaging and that the double-stranded RF is not a substrate for packaging (Cotmore and Tattersall, 2005). The process of AAV-2 (a dependovirus) packaging has been studied in detail by King et al. (2001) who found that the genomic DNA is forced into the pre-formed capsids by the action of helicase rep52/rep40 immobilized on the capsid. The packaging proceeded in 3'→5' direction, which is also the direction for rep52/rep40 processivity. It is not known whether these findings are applicable to the autonomous parvoviruses. The rep52/rep40 complex – a truncated version of major non-structural proteins rep78/rep68 – is unique to adeno-associated

viruses. The 5'→3' mode of packaging is thought to occur in MVM, as the defective virions resulting from interrupted packaging invariably contained 5'-sequences (Cotmore and Tattersall, 1995).

The patterns of packaging sense selectivity generally depend on the terminal sequences. The viruses with ITR (e.g. *Erythrovirus, Iteravirus,* and *Densovirus* genera) encapsidate equal amounts of positive-flip, positive-flop, negative-flip, and negative-flop genomes (Li et al., 2001; Shade et al., 1986; Tijssen et al., 2003). The viruses with unique termini (e.g. *Parvovirus* and *Brevidensovirus* genera) tend to exhibit a strong packaging preference for negative-sense strands. For example, MVM packages over 90% of negative-sense genomes, all with a single conformation at the left end and flip-flop conformations at the right end (Cotmore and Tattersall, 1995). A notable exception to this rule is LuIII, which is closely related to MVM, but packages all possible genomic species equally. Possible explanations of this phenomenon include the differences in the left replication origin activity between the two viruses (Diffoot-Carlo et al., 2005), disruption of cell protein binding sites around the right replication origin of LuIII by AT-rich insertion element (Corsini et al., 1995), and dampening of the right replication origin of LuIII by a single AT insertion at the nick site (Cotmore and Tattersall, 2005). Importantly, the findings of these authors corroborate the unified kinetic hairpin transfer hypothesis postulated by Chen et al. (1989). According to this hypothesis, selectivity of packaging of any parvoviral genome is solely determined by the rates of reactions that comprise rolling hairpin transfers, while the capsid proteins play no role in the sense selection. Indeed, the LuIII genomes of all senses could be packaged equally into MVM

and parvovirus H-1 capsids, despite these viruses' natural preference for negative-sense genomes (Corsini et al., 1995).

Unfortunately, not much is known about packaging patterns of mosquito densoviruses. However, the finding that about 85% of all packaged genomes are negative-sense indicates that brevidensoviral replication and packaging is likely similar to that of *Parvovirus* genus members. Afanasiev et al. (1991) reported that all 3 clones of *Ae*DNV left terminus were found to be in the same conformation. This observation is important because it indicates that *Ae*DNV may share some specific replication details with MVM. However, more clones of either terminus have to be sequenced before any definitive conclusions can be made.

The final step of any virus life cycle is the exit of progeny virions from the host cells. In parvoviruses, this step is preceded by nuclear egress, which prevents retention of the newly-formed virions in the nuclei of infected cells. Miller and Pintel (2002) demonstrated that parvoviral replication and packaging could be shut down by negative feedback mechanisms unless the progeny virions are removed. Two requirements for successful nuclear egress of MVM virions have been identified. First is the synthesis of NS2 and its interaction with Crm1, a nuclear export protein which binds to leucine-rich nuclear export signals (NES) and facilitates nuclear export of proteins in a Ran-GTP-dependent manner (Bodendorf et al., 1999; Miller and Pintel, 2002). When murine cells were infected with a strain that had a mutation in NS2 NES region, the progeny virions accumulated in the nucleus and interfered with further virion production. These virions

were otherwise normal and fully infective, which indicates that the NS2 NES mutation specifically affected nuclear egress of MVM virions. In transformed human cells, which are known to support replication of NS2-null and NS2-defective mutants, NS2-null virions were efficiently transported out of nucleus. Interestingly, some nuclear retention of virions was seen in human cells infected with NS2 NES mutant, which according to the authors suggested a dominant-negative phenotype for NS2 NES mutation. One possible explanation is that Crm1 is still required for efficient egress of MVM virions in human cells, but its interaction with progeny virions is mediated by some cellular protein. When NS2 NES mutant protein interacts with the virions, it interferes with that cellular protein, and consequently with the nuclear export.

Second requirement for efficient nuclear egress of MVM virions is presence and availability of 2Nt – an unordered nuclear export signal located in amino-terminus of major capsid protein VP2 (Maroto et al., 2004). This signal is located on the interior of empty capsids but becomes externalized after the genome is packaged. Alternatively, the signal can be exposed by heat treatment of empty capsids. The authors demonstrated that in permissive human cells full or empty heat-treated capsids were efficiently transported out of nucleus, and that the exposure of 2Nt signal was necessary and sufficient for this transport. However, ongoing viral infection was required for nuclear egress in murine cells. Considering the fact that the viral replication in these cells is NS2-dependent, it is likely that both 2Nt signal and NS2-Crm1 mediated export mechanisms are required for the nuclear egress to occur.

Generally, the release of non-enveloped viruses (such as parvoviruses) is thought to occur through host cell lysis or apoptosis, while relatively non-destructive processes of membrane budding and exocytosis are reserved for enveloped viruses. However, there is some evidence for non-destructive exit of parvoviruses from infected cells under certain conditions. For example, Cotmore and Tattersall (1989) describe accumulation of predominantly full virions in the supernatants of the cell cultures infected with MVM, which indicates that the full virions were selectively released from the cell. If these virions were released through a destructive pathway, the proportion of empty capsids would be much larger. The authors argued that exposed genomic sequence with covalently attached NS1 protein could play a role in such selective virion release. Miller and Pintel (2002) also mention that non-destructive exit of virions is possible in some cases. Unfortunately, neither group of authors offered a possible model to explain this phenomenon: they only commented that it might represent a novel mechanism of viral shedding, and that parvoviruses could make a good model to study this mechanism.

The shedding pathway for mosquito densoviruses is equally unclear. Most members of this group do not cause any CPE when grown in mosquito cell cultures (our observations). The notable exception is *Haemagogus equinus* densovirus (*He*DNV) that completely disrupted C6/36 cells within several days post-infection. Paterson et al. (2005) demonstrated that *He*DNV but not *Ae*DNV induced apoptosis in infected cells. Interestingly, *He*DNV was only moderately virulent in *Aedes aegypti* mortality assays, less virulent then *Ae*DNV, indicating that induction of apoptosis in cell culture is not a good trait to predict infection outcome in mosquito larvae (Ledermann et al., 2004).

Obviously, in those infected individuals who succumbed to the disease the viral shedding was associated with cell destruction. However, *A*PeDNV, another mosquito densovirus discussed in detail later in this work, was efficiently amplified in infected host, yet the infection was completely asymptomatic (Ledermann et al., 2004). This may be another indication of the mysterious non-destructive exit pathway.

Section 1-3. Properties of NS2 proteins from mammalian and insect parvoviruses

NS2 proteins of mammalian parvoviruses are not encoded on a single uninterrupted ORF, as is the case with *Densovirinae* subfamily members. Instead, several small ORFs scattered throughout the viral genome contain exons that are joined by splicing. In MVM, alternative splicing of a long primary transcript results in a single isoform of NS1 whose transcript contains unspliced intron 1, and three isoforms of MVM NS2 (Y, P, and L – Cotmore and Tattersall, 1990). Exon 1 of NS2 transcript is identical to the 5'-end of the primary transcript; consequently, NS1 and all NS2 isoforms share the first 85 amino-terminal residues. The next 97 residues come from exon 2 and are shared by all NS2 isoforms but differ from NS1 sequence. The final 6 to 15 residues come from the rest of exon 2 or from alternative versions of exon 3. These residues uniquely define each isoform, but they do not seem to have much influence on the protein's basic properties. Despite the common amino-terminus, the properties of NS1 and NS2 are dramatically different. In the onset of infection, NS2 accumulates faster and to higher concentrations than NS1 despite the fact that NS2 is very unstable and has a high

turnover rate. Whereas NS1 is primarily nuclear protein, NS2 is strictly cytoplasmic in its phosphorylated form or diffusely localized in unphosphorylated form. Phosphorylated or not, NS2 does not seem to have any NLS, and the authors explain its presence in the nucleus by its small size (25 kDa), which allows it to diffuse freely through the nuclear pore complexes. At the same time, some of the functions of NS2 described next specifically require its presence in the nucleus, and there is always a possibility that NS2 could be delivered to the nucleus in a complex with some cellular or viral protein.

The role of NS2 in the MVM life cycle strictly depends on the host cell type. In most cell types, including transformed human cells, this protein is completely dispensable. The phenotype of NS2-null mutants grown in these cells is indistinguishable from the wild type. As discussed in previous section, some of the defective NS2 mutants can cause a slightly abnormal phenotype by a dominant-negative mechanism (Miller and Pintel, 2002). However, in cells of murine origin, such as the A9 cell line, NS2-null and most defective NS2 mutants are severely impaired (Naeger et al., 1990). Naeger et al (1992) compared the phenotypes of wild type MVM and NS2-deficient mutants in A9 cells and determined that the mutants synthesized less double-stranded RF DNA and single-stranded genomes. The synthesis of viral proteins, especially VP2, was also impaired. At the same time, transcription did not appear to be affected, as the ratio of viral mRNA to viral DNA synthesis was comparable for all strains. This observation prompted the authors to conclude that MVM NS2 is required for efficient translation of viral mRNA.

The studies conducted by Cotmore et al. (1997) revealed that the translation per se was likely unaffected by the absence of functional NS2, because the synthesis of VP2 was efficient during the early stages of infection. However, the capsid assembly did not proceed normally, which resulted in accumulation of unassembled VP2 in the nucleus. This probably activated some kind of negative feedback mechanisms that stopped viral DNA replication and down-regulated translation of viral mRNA. In other words, the authors traced defective phenotype to inefficient processing of VP2 capsomers.

Since some capsids were still formed under NS2-null conditions, the authors concluded that VP2 processing and assembly under wild-type conditions is unlikely to involve direct interaction of these viral proteins. Rather, expression of NS2 caused some changes in cellular environment that were conducive to proper processing and efficient assembly of VP2 into functional capsids. As one of possible mechanisms to induce these changes, the authors considered binding of NS2 to 14-3-3 proteins. According to Mhawech (2005), 14-3-3 is a highly conserved group of acidic proteins with multiple regulatory functions. Over 200 14-3-3 ligands have been identified, and while most of them are cellular proteins, MVM NS2 was also found to bind two proteins of this group (Brockhaus et al., 1996).

In addition to 14-3-3 family and previously discussed Crm1 protein, MVM NS2 was found to interact with survival-of-motor-neuron protein 1 (Smn1). As reviewed in Gubitz et al. (2004), Smn proteins participate in multiprotein complexes identified in all metazoans. These proteins can interact with other proteins and various RNA species, and

they appear to participate in assembly and function of snRNP and splicosomes. According to Young et al. (2005), both NS1 and NS2 proteins of MVM were found to interact with Smn1 *in vivo* and *in vitro*. Interactions of Smn1 with MVM non-structural proteins *in vivo* were mapped to the novel type of nuclear bodies called SAABs (Smn1-associated autonomous parvovirus-associated replication bodies). SAABs were found to be distinct from other known nuclear bodies, and they were induced by parvoviral infection, but not by mere expression of the non-structural proteins. SAABs were formed by agglomeration of smaller and earlier structures called APARs (autonomous parvovirus-associated replication bodies). The latter structures were found in MVM and rat H-1 parvovirus infections (Bashir et al., 2000; Cziepluch et al., 2000). APARs were found to contain NS1, PCNA, and SGT – another cellular protein considered to be important in parvoviral DNA replication. While the exact function of APARs and SAABs is not known to date, they are thought to be the sites of active replication and expression of parvoviral genomes.

While MVM is a representative member of genus *Parvovirus* and mammalian parvoviruses in general, other members of this group may be very different in some aspects, including the function of NS2. Canine parvovirus (CPV; genus *Parvovirus*) is not as closely related to MVM as the rodent parvoviruses, such as H-1. Because of a termination codon in exon-2, the second splice site has no effect on CPV NS2 sequence – this protein exists in a single isoform, and it is shorter than its MVM homologues. Wang et al. (1998) attempted to determine the role of CPV NS2 by constructing a number of nonsense mutations in the exon 2. The authors determined that these mutations had no

effect on CPV phenotype when grown in canine and feline cells, as well as in dog infections. One possible interpretation of these results is that NS2 has no function at all in CPV life cycle. In this case, it can be viewed as a rudiment retained from some ancestral strain, for which NS2 was important for interactions between the virus and its host. This ancestor must be preceding FPLV (the known immediate ancestor of CPV) since feline cells were also found to be permissive for replication of CPV NS2 mutants. Alternative explanation to these results is also possible – all determinants of CPV NS2 function may be located in the common NS1/NS2 region encoded by exon 1. Although the sequence of this region is identical in both non-structural proteins, the absence of downstream sequence in NS2 could completely alter protein's conformation and properties, similarly to the p52/p40 complex of AAV2 reviewed in the previous section of this work (King et al., 2001). In addition to exon 2 truncations, Wang et al. (1998) attempted to construct splice mutants and found that all of them replicated poorly. The authors downplayed importance of this finding and did not follow up on it, which is especially unfortunate because this report is the only one to date that addressed NS2 function in mammalian parvoviruses other than MVM. It would be, therefore, interesting to see more data on NS2 function in CPV and other closely-related parvoviruses.

Even less is known about NS2 proteins of insect parvoviruses. Attempts to find sequence similarity between mosquito densovirus NS2 and its counterparts from other members of *Densovirinae* subfamily failed despite all sophisticated search tools available today for homology searches. As reviewed in previous section, striking similarities can be found between brevidensoviruses and other insect parvoviruses in organization of

middle ORF and expression strategy of NS1/NS2 proteins. Consequently, the function of densoviral NS2 proteins is also likely to be similar. Unfortunately, no work outside of our lab has been done to elucidate the functions of densoviral NS2 proteins.

Based on the sequence data, calculated size of mosquito densovirus NS2 proteins is between 262 and 263 residues, MW = 41 kDa, pI = 9. To visualize NS2 and other mosquito densovirus proteins *in-vivo*, Dr. Joe Corsini developed a series of antibodies that would recognize linear epitopes of *Ae*DNV proteins. One of these antibodies efficiently recognized the amino-terminal sequence of the NS2 protein. This antibody was used in indirect immuno-fluorescence assays (IFA) as described in Azarkh, Robinson, et al. (2008). Using this technique together with GFP-labeled NS1 protein (described in Afanasiev et al., 1994) allowed the study of co-localization patterns of the two non-structural proteins in C6/36 cell culture. Some of the cells displayed strict co-localization of NS1 and NS2, while in other cells NS2 was localized more diffusely, concentrating in the nuclear periphery and cytoplasm. To study temporal and spatial patterns of NS2 expression, Erin Robinson monitored progression of *Ae*DNV infection in highly synchronized *Aedes albopictus* ATC-15 cells. The serial confocal microscopy images (Figure 4) reveal striking similarities in the patterns of NS2 expression and the formation of APAR and SAAB nuclear bodies described earlier in this section. NS2 expression first appears in small punctate regions in the nuclei of infected cells. As the infection progresses, these regions grow and coalesce to form larger structures. Eventually, NS2 is detected diffusely in the nucleus. During the later stages of infection, NS2 moves to the nuclear periphery and into the cytoplasm (Azarkh, Robinson, et al.,

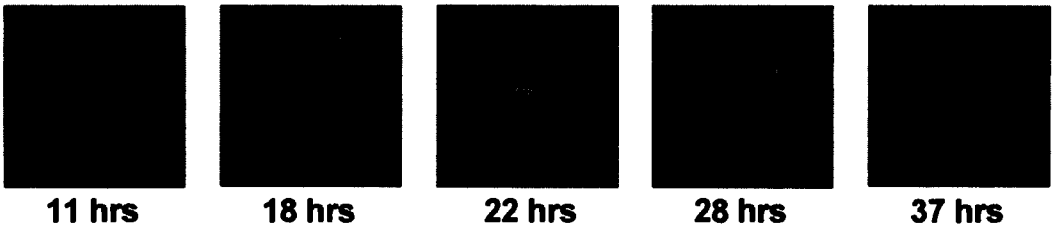

Figure 4. Distribution of NS2 in ATC-15 cells as a function of time (from Azarkh, Robinosn, et al. 2008).

Experiment was conducted in highly-synchronized cells. The time since hydroxyurea block removal is indicated under each image. NS2 is stained with fluorescent antibodies (green). Nuclei are stained with DAPI (blue).

2008). Further studies are needed to understand molecular mechanisms that underly NS2 transport into, within, and out of the nucleus.

Little is known about NS2 function. Dr. Boris Afanasiev constructed an NS2-null mutant of *Ae*DNV by changing the first ATG of the middle ORF to ACG. Similarly to MVM NS2 mutants grown in murine cells, this mutant replicated poorly in cell culture (personal communication), which indicated that mosquito densovirus NS2 was required for efficient reproduction of mosquito densoviruses.

I decided to study this mutant and brevidensoviral NS2 proteins in more detail. One of the main challenges to be addressed in the course of studies was the lack of an observable cytopathic effect (CPE) in cell cultures infected with mosquito densoviruses (*He*DNV-induced apoptosis of infected cells is a single exception – Paterson et al., 2005). This precluded characterization of brevidensoviruses using plaque morphology and counts and necessitated other, sometimes indirect, methods to characterize the viruses. In the course of my research, I evaluated four different experimental approaches to NS2

characterization: mutagenesis, promoter activity assays, imaging studies, and *in-vitro* DNA pull-down assays. These experimental approaches addressed sub-hypotheses that had arisen at various timepoints of my research. The sub-hypotheses are listed below.

1. NS2 is required for efficient replication of viral DNA in the course of viral propagation in both cell cultures and mosquito hosts.
2. NS2 enhances trans-activation effect that is exerted by NS1 towards the structural gene promoter P(VP).
3. NS2 is targeted to the nucleus. It's co-localization with NS1 in the punctate nuclear bodies is accompanied with a direct interaction between the two non-structural proteins.
4. NS2 is a DNA-binding protein (the rationale for this sub-hypothesis is discussed in Section 2-5).

The Chapter 2 contains detailed description of all experiments conducted in the course of my research, while the discussion of the results, conclusions, and prospects are presented in the Chapter 3.

Chapter 2. Experiments and their results

Section 2-1. Materials and methods

Plasmids and cloning. The overview of the plasmids constructed and/or used in the course of my research is given in the Table 3 (pp. 38-40), followed by a detailed explanation of the origins and cloning strategy for each plasmid.

Plasmid	Description	Source	Notes
pUCA	Complete genomic sequence of *Ae*DNV in pUC19 background	Our lab	See Afanasiev et al., 1994
pUCP	Complete genomic sequence of *A*PeDNV in pUC19 background	Our lab	See Ledermann et al., 2004
pAPA series	pUCA with the middle of the viral genomic sequence replaced with a homologous fragment from *A*PeDNV	Our lab and this work	
pUCP-G172E	pUCP with NS2 protein G172E mutation	This work	
pUCP-G172A	pUCP with NS2 protein G172A mutation	This work	
pUCA-NS2-null	pUCA with NS2 gene starting ATG→ACG mutation	Our lab	
pUCA-INV	pUCA with an inversion of the right end of the viral genomic sequence	Our lab	See Afanasiev et al., 1994
pUCA-IM	pUCA-INV with NS2 gene starting ATG→ACG mutation	This work	
p61-*Nco*RE	Derivative of pUCA with deleted left end of the viral genomic sequence, intact P(VP) promoter, intact 5' end of VP gene fused in-frame with β-galactosidase gene, followed by intact right end of the viral genomic sequence	Our lab	See Ward et al., 2001

Plasmid	Description	Source	Notes
p61-ΔPBR	p61-*Nco*RE with deleted putative NS2-binding region upstream from P(VP)	This work	
pBS-Luc	Firefly luciferase gene under control of *Drosophila* Hsp70 promoter in pBluescript background	Our lab	See Ward et al., 2001
pBS-Luc-Δ*Xba*I	pBS-Luc with *Xba*I site removed from the multiple cloning region	Our lab	
Hsp-NS2 series	Derivatives of pBS-Luc-Δ*Xba*I with *Luc* gene replaced with an NS2 gene of interest	This work	See Table 4 for individual constructs
pECFP	Cloning vector; the source of eCFP	Commercial (Clontech)	Gift from Dr. Olson's lab
pEYFP	Cloning vector; the source of eYFP	Commercial (Clontech)	Gift from Dr. Olson's lab
NS1-CFP	Derivative of pUCA with 3' end of NS1 gene fused in-frame with the 5' end of CFP gene	This work	
NS2-YFP	Derivative of pUCA with 3' end of NS2 gene fused in-frame with the 5' end of YFP gene	This work	
YFP-NS2	Derivative of pUCA with the 3' end of YFP gene fused in-frame with the 5' end of NS2 gene	This work	
pANS1-GFP	Derivative of pUCA with 3' end of NS1 gene fused in=frame with the 5' end of GFP gene	Our lab	See Afanasiev et al., 1999
pET-21b	Expression vector for use in *E. coli* expression systems	Commercial (Novagen)	
pET-42b	Expression vector for use in *E. coli* expression systems	Commercial (Novagen)	
pET21-PNS2	Construct for expressing full-length *A*PeDNV NS2 protein in *E. coli* expression systems	This work	
pET21-trPNS2-1	Construct for expressing truncated *A*PeDNV NS2 protein in *E. coli* expression systems	This work	
pET21-trPNS2-2	Construct for expressing truncated *A*PeDNV NS2 protein in *E. coli* expression systems	This work	

Plasmid	Description	Source	Notes
pET42-PNS2	Construct for expressing full-length *A*PeDNV NS2 protein fused to GST tag in *E. coli* expression systems	This work	
pET42-trANS2	Construct for expressing truncated *Ae*DNV NS2 protein fused to GST tag in *E. coli* expression systems	This work	

Table 3. The overview of the plasmids (begins on p. 38)

pUCA is an infectious clone that contains complete *Ae*DNV sequence in pUC19 background as described in Afanasiev et al. (1994). pUCP is an infectious clone that contains complete *A*PeDNV sequence in pUC19 background; first mentioned in Ledermann et al. (2004). Hybrids are chimeric mosquito densoviruses with termini derived from one virus and the middle part from another. pAPA series plasmids are infectious clones of the hybrids described in this work. These plasmids can be viewed as pUCA derivatives in which the middle part of viral genome is replaced with homologous region of pUCP. pAPA-4 and pAPA-5 were constructed by Dr. Boris Afanasiev by replacing *Msc*I x *Bam*HI and *Bst*API x *Bam*HI fragments of pUCA, respectively, with homologous fragments from pUCP (these restriction sites are conserved between the two viral species). Starting with pAPA-6, the new pAPA constructs were made from preceding constructs rather than from pUCA. In pAPA-6, *Bst*BI (747) x *Bsr*GI (1744) fragment of pAPA-4 was replaced with a PCR-amplified homologous fragment of pAPA-5. When describing construction of pAPA series of plasmids, the numbers in parentheses indicate the first base position of each restriction site as it can be located on ClustalW alignment of *Ae*DNV and *A*PeDNV. PCR was needed to engineer a *Bst*BI site present in

*A*PeDNV, but absent in *Ae*DNV because of a single point mutation. pAPA-7 was originally planned with the junction between the fragments at *Sal*I (1103) site, but this plasmid was later determined to be unnecessary and its construction was never finished. In pAPA-8, *Hpa*I (935) x *Xba*I (2788) fragment of pAPA-5 was replaced with a homologous fragment of pAPA-6. Partial digestion technique was used to avoid cutting additional *Hpa*I site located within this fragment. In pAPA-9, PCR fusion technique was used to generate a chimeric (*Ae*DNV/*A*PeDNV) fragment with junction at alignment position 805. pAPA-5 and pAPA-6 served as templates for initial PCR fragments that were fused by additional PCR reaction. The final PCR product was cloned into *Dra*III (327) x *Bst*API (1349) sites of pAPA-6, which required three-piece ligation because of an additional *Bst*API site in the pUC-19 backbone. In pAPA-10, PCR fusion technique was used to generate a chimeric fragment with junction at alignment position 887. *Hin*dIII (720) x *Sal*I (1103) fragment of pAPA-6 was replaced with the final PCR product, which required a sub-cloning step because of multiple additional *Hind*III sites in the right end of the viral sequence and in the pUC19-backbone. pAPA-11, pAPA-12, and pAPA-13 were constructed using the same scheme. For each plasmid, a set of two complimentary 5'-phosphorylated oligonucleotides was synthesized by CSU core facility. The ends of these oligonucleotides contained unmatched sequences that corresponded to the "sticky" ends generated by *Eco*O109I x *Hpa*I restriction digest. These fragments were heated to 95° C in STE buffer and slowly cooled down over a 2-hour period. This procedure resulted in double-stranded ligation-ready DNA fragments, which were cloned into *Eco*O109I (847) x *Hpa*I (935) sites of pAPA-10. One sub-cloning step was required

because neither of the restriction sites is unique in pAPA-10. The oligonucleotides were designed based on *Ae*DNV and *A*PeDNV sequence to produce chimeric DNA fragments with junctions at alignment positions 907, 901, and 895 for pAPA-11, pAPA-12, and pAPA-13, respectively. pUCP-G172E and pUCP-G172A plasmids are point mutants of pUCP with a guanine at alignment position 895 substituted to adenine or cytosine, respectively. These substitutions were made by PCR-mediated site-directed mutagenesis, with final PCR product cloned into *Dra*III (327) x *Bst*API (1349) sites of pUCP. pUCA-NS2-null plasmid was constructed by Dr. Boris Afanasiev. It carries a single thymine-to-cytosine substitution in the first ATG triplet of NS2 gene.

pUCA-INV is a plasmid similar to pUCA, but with an inverted right terminus of the viral sequence; described in Afanasiev et al. (1994). pUCA-IM is an NS2 knockout variant of pUCA-INV constructed by cloning the *Dra*III x *Bst*EII fragment from pUCA-NS2-null into pUCA-INV. p61-NcoRE is a derivative of pUCA with a deletion of viral sequence upstream of *Nco*I site and with a 3' portion of VP gene replaced in-frame with β-Galactosidase gene; described in Ward et al. (2001). p61-ΔPBR is a derivative of p61-NcoRE that carries a deletion of *Bst*API x *Ale*I fragment. This was achieved by PCR amplification of *Ale*I x *Bpu*10I fragment of p61-NcoRE with simultaneous site-directed mutagenesis that changes *Ale*I restriction site to *Bst*API. This fragment was then cloned into *Bst*API x *Bpu*10I sites of p61-NcoRE. pBS-Luc is a pBluescript-based plasmid that contains the *Drosophila melanogaster* Hsp70 promoter, the firefly luciferase gene, and the SV-40 poly-adenylation site used by Ward et al. (2001). pBS-Luc-Δ*Xba*I (constructed by Jennifer Chiniquy) carries a deletion in a multiple cloning site of pBS-

Luc, which makes *Nco*I and *Xba*I restriction sites flanking *luc* gene unique and allows for a simple replacement of this gene with any gene of interest. Hsp-NS2 series plasmids were constructed by PCR amplification of different variants of NS2 gene with simultaneous site-directed mutagenesis to engineer *Nco*I and *Xba*I restriction sites at the ends of the amplified gene. The PCR fragment was then cloned into the matching sites of pBS-Luc-Δ*Xba*I. The plasmids of this series are summarized in Table 4.

Plasmid name	PCR template	NS2 gene variant
Hsp-ANS2	pUCA	Wild type full-length *Ae*DNV NS2 gene
Hsp-trANS2	pUCA	Wild type *Ae*DNV NS2 gene truncated after base position 771 (residue T257)
Hsp-PNS2	pUCP	Wild type full-length *A*PeDNV NS2 gene
Hsp-G172E	pUCP-G172E	Full-length *A*PeDNV NS2 gene with a point mutation resulting in G172E substitution

Table 4. Plasmids of Hsp-NS2 series.

Plasmids pECFP and pEYFP (Clontech) are the sources of fluorescent protein tags eCFP and eYFP, respectively; generously provided by Chris Cirimotich and Dr. Olson's lab. The NS1-CFP plasmid expresses full-length *Ae*DNV NS1 protein with a carboxy-terminus fused in frame with eCFP. It was constructed by PCR amplification of eCFP gene with simultaneous site-directed mutagenesis to engineer *Nru*I and *Nsi*I sites at the 5' and 3' ends of amplicon, respectively. This PCR fragment was cloned into *Sna*BI x *Nsi*I sites of pUCA. The NS2-YFP plasmid expresses full-length *Ae*DNV NS2 protein with a carboxy-terminus fused in frame with eYFP. It was constructed by cloning eYFP

gene flanked by *Stu*I and *Nco*I restriction sites into *Ale*I and *Nco*I sites of pUCA. The gap between NS2 and eYFP genes was closed by replacing *Dra*III x *Nco*I region with a PCR fragment containing complete NS2 gene with modified upstream and downstream sequences. The upstream sequence included original *Dra*III restriction site, but contained a point mutation that introduced a stop codon in the NS1 frame. This prevented expression of a large, but truncated version of NS1 protein with unpredictable and possibly toxic properties. The downstream sequence consisted of an *Nco*I site engineered by site-directed mutagenesis immediately at the end of the NS2 gene, which effectively deleted unwanted sequence between the end of NS2 and beginning of eYFP gene and positioned the latter in frame with the former. The YFP-NS2 plasmid also expresses YFP-labeled *Ae*DNV NS2 protein, but with the eYFP domain fused to the amino-terminus of NS2. It is derived from pUCA by deleting one fragment and inserting three fragments through a series of sub-cloning steps (Figure 5). The deletion of the *Ale*I x *Bst*BI fragment followed by blunt-ending and re-circularization is necessary to keep the size of the viral genome close to original 4 kb, which in turn allows for packaging in the presence of a helper virus. The insert 1 is a ligation-ready 5'-phosphorylated synthetic DNA duplex that contains the sequence found upstream of NS2 gene with a single mutation that creates a stop codon in NS1 frame. The 5' end of this fragment contains the original *Dra*III site, while the 3' end contains the start codon in NS2 frame and *Nco*I site engineered around it. The insert 2 is an *Nco*I x *Bsr*GI fragment from pEYFP that contains the entire eYFP sequence except the last two bases. The insert 3 is a PCR product that contains 5' portion of NS2 gene including *Bst*EII restriction site. Site-

directed mutagenesis was used to engineer *Bsr*GI site and the last two bases of the eYFP gene adjacent to the 5' end of NS2 gene. pANS1-GFP plasmid expresses full-length *Ae*DNV NS1 protein with a carboxy-terminus fused with the *Av*GFP; described in Afanasiev et al. (1999).

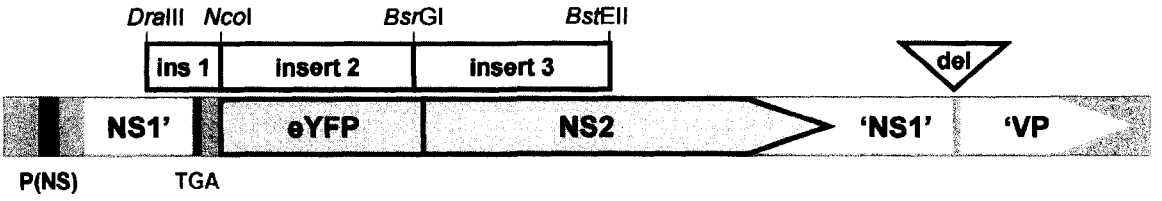

Figure 5. Genetic organization and cloning strategy of YFP-NS2 plasmid.

P(NS) – non-structural gene promoter; TGA – stop codon for early termination of NS1 translation; ins – insert; del – deletion.

Plasmids pET-21b and pET-42b (Novagen) are T7-*lac* vectors for expression of heterologous proteins in *E. coli* cells. pET21-PNS2 series plasmids were constructed by cloning PCR amplified full-length or truncated NS2 gene from *A*PeDNV into *Nde*I x *Xho*I-digested pET-21b vector. *Nde*I and *Xho*I restriction sites flanking NS2 gene were engineered in the course of PCR through the use of mutagenic primers. In pET21-PNS2, the full-length gene is cloned. In pET21- trPNS2-1, only bases 1-774 (residues 1-258) were cloned, which resulted in a loss of carboxy-terminus. In pET21-trPNS2-2, bases 772-1089 (residues 258-363) were cloned, which resulted in a loss of amino-terminus. pET42-PNS2 was constructed by a 3-piece ligation combining the plasmid backbone obtained by *Kpn*I x *Xho*I digestion of pET-42b vector, NS2 gene fragment obtained by *Bse*RI x *Xho*I digestion of pET21-PNS2 plasmid, and a synthetic 5'-phosphorylated ligation-ready DNA duplex containing the junction between the GST and NS2 domains

and flanked by *Kpn*I x *Bse*RI restriction sites. pET42-trANS2 was constructed by cloning PCR-amplified full-length NS2 gene from *Ae*DNV into *Nco*I x *Xho*I-digested pET-42b vector. *Nco*I and *Xho*I restriction sites flanking NS2 gene were engineered in the course of PCR through the use of mutagenic primers.

The DH5-α strain of *Escherichia coli (E. coli)* was used for general cloning purposes. These cells were made electro-competent and transformed with the plasmids of interest using standard electroporation protocols. TOP-10 chemically-competent *E. coli* cells (Invitrogen) were used in accordance with the manufacturer's recommendations to propagate TOPO-clones of PCR products. Commercially-available kits were used to isolate, purify, and gel-extract DNA in the course of cloning (FastPlasmid mini-kit from Eppendorf; QIAGEN midi- and maxi-kits and QIAquick gel extraction kit from Qiagen). Unless explicitly stated otherwise, all enzymes used in cloning were purchased from the New England Biolabs.

Mosquito cell cultures. *Aedes albopictus* C6/36 cells were used for the majority of mosquito cell culture experiments and procedures. These cells were grown in Leibovitz-15 (L-15) medium with 2 mM L-glutamine, supplemented with penicillin (100 μg/mL), streptomycin (100 U/mL), and fetal bovine serum (10% v:v). The cells were incubated at 28° C and passed every 3-4 days at 20% - 30% confluency. A modified serum-free line of C6/36 cells (SF) was developed in our lab (Suchman and Carlson, 2004) and used for virus preparations. This line was grown in Sf-900 SFM medium supplemented with penicillin (100 μg/mL) and streptomycin (100 U/mL). The cells were incubated at 28° C and passed every 2-3 days at 10% - 25% confluency. *Aedes aegypti*

Aag2 cells (a gift from Jackie Scott and the AIDL group) were used for confocal microscopy experiments. These cells were grown in Schneider's medium supplemented with penicillin (100 μg/mL), streptomycin (100 U/mL), and fetal bovine serum (10% v:v). The cells were incubated at 28° C and passed every 3 days at 10% - 20% confluency.

Transfection. Mosquito cells that reached 40% - 60% confluence were transfected with plasmids of interest using Effectene kit (Qiagen) in accordance with the manufacturer's recommendations for transient transfection of attached cells. Amount of each reaction component depended on the size of tissue culture, as shown in Table 5. Transfected cells were incubated at 28° C. Other details of transfection procedure varied depending on experiment setup; they are discussed later in this section.

Culture size		Amount of components in reaction mixture				Medium to add to	
Actual	Qiagen equivalent	DNA (μg)	DNA in buffer EC	Enhancer	Effectene	cells	mixture
35 mm dish	6-well plate	0.4	100	3.2	10	600	1900
25 mm^2 flask (T-25)	60 mm dish	1	150	8	25	1000	4000
75 mm^2 flask (T-75)	100 mm dish	2	300	16	60	3000	7000

Table 5. Amount of reagent components used to transfect cell cultures of various size.

All amounts are in milliliters unless indicated otherwise.

Virus preparation (for use in subsequent infection of the cells or mosquito larvae). SF cells were transfected with plasmids of interest and incubated at 28° C overnight. Next day (no later than 24 hr post-transfection) the medium containing

untransfected plasmid DNA was removed, and the cells were washed twice with sterile PBS (the amount of each portion of PBS was equivalent to the original culture volume). The fresh medium was then added to the cells, and the incubation continued for another 3-5 days depending on the culture density. At the end of incubation, the cells were lysed by 3 cycles of alternating freezing at -80° C and thawing at 37° C. The lysates were cleared by low-speed centrifugation (Beckman G56R centrifuge, 3750 rpm for 5 min), followed by high-speed centrifugation (DuPont centrifuge, SW-34 rotor, 15000 rpm for 10 min). The virus particles (along with some cellular constituents) were pelleted by ultracentrifugation (Beckman L7 ultracentrifuge, SW-28 Ti rotor, 28000 rpm for 2.5 hr) and resuspended in 1 mL of sterile distilled water. For infection of mosquito cell cultures, the virus preparation was filter-sterilized. To determine virus concentration, viral DNA was extracted from 20-μL aliquots of virus preparation using QIAamp blood mini-kit (Qiagen). Quantitative real-time PCR (qPCR) was then performed as described later in this section.

Quantitative PCR. Real-time PCR developed in our lab (Lederman et al., 2004) is a TaqMan assay that targets a 181-base region of NS1 gene.
The forward primer CATACTACACATTCGTCCTCCACAA,
the reverse primer CTTGGTGATTCTGGTTCTGACTCTT,
and the probe FAM-CCAGGGCCAAGCAAGCGCC-TAMRA were designed to bind to highly conserved sequences of NS1 gene, so that the same assay could be used to detect different strains of mosquito densoviruses. The original protocol for this assay was

followed, except ABI 7700 instrument was no longer available, so it was substituted with Opticon 2 (MJ Resesarch) and iQ-5 (Bio-Rad) real-time PCR systems.

Immuno-fluorescence assays (IFA) were developed in our lab to detect viral proteins in the cells transformed with infectious clones or infected with mosquito densoviruses. Two kinds of primary antibodies were used in this work: α-NS2 and α-*Ae*DNV. The former (developed by Dr. Joe Corsini) was raised against a synthetic peptide that represented an amino-terminal region of *Ae*DNV NS2 protein (VSAGGENWIWEHQLESKEDWPTITNN). The latter (a gift from Dr. Leon Buchatsky) was raised against the whole capsid of *Ae*DNV. Both kinds of antibodies were produced in rabbits and are polyclonal in nature. Secondary antibody (Zymed) was raised in goats against rabbit IgG and conjugated to FITC. To perform IFA, the cells were washed once with PBS and fixed with a cold mixture of equal volumes of absolute ethanol and acetone for 15 min. After removing the fixative, the cells were dried and re-hydrated with PBS for at least 5 min. The staining consisted of primary antibody (1:200 dilution of α-NS2 or 1:1000 dilution of α-*Ae*DNV) and secondary antibody (1:200 dilution), each followed by three PBS washes. When nuclear counterstain was necessary, it was performed using a 1:1000 dilution of crystallized DAPI stock in distilled water, followed by a single PBS wash. Conventional microscopy was performed using a Nikon Diaphot 200 fluorescent microscope. The images generated under FITC and DAPI filter settings were collected using CoolSnap camera and saved in 24-bit RGB TIFF format. Adobe Photoshop and ImageJ software was used for image processing and analysis.

Quick test for infectivity. C6/36 cells grown in T-25 flask were transfected with the plasmid of interest. Untransfected plasmid DNA was removed by washing within 24 hr post-transfection. One mL of the medium was removed from the transfected cell culture 72 hr post-transfection and added to a fresh cell culture grown to 30% - 50% confluence in 4 mL of medium. Infected cell culture was grown for 72 hr, fixed, and stained with α-*Ae*DNV antibodies (see IFA procedure). Those infected cell cultures that displayed at least one positive cell in the majority of fields were considered overall positive, and the corresponding construct was considered infective.

Encapsidation efficiency (no DNase I treatment). For each cell culture sample transfected with a plasmid of interest, two samples were assayed by qPCR and compared: one of the cleared lysate before ultracentrifugation, and the other of the virus-containing pellet after centrifugation and reconstitution with distilled water to the starting volume.

Encapsidation efficiency (DNaseI treatment). For each cell culture sample transfected with a plasmid of interest, three samples were assayed by qPCR and compared: cleared lysate before ultracentrifugation, untreated virus-containing pellet, and DNaseI-treated pellet. The treatment step consisted of mixing 500 μL of cleared lysate with 500 μL of 2x DNase buffer (100 μL of 10x DNase buffer from Fermentas; 400 μL distilled water). In case of treated samples, 20 U of DNaseI (Fermentas) were added to the buffer prior to mixing it with the sample, while untreated samples were mixed with the buffer alone. Untreated and treated samples were incubated at 37° C for 30 min, followed by ultracentrifugation in Beckman Optima TLX centrifuge (TLA-110 rotor, 55000 rpm, 2 hr). The pellets were resuspended in 500 μL of Sf-900 medium. 500 μL of

DNase inactivation buffer (5 mM EDTA and 0.2% SDS in PBS) were added to all samples (cleared lysates, untreated pellets, and treated pellets). Samples were incubated until complete clearing (10-20 min) at room temperature, followed by 20 min incubation at 75° C. 200 μL of each sample was then processed using QIAamp blood mini-kit (Qiagen) to extract viral DNA, and the extracts were tested by qPCR.

Virus propagation curve. Virus preparations of wild type *A*PeDNV and its G172E mutant were produced as described above. C6/36 cells grown in 5 mL of medium to 35%-40% confluence in T-25 flasks were infected with the viral preparations to the final concentration of 1 E+09 copies of viral genome per mL. The cells were incubated at 28° C for 2 hr, at which point (considered time zero) the cells were washed and the medium was replaced as described above. Infected cells were then incubated at 28° for 72 hr. 20-μL aliquots of the medium were taken from infected cell cultures at 0 hr, 24 hr, 48 hr, and 72 hr post-infection. These aliquots were processed using QIAamp viral DNA isolation mini-kit (Qiagen), and the resulting DNA samples were analyzed by qPCR.

***In-vivo* infectivity study.** Virus preparations of wild type *Ae*DNV, its NS2-null mutant, hybrids 12 and 13, and *A*PeDNV G172E mutant were produced as described above. The eggs of *Aedes aegypti* strain Rexville D mosquitoes were hatched in tap water at 28° C. Three hr post-hatch, the instar I larvae were transferred into 18 15-mL conical tubes (50-100 larvae per tube) and exposed to 5 E+08 copies of each virus in total volume of 5 mL (final concentration 1 E+08 copies of viral genome per mL). Uninfected instar I larvae in 5 mL of tap water served as a control. Each infection and control was set up in triplicates. The infection step proceeded for 24 hr, after which the larvae were

transferred into plastic cups, and 75 mL of tap water was added to each cup. A 100-μL water sample was then taken from each cup and stored at -20° C. Experiment continued until day 10 post-infection. During this time, the larvae were incubated at 28° C with 12 hr light / 12 hr dark cycles. Each sample of the triplicate was put on a different tray, so that three experimental groups were formed. The larvae were fed 10% liver powder (100 μL per cup), and the water was added to the cups as needed. In addition to day 1 water sample, 100-μL aliquots of rearing water were collected on days 4, 7, and 10 post-infection and stored at -20° C. At the end of experiment, each water sample was thawed and mixed with 900 μL of distilled water and analyzed by qPCR. Each qPCR plate contained samples from a single experimental group.

Transactivation and complementation experiments. C6/36 cells were transfected with plasmids of interest as shown in Table 6 and incubated for 48 hr. Assays for β-galactosidase and firefly luciferase were conducted as described in Ward et al. (2001), except the following modifications. The amount of lysis buffer was increased 6-fold (to 1.5 mL per T-25 flask). No additional dilution was required, and the amount of sample tested was increased from 5 μL to 20 μL per reaction.

Co-localization and FRET (Fluorescence Resonance Energy Transfer) studies in Aag2 cells. The cells were seeded into T-25 flasks at 30% confluence or into 35 mm glass-bottom dishes (MatTek) at 20% confluence. After the cells reached about 60% confluence, they were transfected with fluorescent protein constructs. The total amount of DNA per dish was the same for a given cell culture size (1 μg per T-25 or 0.4 μg per 35 mm dish), but the proportion of different plasmids depended on the sample,

	Source of luciferase: pBS-Luc	Source of β-galactosidase: p61-NcoRE p61-ΔPBR	Source of NS1/NS2: pUCA-INV pUCA-IM	Source of NS2 complementation: Hsp-ANS2 Hsp-PNS2 Hsp-G172E
Experiments without complementation *	0.1	0.5	0.5	---
Experiments with complementation	0.1	0.1	0.4	0.4

Table 6. Amount of each plasmid used for transfections in trans-activation and complementation experiments.

(*) Early experiments conducted before the complementation plasmids were constructed

as shown in Table 7. At 20 to 24 hr post-transfection, the samples were washed once with PBS and fixed for 15 min with 2% formaldehyde solution in PBS, which was prepared immediately before use from the 16% stabilized formaldehyde ampules (Pierce). Fixation was stopped by removing the fixative, replacing it with PBS, and incubating for 5 min. In case of T-25 flasks, this portion of PBS was replaced with another, which kept cells hydrated throughout the assay. In case of glass-bottom dishes, PBS was removed, and an 18-mm round coverslip was mounted on top of the fixed cells using FluorMount medium (Southern Biotech).

	Donor: NS1-CFP or NS1-GFP	Acceptor: NS2-YFP or YFP-NS2	Helper: NS2-null
Donor only	1	---	---
Donor with helper	$^1/_2$	---	$^1/_2$
Acceptor with helper	---	$^1/_2$	$^1/_2$
FRET sample	$^3/_8$	$^3/_8$	$^1/_4$

Table 7. Proportion of different plasmid DNA species used to transfect Aag2 cells in the course of colocalization and FRET experiments.

Channels	Illumination settings			Detection settings	
	Laser	Line (nm)	Power (% of maximum)	Gain	Detection window (nm)
GFP	Argon	458	20	604	465-510 filter
YFP	Argon	514	8 / 12 *	604	561-657 meta
FRET	Argon	458	20	604	561-657 meta

Table 8. Confocal microscopy settings to acquire FRET experiment images

(*) Different power was required for optimal excitation of acceptor in NS2-YFP and YFP-NS2 samples (first and second value, respectively)

Confocal microscopy and FRET assays were performed using Zeiss 510-LSM confocal microscope. The settings (summarized in Table 8) were adjusted empirically to provide the best separation of YFP and GFP signals and the most complete representation of grayscale values possible, as described in Baumann et al. (1998) and Hachet-Haas et al. (2006). Line-by-line pixel averaging technique built in Zeiss LSM software was used to improve signal-to-noise ratio. The images were collected and saved in uncompressed 8-bit TIFF format. Each field was represented by four images (GFP, YFP, FRET, and brightfield). ImageJ program (http://rsb.info.nih.gov/ij/download.html) was used to process the images as follows:

1. Brightness and contrast were auto-adjusted for all brightfield images. This was done exclusively to enhance visibility of cell boundaries in merged co-localization images. Brightfield images are not used in calculating the FRET indices.
2. The four images of each field were temporarily stacked and cropped to 85 x 85 pixel size. The stack was then converted to separate images.

3. The cropped images of all fields collected from the same sample and through the same channel were combined in a single montage. This procedure was repeated to process all sample-channel combinations.
4. The montages were further processed and analyzed using FRET and Co-localization Analyzer and PixFRET plugins, as outlined in Hachet-Haas et al. (2006) and Feige et al. (2005), respectively.
5. The lookup tables (LUTs) were modified for the final outputs of each program (Figure 6). The original LUT of the Co-localized FRET Index image was replaced with "coloc fret index.lut" in which the first 16 values are displayed in the same shade of grey (RGB = 200;200;200). The original LUT of the PixFRET FRET index was replaced with "smart.lut" (one of ImageJ pre-sets).

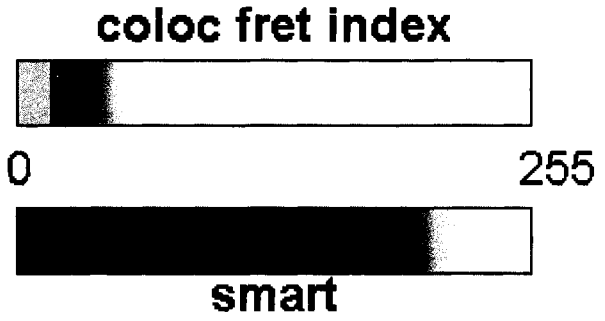

Figure 6. The LUTs applied to the final output images generated by FRET and Co-localization Analyzer and PixFRET plug-ins.

The numbers indicate the beginning and the ending values in 8-bit format images.

Expression of recombinant NS2 protein in bacterial cells. Rosetta2 chemically-competent *E. coli* cells (Novagen) were used to express NS2 proteins in prokaryotic system using T7-*lac* approach. This strain is a derivative of BL-21(DE-3) strain

containing a proprietary plasmid pRARE-2, which over-expresses 7 tRNA species underrepresented in *E. coli* to overcome the codon usage problem. To express NS2 protein, the cells were chemically transformed with the plasmids of interest in accordance with the manufacturer's recommendations. The transformed bacteria were grown in LB medium containing 34 μg/mL chloramphenicol (to maintain pRARE-2 plasmid) and either 100 μg/mL ampicillin or 30 μg/mL kanamycin (to maintain pET-21 or pET-42 derivatives, respectively). When the cell density reached OD[600 nm] between 0.6 – 0.8 A, expression of recombinant NS2 protein was induced by addition of 100 mM IPTG solution to the final concentration of 1 mM. The cells were harvested 3 hr post-induction by low-speed centrifugation (Beckman G56R centrifuge, 3750 rpm for 5 min), washed once with cold 50 mM Tris-HCl pH 7.4 (1/10 of original culture volume), and frozen at -20° C overnight. Next morning, the cells were thawed and resuspended in lysis buffer (5% v:v glycerol, 1% v:v Triton X-100, 300 mM NaCl, 50 mM Tris-HCl pH 7.4; 1/50 of original culture volume). Fresh lysozyme solution in the lysis buffer (50 μg/mL) was prepared and added to the cell suspension to final concentration of 1 μg/mL. The cells were vortexed for 5 min, followed by incubation on ice for 15 min. The cell debris was removed by high-speed centrifugation (DuPont centrifuge, SW-34 rotor, 15000 rpm for 10 min), followed by filtering through 0.22 μ filter. The resulting clear lysate was aliquoted and stored at -20° C. To express GST-only control, the same procedure was followed, except the original pET-42b plasmid was used instead of NS2-containing derivatives. Alternative methods of cell disruption and protein extraction have been

attempted in the course of some experiments. These methods will be discussed along with corresponding experiment results.

Analysis of protein expression. SDS-PAGE was used to separate proteins for subsequent analysis by Coomassie stain and Western blot methods. All reagents used for SDS-PAGE electrophoresis and blotting were from Invitrogen, except the nitrocellulose membrane, which came from Amersham Bioscience. The samples were mixed with 4x SDS loading buffer in 3:1 ratio by volume and heated to 70° for 10 min. They were then loaded onto NuPage bis-tris 4-12% mini-gel and run in MES buffer with antioxidant at 200 V for 35 min.

For Coomassie stain, the gels were covered with the stain (0.0025% w:v Coomassie Blue R-250, 7% v:v glacial acetic acid, 40% v:v methanol, distilled water to 1L) and microwaved at high power for 1 min followed by 20 min incubation at room temperature on the orbital shaker. The samples were then destained in a mixture of glacial acetic acid (7% v:v), methanol (40% v:v), and water (to 1 L) overnight with several changes of destaining solution. The images were taken using GelDoc camera (Bio-Rad).

Western blots were performed as described in Azarkh, Robinson et al. (2008), except for a different antibody used to stain trPNS2-2 protein, which lacks the amino-terminal epitope recognized by α-NS2 antibodies. This protein was stained with α-His_6 (C-term) HRP-conjugated antibodies (gift from Dr. Shuhui Wang) diluted 1:5000. No secondary antibody was required for this stain.

For the dot blots, 9 volumes of lysate was mixed with 1 volume of 10% SDS and incubated at 70° C for 10 min. 5 μL of the lysate was then spotted onto a nitrocellulose filter and incubated at 37° C for 10 min or until the spot became completely invisible. The filter was then blocked in UniBlock solution (AGTC) and stained against NS2 as described in Azarkh, Robinson et al. (2008).

Purification and concentration of recombinant trANS2 protein. MagneGST protein purification system (Promega) was used to purify GST-tagged recombinant NS2 protein. This system was also used for DNA pull-down experiments described later in this section. The original manufacturer's protocol for protein purification was optimized, which resulted in the following modifications:

- The starting amount of magnetic particles was set at 0.5 mL
- The amount of binding and wash buffer (BWB) was set at 1 mL for all washing steps; all washing steps were conducted at room temperature
- The amount of protein-containing lysate was set at 1 mL
- Protein binding was conducted at 4° C for 30 min with shaking
- Composition of elution buffer was changed to include 1% v:v Triton X-100 and 500 mM NaCl and to increase concentration of reduced glutathione (GSH) to 100 mM (2x) – these changes were either allowed or specifically recommended by the manufacturer to increase elution efficiency.
- Elution was conducted at room temperature for 30 min with shaking
- To determine efficiency of elution, the beads were incubated in 1 mL of 8 M urea at 70° C for 10 min.

iCon Concentrator devices (Pierce) were used to concentrate eluted protein by ultrafiltration method in accordance with manufacturer's recommendations. The table provided by the manufacturer was used to determine total amount of liquid in the upper and lower chambers of the device required to reach desired deadstop volumes. The deadstop volume is the sample volume remaining in the upper chamber after the levels of liquid in the upper and lower chambers equalized, and the filtration stopped. Exchange buffer used to dilute the protein samples and to fill the bottom chamber of the device consisted of 5% v:v glycerol, 50 mM NaCl, and10 mM Tris-HCl pH 7.4. The starting volume of protein sample in exchange buffer was 5 mL, and the deadstop volumes were 1 mL, 500 µL, 200 µL, and 100 µL. The iCon device was centrifuged in Beckman G56R centrifuge at 3750 rpm in 20-min increments until the desired deadstop volume was reached. Small samples were collected throughout the concentration process to assess the progress by SDS-PAGE, including 15 µL upper chamber sample before the first concentration cycle, 15 µL upper and lower chamber samples after the first concentration cycle, and the upper chamber samples after concentration cycles 2 (15 µL), 3 (5 µL), and 4 (5 µL). To check for protein precipitation during the concentration process, the final sample remaining in the upper chamber was centrifuged for 15 min in microcentrifuge at 14000 rpm. The supernatant was removed, and 5 µL of it was saved for analysis by SDS-PAGE. One mL of exchange buffer was used to gently rinse the walls of the upper chamber. The wash was added to the pellet from the previous step and centrifuged as above. The supernatant was discarded, and the pellet was solubilized in 100 µL of 8 M urea. Five µL of the solution was saved for analysis by SDS-PAGE.

DNA pull-down assays using MagneGST system (Promega). Cleared lysates containing GST-trANS2 fusion protein or GST-only control were prepared as described above and served as baits. To immobilize the bait on MagneGST beads, 1 volume of beads (50-100 µL depending on specific experiment) was washed 3 times in 8 volumes of binding and wash buffer (BWB – 4.2 mM Na_2HPO_4; 2 mM KH_2PO_4; 140 mM NaCl; 10 mM KCl), reconstituted with BWB to 2 volumes, and incubated with 4 volumes of protein-containing cleared lysate at 4° C for 30 min with shaking. The beads were washed 5 times with 8 volumes of BWB per wash, with wash #3 extended to 5 min at room temperature with shaking, and reconstituted to the original volume with BWB.

To prepare non-specific prey samples, total nucleic acid preparations from *E. coli* DH5-α cells were made using a protocol adapted from Zhang et al. (2005). Briefly, the cells were grown overnight in LB broth, spun down, and resuspended in 1/100 of original culture volume of 20 mM Tris-HCl pH 7.4. This suspension was put on ice and sonicated at power output 6, 45% duty cycle, 1 min ON / 1 min OFF. 100-µL samples were collected after 2 min, 4 min, 6 min, 8 min, and 10 min of total sonication time. The sonicated samples were pooled, heated at 95° C for 10 min, and chilled on ice. Heat-precipitated proteins and salts were removed by centrifugation, and the nucleic acids (DNA/RNA mixture) were purified using ethanol precipitation. The nucleic acid pellets were reconstituted in distilled water and adjusted to 1 µg/µL of DNA equivalent.

To prepare specific prey samples, 12 ug of pUCA plasmid DNA was digested with restriction enzymes as follows. *AleI* x *Blp*I x *Bst*BI digest was used to generate restriction fragments of 592 bp, 706 bp, and 5405 bp. *Bst*BI x *Hpa*I x *Nco*I digest was

used to generate restriction fragments of 908 bp, 1115 bp, and 4680 bp. The DNA digests were purified using ethanol precipitation, and the pellets were reconstituted with 50 μL of distilled water and diluted to 250 μL with BWB.

To conduct pull-down experiments with non-specific prey, 40 μL of beads with immobilized bait were mixed with 300 μL of prey and 300 μL of BWB and incubated at room temperature for 30 min with shaking. The beads were washed 5 times in 300 μL of BWB per sample with extended wash #3. The pellet was reconstituted with 40 μL of BWB, and 3 5-μL aliquots were taken for the further analysis. Additionally, 3 5-μL aliquots were taken from the non-specific prey sample. The aliquots were treated with 2 U of DNaseI (Fermentas), 2 μg of RNaseA (Qiagen), or no enzyme in 25-μL reactions at 37° C for 30 min. The treated magnetic beads samples were washed once with 300 μL of BWB, all liquid was removed, and the beads were used in elution step. The treated prey samples were stored on ice until analysis step.

To conduct pull-down experiments with specific prey, 20 μL of beads with immobilized bait were mixed with 245 μL of the prey. Remaining 5 μL of each prey sample was stored on ice until analysis step. The mixture of beads and prey was incubated at room temperature for 30 min with shaking. The beads were washed 5 times in 300 μL of BWB per sample with extended wash #3, and all liquid was removed from the beads, which were then used in elution step.

DNA bound to the beads was eluted by incubating with 20 μL of lysis buffer (10% v:v Proteinase K from Qiagen and 1% w:v SDS in BWB) at 56° C for 20 min with frequent vortexing. Liquid phase was separated from the beads and loaded on 1.2%

agarose gel. The prey samples were loaded on the same gel. Electrophoresis was conducted at 75 V for 1 hr in 1x TAE buffer, followed by ethidium bromide stain (0.5 μg/mL EtBr for 30 min with shaking and brief destaining in distilled water). The gel images were acquired using GelDoc camera (Bio-Rad).

DNA pull-down assays using ReactiBind system (Pierce). Cleared lysates containing GST-trANS2 fusion protein or GST-only control were prepared as described above and served as baits. Additionally, PBS was used as a no-bait control. All bait samples were treated with PMSF at final concentration 0.1 mM and diluted 100-fold with PBS. Prey samples were prepared by digesting 40 ug of pUCA with *Bst*API and *Sal*I, gel-extracting the 250-bp band, and diluting extracted DNA to 1 mL with PBS. One 8-well ReactiBind strip was used for each pull-down experiment. Three wells were filled with 100 μL per well of NS2 fusion protein, next 3 wells were filled with 100 μL per well of GST-only control, and the remaining 2 wells were filled with 100 μL per well of no-bait control. The strip was parafilmed and incubated at room temperature for 30 min. The wells were washed with 3 200-uL portions of wash buffer (0.05% Tween 20 in PBS). 100 μL of the prey sample were added to each well, and incubation and wash steps were repeated as above. 100 μL of elution buffer (10% v:v Proteinase K and 0.1% w:v SDS in PBS) were added to each well. The strip was parafilmed and incubated at 56° for 20 min. Three-fold serial dilutions in water were performed for all eluates, and 81-fold dilution was used in analysis step. Additionally, 3-fold serial dilutions in water were performed for the prey DNA sample, and 6561-fold dilution was used in analysis step. Selected

dilutions were analyzed by qPCR using TaqMan assay that targets a 181-bp amplicon included in the 250-bp prey DNA fragment.

Section 2-2. Studies of viruses with mutations/recombinations in NS2 gene

2-2-1. Characterization of NS2 ATG mutant

As mentioned in the Chapter 1, the NS2 ATG mutant virus has been classified as non-viable based on preliminary observations, so I decided to further characterize this mutant. Immuno-fluorescence assays (Figure 7) revealed that the virus is capable of capsid synthesis and assembly. At 72 hr post-transfection, cells positive for whole capsid antigen were detected. The low overall efficiency of transfecting C6/36 cells with brevidensoviral constructs (estimated 0.5%-2%) precludes accurate calculation of positivity rate, but the fraction of positive cells transfected with the mutant virus appeared to be similar to that for the wild-type *Ae*DNV. Based on relative brightness of fluorescence, the amount of capsid antigen in the cells transfected with the mutant construct appeared to be somewhat decreased compared to the wild-type control. While the expression of NS1 protein was not observed directly in the course of these IFA experiments, it was inferred because NS1 is required for efficient expression from the structural gene promoter P(VP) responsible for the synthesis of brevidensoviral capsid proteins (Ward et al., 2001). No NS2 expression was detected in the cells transfected with the mutant construct and stained with primary antibodies raised against N-terminal peptide of NS2. This finding was consistent with the hypothesis that the second AUG

codon of the left transcript (that was now mutated to ACG) served as initiation codon for NS2 translation (Kimmick et al., 1998).

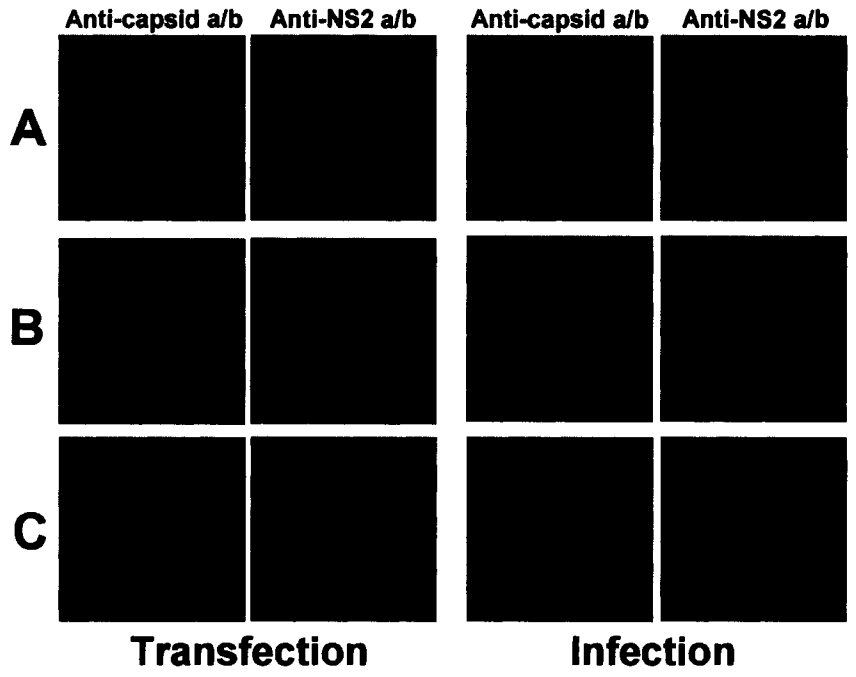

Figure 7. Characterization of wild-type *Ae*DNV and NS2-null mutant phenotypes using immuno-fluorescence assays.

A – wild type. B – mutant. C – negative control (transfected without any DNA).
Transfection – cell were transfected with plasmids of interest, and IFA was performed 72 hr post-transfection. Infection – cell culture medium in which the transfected cells were grown for 72 hr was removed, cleared by centrifugation, mixed 1:4 with fresh medium, and added to the fresh cells. IFA was performed 72 hr post-infection.

When the cells are transfected with infectious constructs, the virions accumulate in the medium, and their concentration is sufficient to establish secondary infection when this medium is added to the new mosquito cell culture. However, the mutant viruses failed this test for infectivity. When the culture medium was collected 72 hr post-

transfection and added to the new cell culture, no positive cells were detected in IFA assay using anti-capsid primary antibodies.

I then decided to compare efficiency of viral DNA synthesis and encapsidation using real time PCR. Upon numerous repeats (four of which are shown in Table 9), amount of viral DNA synthesized by the mutant virus was consistently lower that that in the wild-type control, with the decrease ranging from 50-fold to over 300-fold. In two of these experiments, the amount of viral DNA in the cell lysates was compared to these in viral pellets purified as described in Materials and Methods section and reconstituted to the original lysate volume. In addition, DNase I digestion was used in the course of one experiment to eliminate any free DNA co-precipitating with the virus particles and causing falsely elevated real time PCR results.

Where the DNA concentration was determined for lysate and virus preparation, efficiency of viral DNA encapsidation was calculated by the formula **E = (P/L)*100%**

Analyte	Sample	Experiment			
		1	2	3	4
Cleared cell lysate	Wild type	4.74 E+06	5.06 E+06	8.97 E+05	6.18 E+06
	Mutant	9.17 E+04	3.83 E+04	5.43 E+03	1.86 E+04
	Ratio	52	132	165	332
Virus prep. without DNaseI digestion	Wild type	2.35 E+06	2.97 E+06		
	Mutant	5.73 E+04	1.85 E+04		
	Ratio	41	161		
Virus prep. with DNaseI digestion	Wild type		1.67 E+06		
	Mutant		9.91 E+03		
	Ratio		169		

Table 9. Viral DNA synthesis by *Ae*DNV (wild-type control) and the NS2 ATG mutant.

All DNA concentrations are in copies per μL

where E = encapsidation efficiency, L = concentration of viral DNA in cell lysate, and P = concentration of viral DNA in the virus preparation reconstituted to the original lysate volume. Encapsidation efficiency data are summarized in Figure 8. While NS2 ATG mutant synthesizes less viral DNA and produces lesser number of viral particles, its encapsidation efficiency does not appear to be compromised: it is comparable to encapsidation efficiency of wild-type *Ae*DNV.

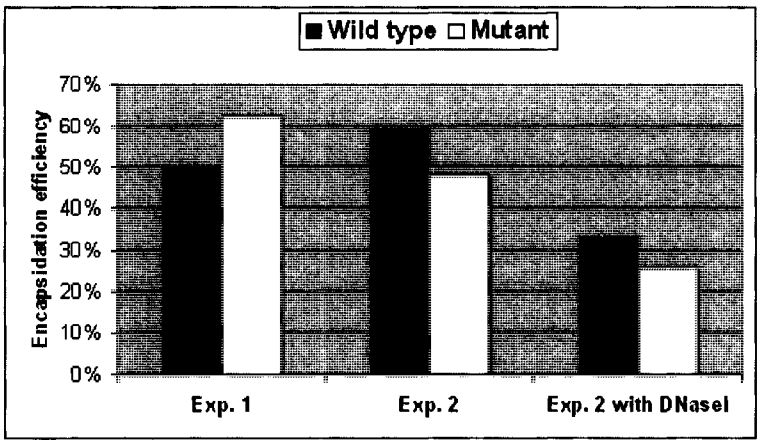

Figure 8. Encapsidation efficiency for wild-type *Ae*DNV and NS2 ATG mutant measured in two separate experiments (exp. 1 and exp. 2).

Encapsidation efficiency is a proportion of encapsidated DNA in the total amount of viral DNA synthesized in a given cell culture. Experiment 1 was conducted without DNase I treatment; encapsidated DNA was presumed to have separated from free DNA in the course of ultracentrifugation. Experiment 2 was conducted with and without DNase I treatment. DNase I treatment ensured that any DNA not protected by capsids is destroyed.

2-2-2. Construction and characterization of hybrids 6-13 and point mutants G172E and G172A

Originally, the hybrid project was not associated with NS2 study. It was started by Dr. Boris Afanasiev, who was interested in finding genetic determinants of the

differences in *Ae*DNV and *A*PeDNV phenotypes. The latter virus was isolated from a mosquito cell culture in Peru (hence the name *Aedes* Peruvian strain densovirus). It shared 80.8% nucleotide sequence identity with *Ae*DNV, and appeared to be more robust than *Ae*DNV when grown in cell cultures, as judged by the number of infected cells (Paterson et al., 2005). Unfortunately, *A*PeDNV did not produce any apparent disease in mosquitoes infected with this virus (Ledermann et al., 2004), so Dr. Afanasiev attempted to construct chimeric viruses that would combine pathogenicity of *Ae*DNV with robustness of *A*PeDNV. Five such chimeric viruses were initially constructed and named hybrids 1 through 5 (Figure 9).

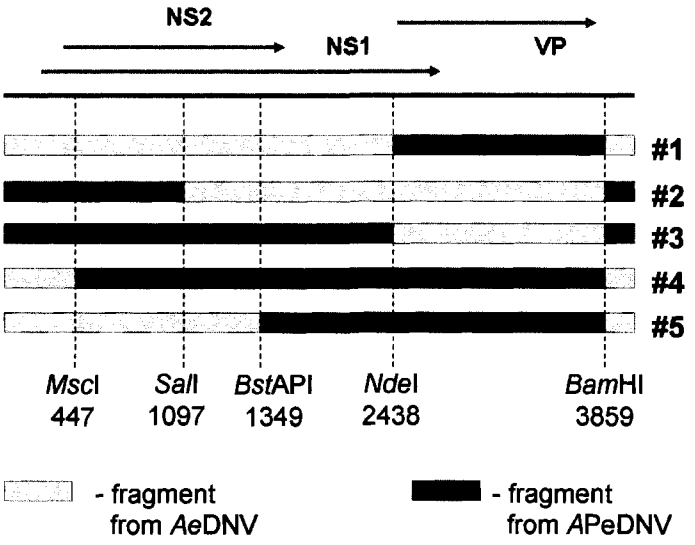

Figure 9. Genomic organization of hybrids 1 through 5.

The origins of fragments and the locations of junctions are shown.

Surprisingly, hybrid 4 was the only one viable, and it displayed a phenotype similar to that of *A*PeDNV. Of the remaining four chimeric viruses, hybrid 5 presented a special interest: it was similar to hybrid 4 in its genomic organization, successfully

synthesized viral proteins (based on IFA) and viral DNA (based on qPCR), yet it produced no infective progeny based on the quick test for infectivity (Table 10). It was then hypothesized that viability of these hybrids depends on the extent of *Ae*DNV sequence at the left end of genome.

Hybrid	Left junction position**	Viral DNA concentration***	Cells positive for capsid antigen	
			Transfected	Infected
4*	447 (<895)	2.85 E+07	Present	Present
5*	1349 (>895)	1.85 E+07	Present	Absent
6	747 (<895)	8.15 E+07	Present	Present
7	Originally planned, but never constructed – determined to be unnecessary			
8	935 (>895)	4.45 E+07	Present	Absent
9	805 (<895)	Not determined	Present	Present
10	887 (<895)	Not determined	Present	Present
11	907 (>895)	Not determined	Present	Absent
12	901 (>895)	1.53 E+07	Present	Absent
13	895	1.30 E+07	Present	Present

Table 10. Characterization of hybrids 4-13

(*) These hybrids were constructed by Dr. Afanasiev and co-workers

(**) Defined as the most upstream base at which the hybrid differs from *Ae*DNV. Numeration is based on ClustalW alignment between *Ae*DNV and *A*PeDNV genomes.

(***) Concentration of viral DNA in partially purified virus preparation (copies per μL); average of two or more experiments.

To check this hypothesis, I constructed seven additional hybrids, which were only different in the position of junction between the left fragment from *Ae*DNV and middle fragment from *A*PeDNV. Each hybrid was checked for production of viral capsids inside transfected and infected cells (quick test for infectivity); qPCR was performed on partially-purified virus preparations of selected hybrids to assess ability of the virus to produce complete virus particles with encapsidated genomic DNA inside (Table 10). The

decision to move this junction upstream or downstream was based on the results of quick infectivity test for the previous hybrid (Figure 10).

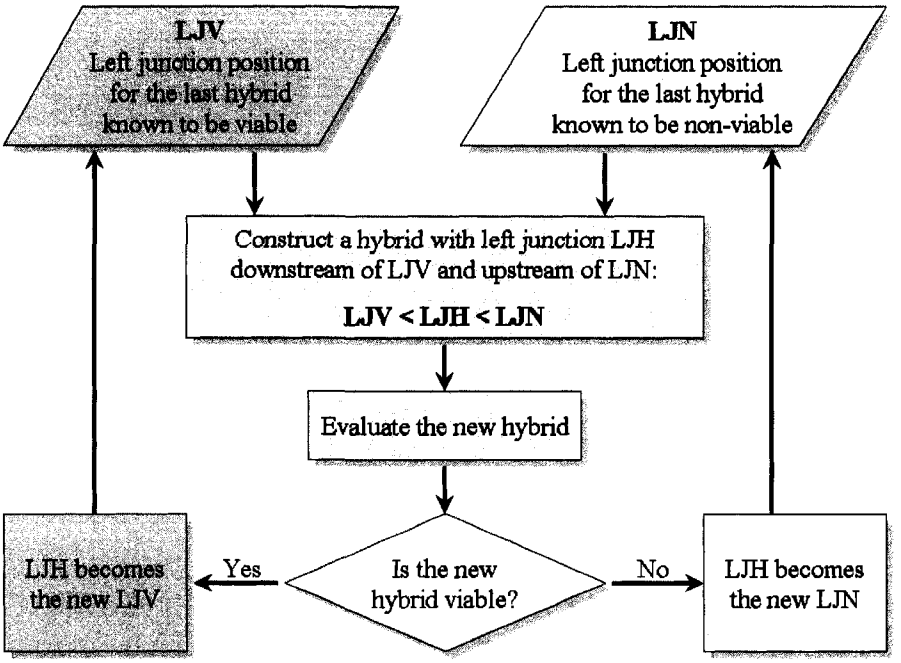

Figure 10. Flowchart for planning hybrids 6 – 13.

Hybrids 12 and 13 concluded the series, as all nucleotides between these hybrids' junction points are identical. As is apparent from Table 10, all hybrids with left junction placed downstream from the nucleotide 895 were non-infective, even though they produced DNA-containing virions upon transfection and the concentration of these virions was comparable to those produced by infective hybrids. Comparison of hybrid 12 and hybrid 13 sequences revealed that a single nucleotide base change from guanine to adenine changed NS2 protein amino-acid residue 172 from glycine to glutamate (G172E), while being silent in NS1 reading frame (Figure 11).

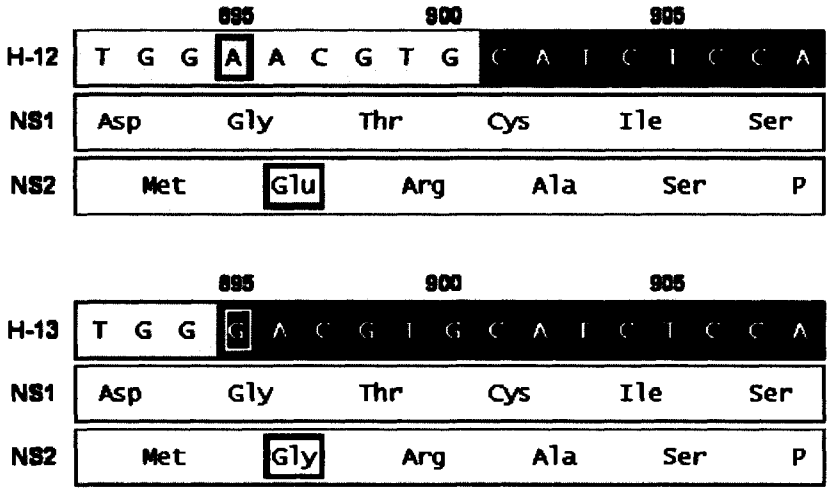

Figure 11. Left end junction of hybrids 12 (non-infective) and 13 (infective).

The changes in nucleotide and amino-acid sequences are enclosed in boxes.

To determine whether G172E mutation alone was sufficient to render virus non-infectious, a mutant of *A*PeDNV carrying single G172E mutation has been constructed. The phenotype of this mutant was similar to that of the non-infective hybrids: it produced normal amounts of DNA-containing virions upon transfection, but failed to establish secondary infection in quick infectivity test. Additionally, no viral DNA accumulation was observed in culture medium of C6/36 cells infected with mutant virus (Figure 12).

To determine the importance of glycine at the residue 172 of NS2, another mutant of *A*PeDNV was constructed that carried single G172A mutation. In a quick test for infectivity, the virions produced after transfection failed to infect fresh C6/36 cells, indicating that alanine could not substitute for glycine despite size and charge similarities.

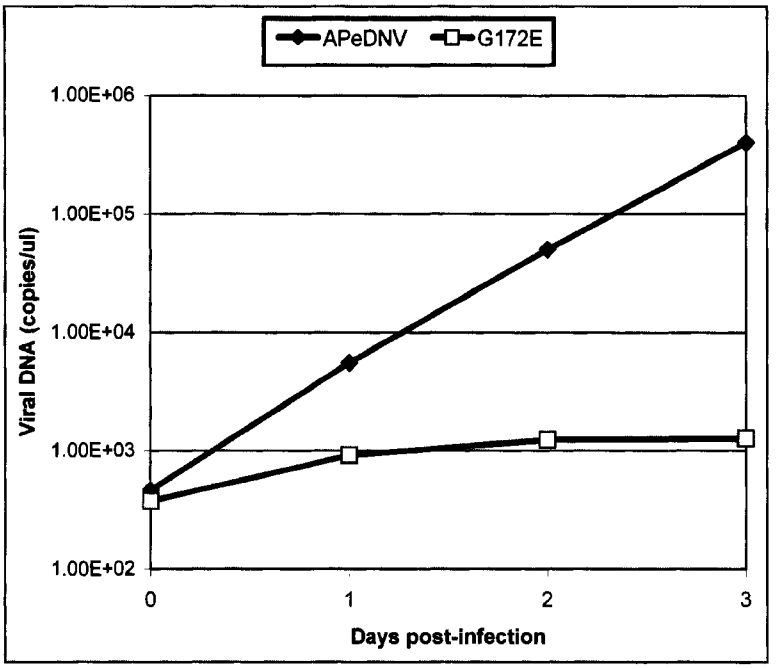

Figure 12. Viral propagation curves for wild-type *A*PeDNV and NS2 $G^{172}E$ mutant.

Assays were carried out in C6/36 cells. Viral replication was scored by assessing the accumulation of viral DNA.

2-2-3. Accumulation of viral DNA in rearing water samples following infection of *Aedes aegypti* mosquito larvae with wild type and mutant viruses

The majority of studies described in this work have been performed in mosquito cell cultures, which provide well-controlled environment for conducting our experiments and for a straightforward interpretation of data. At the same time, characterization of mosquito densoviruses carrying mutated or chimeric variants of NS2 gene would not be complete without looking at the phenotype displayed by these viruses following their entry into the mosquito host. Even those brevidensoviruses that do not cause any visible symptoms upon infecting mosquito larvae (e.g. *A*PeDNV) are amplified by their mosquito hosts, leading to increased viral titers in rearing waters and inside individual

mosquito hosts (Ledermann et al., 2004). On the other hand, the non-viable hybrids, such as H-12, and mutants (NS2-null, G172E) fail to establish productive infection of C6/36 cells, and if this is also true for other types of mosquito cells then propagation of these strains in the mosquito host is not possible.

To elucidate the phenotype of NS2 mutants and chimeric constructs *in vivo*, instar I larvae of *Aedes aegypti* mosquitoes (Strain Rexville D) were exposed to the same dose of partially purified viral preparations of *Ae*DNV (positive control), NS2-null mutant of *Ae*DNV, hybrid 12 (non-viable), hybrid 13 (viable), and G172E NS2 mutant of *A*PeDNV. Water containing no virus was used to infect the larvae in the negative control group. The larvae were infected in triplicate and placed on three trays such that each tray contained one of the triplicates from each group. Each tray therefore represented a single experimental series. Accumulation of virus in rearing water was assessed by qPCR using water samples collected on days 1, 4, 7, and 10 post-infection.

The results of these experiments are summarized in Figure 13. Significant (over 2 logs) increase in viral DNA concentration by day 10 post-infection was observed in *Ae*DNV samples in two out of three experimental series. One *Ae*DNV sample did not show any signs of viral DNA accumulation. The most likely explanation for this anomaly is overgrowth of microflora (bacteria, yeast, algae), which resulted in death of infected larvae occurring before these individuals could excrete significant amount of virus. Since this happened only in one of three control samples, this is likely a problem with an isolated sample and not with the experiment in general.

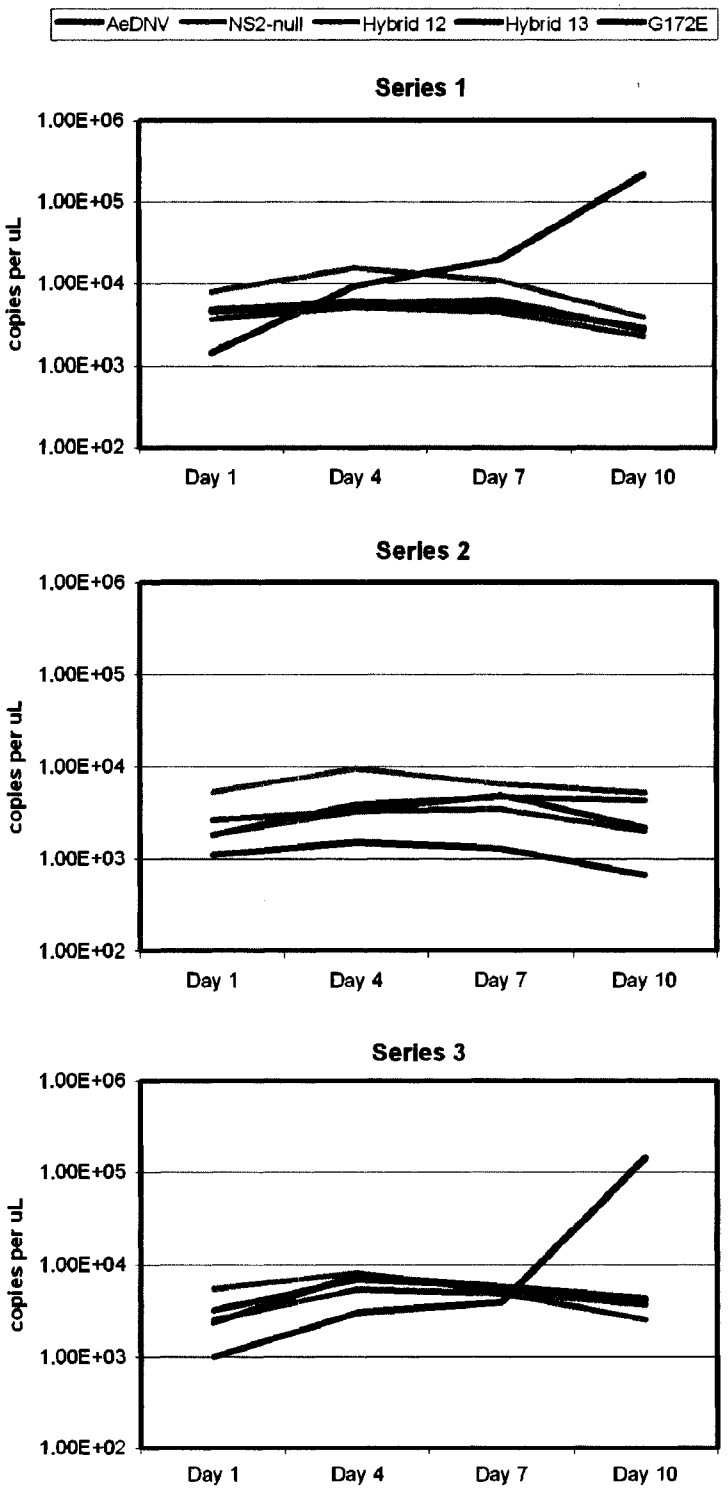

Figure 13. Accumulation of viral DNA in rearing waters following infections with different densoviral strains.

No viral DNA was detected in uninfected samples except for a single data point (Series 1; day 1; 32 copies per μL), which appears to be a result of contamination. Likewise, no signs of viral DNA accumulation were detected in any of the mutant / chimeric samples. This result was largely expected with a lone exception of hybrid 13, which was characterized by the viable phenotype in cell culture experiments. Perhaps, chimeric non-structural proteins (NS1 and/or NS2) carry some sort of defect that is not apparent during viral propagation in C6/36 cell culture, but becomes an obstacle to establishing the viral host infection *in-vivo*.

Section 2-3. Trans-activation and complementation studies: effect of NS2 on P(VP) promoter

2-3-1. The novelty of experimental design

As described in the Chapter 1 of this work, the non-structural protein NS1 trans-activated the structural gene promoter P(VP) of *Ae*DNV when it was co-expressed with NS2 in C6/36 mosquito cells (Ward et al., 2001). Expression of NS2 in these experiments resulted from both proteins translated from the same transcripts by a "leaky scanning" mechanism, and the contribution of this protein to the NS1-mediated activation of P(VP) promoter has not been studied. I decided to address this issue by designing a modified version of the trans-activation experiment.

In the original experiment by Ward et al. (2001), C6/36 cells are transfected with three different plasmids (Figure 14, original setup). NS1 is expressed from plasmid pUCA-INV. This plasmid contains inversion of the right viral terminus, which disables

VP gene and makes viral replication impossible. However, the left terminus is intact, so NS1 is co-expressed with NS2, just like in a wild-type *Ae*DNV. The plasmid p61-NcoRE is a reporter construct that contains structural gene promoter P(VP), driving expression of a VP-β-galactosidase (β-Gal) fusion which can be quantified by a chemiluminescent method. To minimize impact of sample-to-sample transfection efficiency and cell density variations, a third construct, pBS-Luc is used, which expresses firefly luciferase from *Drosophila melanogaster* Hsp70 promoter (constitutive in mosquito cells). Expression of luciferase is also quantified using a chemiluminescent method.

The original experimental procedure described above cannot provide information about the role of NS2 in P(VP) trans-activation because NS1/NS2 expression in

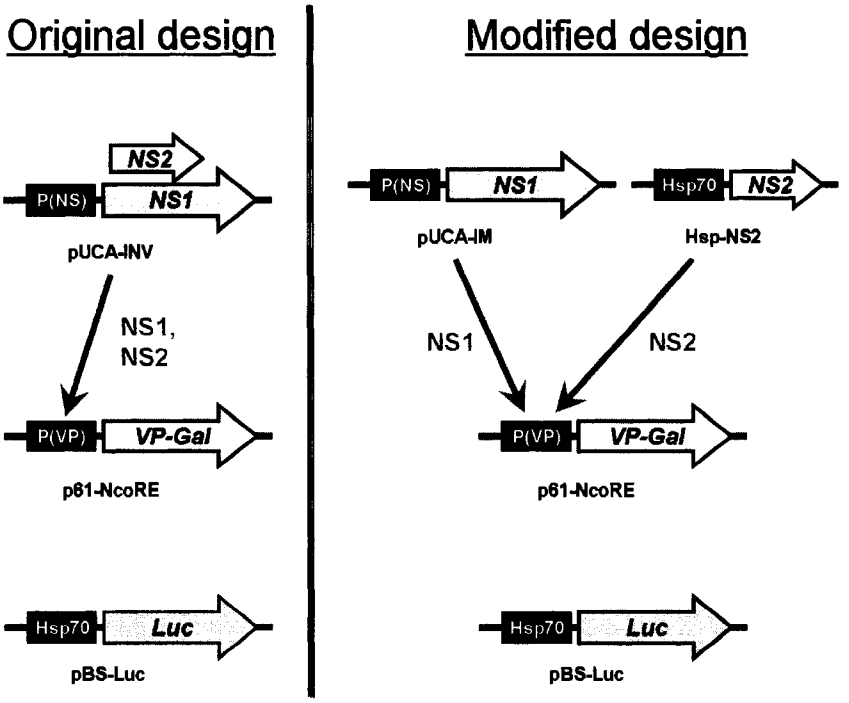

Figure 14. Original and modified experimental procedure to determine the role of non-structural proteins on P(VP) promoter activity.

See explanations in the text.

pUCA-INV is inseparable. I overcame this problem by cloning NS2 ATG→ACG mutation from NS2-null construct described above into pUCA-INV. The new construct called pUCA-IM expressed exclusively NS1. To verify that any differences observed in the course of experiments were caused by NS2 knockout, I designed complementation constructs that expressed different versions of NS2 proteins under control of Hsp70 promoter (Figure 14, modified setup).

2-3-2. Results

When pUCA-INV is replaced with pUCA-IM as a source of non-structural proteins, a drop in VP-β-Gal expression occurs, but it is still expressed at a level higher than that observed in the absence of non-structural proteins (Figure 15A). This observation confirms that, while NS2 is neither necessary nor sufficient for P(VP) trans-activation, it modulates trans-activation effect of NS1 and is required for the maximum activity of this promoter.

To verify that the decrease in trans-activation effect was a result of NS2 knockout, I conducted complementation studies, in which NS2 was supplied *in trans* by co-transfection with Hsp-ANS2 or Hsp-PNS2. These plasmids expressed NS2 protein from *Ae*DNV or *A*PeDNV, respectively, and they were co-transfected with pUCA-IM, p61-NcoRE, and pBS-Luc. The control samples that did not require NS2 complementation (NS1/NS2 expressed from pUCA-INV, NS1 ONLY, and NO NS) received pUC19 plasmid to maintain constant amount of transfected DNA. Upon repeated experiments, complementation with either species of NS2 resulted in increased trans-activation effect

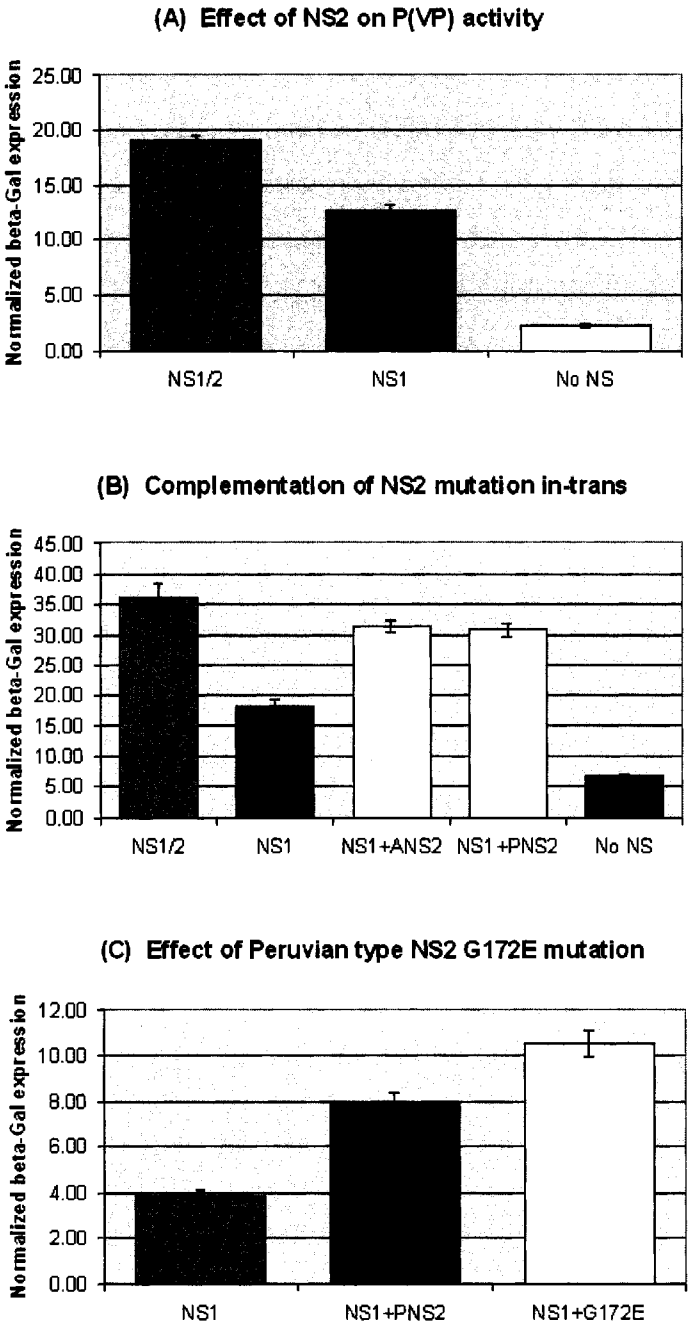

Figure 15. Results of trans-activation and complementation experiments.

Normalized β-Gal expression is calculated as a unit-less ratio of β-Gal to Luciferase luminescence. Each column represents average of two experiments. Error bars mark 95% confidence intervals.
NS1/2 – both NS1 and NS2 are provided by pUCA-INV; NS1 – NS1 only is provided by pUCA-IM, no NS2 is present; No NS – neither NS1 nor NS2 is present, pUC19 plasmid is used to keep amount of transfected DNA constant; NS1+ANS2, NS1+PNS2, NS1+G172E – NS1 is provided by pUCA-IM, while NS2 is provided by Hsp-ANS2, Hsp-PNS2, or Hsp-G172E, respectively.

as judged by VP-β-Gal expression. A significant degree of variability was observed in the extent to which addition of NS2 increased activity of P(VP). In some cases, the levels of activity were indistinguishable from those in positive control, where NS1 and NS2 were expressed from P(NS) promoter of pUCA-INV. In other cases, a smaller degree of trans-activation was observed, possibly because Hsp70 promoter may not provide sufficient levels of NS2 expression in C6/36 mosquito cells (Figure 15B). It is certain, however, that addition of homologous or heterologous NS2 enhances NS1 effect on P(VP) promoter activity.

The ability of the heterologous (Peruvian type) NS2 to trans-activate *Ae*DNV structural gene promoter was used to determine if the single G172E mutation in Peruvian type NS2 described earlier in this work had any effect on VP-β-Gal expression. To do so, additional complementation plasmid Hsp-G172E was constructed by introducing a point mutation into Hsp-PNS2 sequence. All samples were transfected with pUCA-IM, p61-NcoRE, and pBS-Luc, while Hsp-PNS2, Hsp-G172E, or pUC19 plasmid was used as a complementation construct. This experiment was repeated twice, with an interesting finding: Peruvian species of NS2 with G172E mutation has larger effect on P(VP) trans-activation than its wild-type counterpart (Figure 15C). This finding corroborates previous observations of VP expression in the cells transfected with non-viable hybrids and G172E mutant of *A*PeDNV: based on IFA, no defect in capsid synthesis could be detected in such cells.

Section 2-4. Studies of NS2 localization and co-localization

2-4-1. Localization of full length ANS2 vs. trANS2 in the absence of other viral proteins

As discussed in Chapter 1, NS2 protein of *Ae*DNV appears to have a complex subcellular localization pattern, starting out as a nuclear protein localized in punctate bodies and becoming diffusely distributed around the nucleus during the later stages of infection. This localization pattern could result from interactions with other viral proteins (NS1, VP1, and VP2), which are also translocated to nucleus. Alternatively, NS2 could possess nuclear localization signals (NLS) of its own, which facilitate protein's translocation through the interaction with importins (reviewed in Lange et al., 2007). PSORT II program (a freeware available at www.psort.org) was used to analyze NS2 sequences from *Ae*DNV and six other members of *Densovirinae* family in search for putative NLS. While each protein sequence returned several hits of different types (4-residue, 7-residue, and bi-partite), only the bi-partite signals were detected consistently and in a similar location in all analyzed sequences (Table 11). The bi-partite NLS, first discovered in *Xenopus* nucleoplasmin, consist of two basic residues, followed by a 10-residue spacer group, and conclude with a group of 5 residues of which at least 3 must be basic (Dingwall and Laskey, 1991).

To study nuclear translocation of NS2, I constructed two plasmids: Hsp-ANS2 (also mentioned in the previous section) and Hsp-trANS2. These plasmids express full-length or truncated *Ae*DNV NS2 protein, respectively, under control of *Drosophila melanogaster* Hsp70 promoter. Putting NS2 expression under control of Hsp70 promoter, which is constitutive in mosquito cell lines, makes the presence of NS1

Virus	Genus	Location	Sequence
*Ae*DNV	Brevidensovirus	267 – 283	**KR**TGDTSPQPGPS**KRR**V
*A*ThDNV	Brevidensovirus	268 – 284	**KR**TGDTSPQQGPS**KRR**V
*Aal*DNV	Brevidensovirus	268 – 284	**KR**TGDISPQQGPS**KRR**A
*A*PeDNV	Brevidensovirus	268 – 284	**KR**TGDISPQPGPS**KRR**A
*Gm*DNV	Densovirus	256 – 272	**RK**PIRQGNSHTYG**KK**Q**R**
*Bm*DNV	Iteravirus	263 – 295	**RR**NRPSSSRHINTT**RKRK**SITTSKGVLT**KKK**SL (overlap of at least 2 putative bipartite NLS)
*Ce*DNV	Iteravirus	278 – 296	**RKRK**STMMSTGKFM**KKK**LL

Table 11. The bi-partite nuclear localization signals identified within the sequences of NS2 proteins from selected members of family *Densovirinae*.

Location is defined by the first and the last amino-acid position of each signal. The basic residues within each NLS are shown in boldface.

unnecessary and allows studying NS2 expression in the absence of other viral proteins. The truncated variant of NS2 is 257 a.a.-long, thus missing the last 105 residues including the putative bi-partite NLS. It is identical to the truncated NS2 domain of GST-trANS2 fusion protein discussed in the following section. According to protein prediction programs PSIPRED and FoldIndex© (McGuffin et al., 2000; Prilusky et al., 2005), the carboxy-terminal region of NS2 lost as a result of truncation is predicted to be mostly unstructured and composed of random coils, while the region retained is predicted to fold into a globular domain (Figure 16).

C6/36 cells were transfected with Hsp-ANS2 or Hsp-trANS2 plasmid. 48 hr post-transfection the cells were fixed, stained with primary α-NS2 and secondary α-rabbit

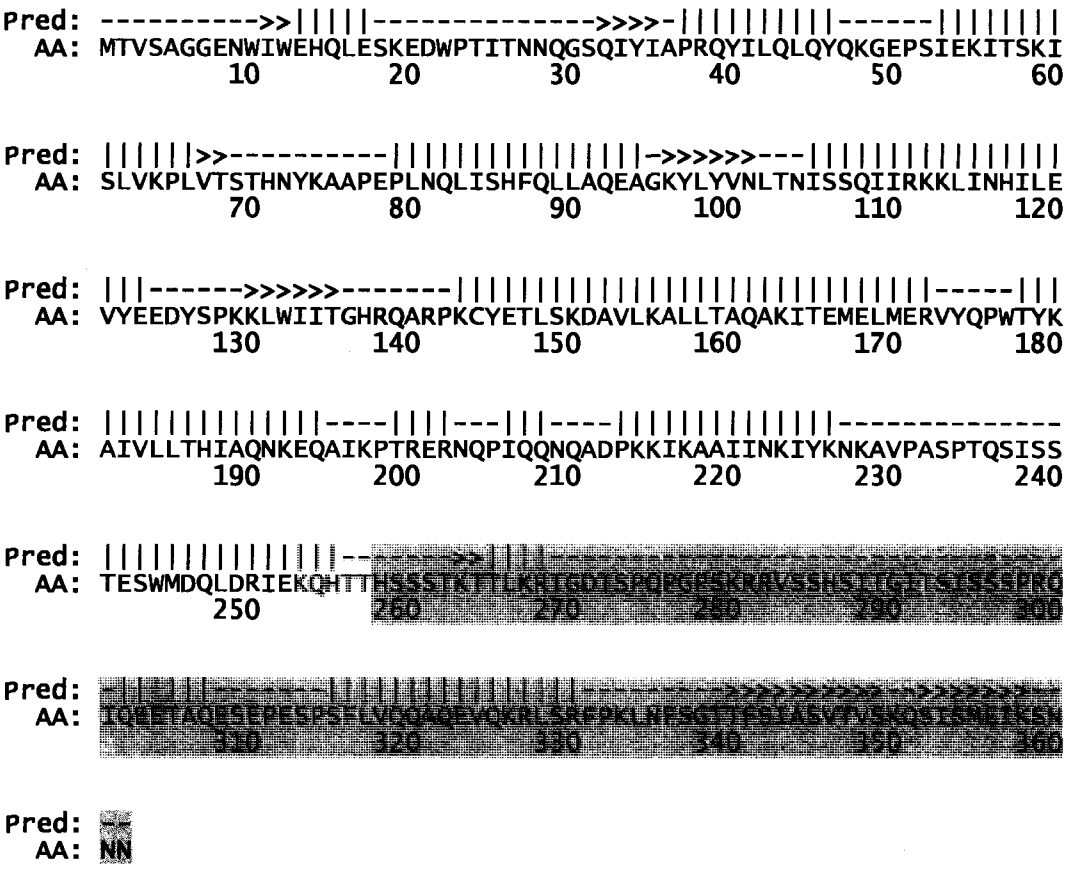

Figure 16. The use of PSIPRED and FoldIndex© protein prediction programs in planning of NS2 truncation.

Pred – predicted secondary structure (| | | | - α-helix; >>>> - β-strand; ---- – random coil);
AA – amino-acid sequence (green – predicted folded domain, red – predicted disordered regions, purple – putative bi-partite NLS). The carboxy-terminal region absent in truncated NS2 is highlighted in grey.

FITC-conjugated antibodies, followed by DAPI counterstain. The cells were then observed using a widefield fluorescent microscope, and the images were collected, processed, and analyzed. Removal of NS2 carboxy-terminus resulted in a change of the protein's subcellular localization (Figure 17), which could be explained in two ways. First, the truncated version of NS2 could become small enough to freely diffuse through the nuclear pores and leak in and out of the nuclei. Second, the loss of putative NLS

could make the protein's transport through the nuclear pores impossible, resulting in its exclusion from the nucleus. Some of the cells transfected with a truncated NS2 construct were characterized by diffuse fluorescence consistent with the former scenario (Figure 17, A). Such cells could not provide any information about the role of putative bi-partite NLS in subcellular localization of NS2. However, other cells (Figure 17, B-C) displayed clearly cytoplasmic localization of NS2, meaning that the loss of NLS resulted in the protein's inability to enter the nuclei of these cells. Strictly nuclear localization of NS2 was found in all cells transfected with a full-length NS2 construct (Figure 17, D-F), indicating that nuclear translocation of this protein does not rely on interaction with other viral proteins. Targeted nuclear localization of *Ae*DNV NS2 sets this protein apart from NS2 proteins of mammalian parvoviruses, which passively diffuse into the nucleus due to their small size.

2-4-2. Co-localization vs. interaction between NS1 and NS2 proteins: a FRET microscopy study

Work conducted in our lab by Erin Robinson (Azarkh, Robinson, et al., 2008) demonstrated that, at least during the early stages of viral infection, the two non-structural proteins co-localize in compact nuclear bodies similar to those observed in other parvoviral infections. At that time, it was not known whether this co-localization resulted from direct NS1-NS2 interaction or from both proteins interacting with a third component, such as a cellular protein. Fluorescent Resonance Energy Transfer (FRET) is a phenomenon in which the energy from excited donor fluorochrome is transferred by a non-radiative mechanism to an acceptor fluorochrome, and excites it. This transfer can

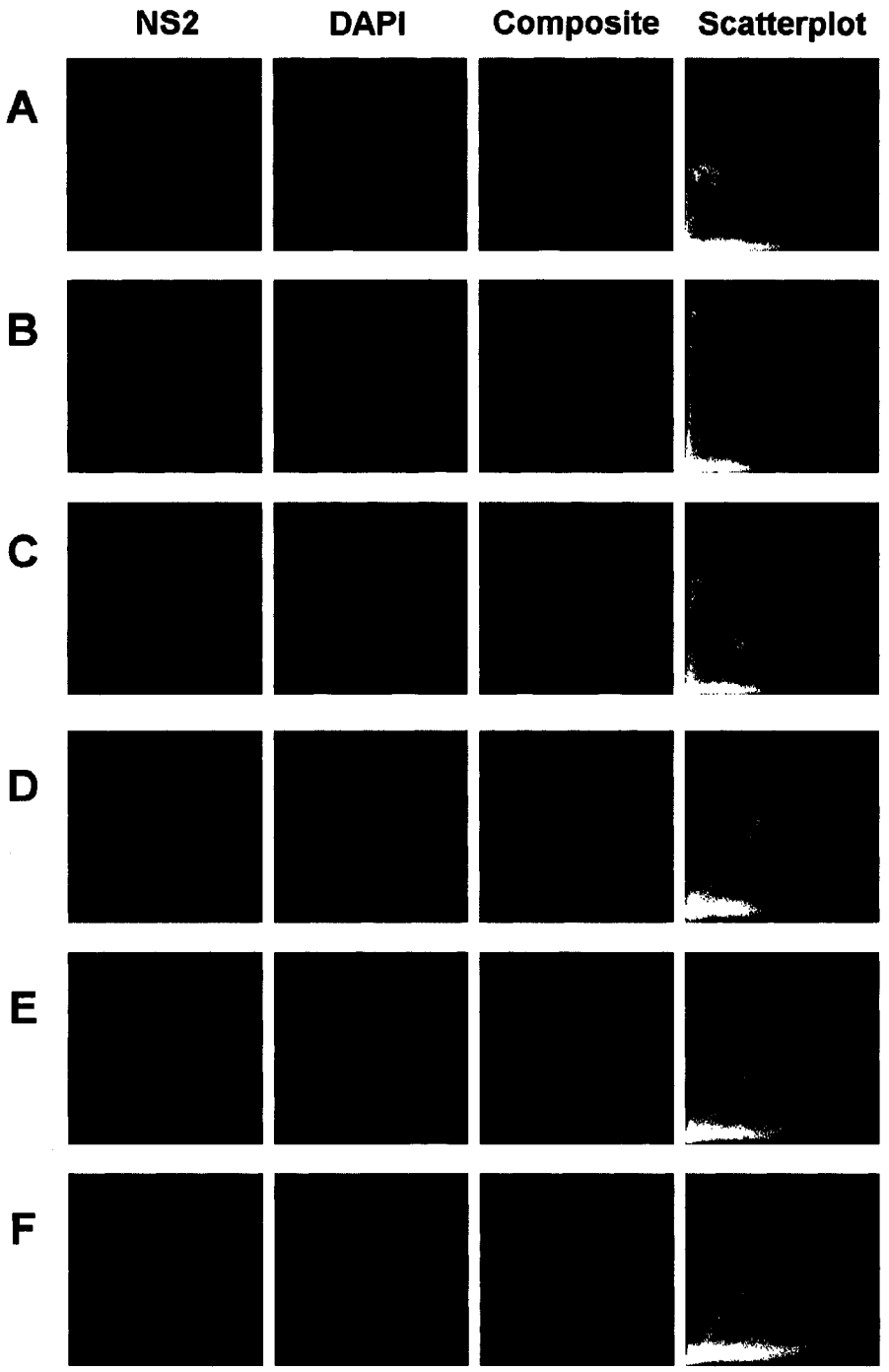

Figure 17. Subcellular localization of NS2.

A-C – truncated NS2; D-F – full-length NS2. Scatterplot – for each pixel of a field image, an 8-bit intensity value in DAPI channel (abscissa) is plotted against the value of the same pixel in FITC channel (ordinate).

only happen when the distance between the fluorochromes is less than about 10 nm, which in practice can only be achieved when the fluorochromes (or other molecules labeled with fluorochromes) interact with each other. Coupled with confocal microscopy, FRET provides a powerful method to detect interactions *in situ*. In case of my research, the goal was to determine whether FRET occurs between fluorescently-labeled NS1 and NS2 proteins as they co-localize in the nuclear bodies of co-transfected Aag2 cells.

Three fluorescent protein fusion constructs were designed: NS1-CFP, NS2-YFP, and YFP-NS2. The last two fusions consisted of the same NS2 and eYFP domains, but the eYFP domain was fused to the carboxy-terminus of NS2 in the former construct and to the amino-terminus in the latter construct. The constructs were tested by transfecting *Aedes aegypti* Aag2 cells (chosen over C6/36 cells for better cell morphology and firmer attachment to the surface). Transfected cells were incubated in T-25 flasks for 20-24 hr and then observed *in situ* under 10x power using Zeiss LSM-510 confocal microscope. Expression of NS2 fluorescent fusion proteins was readily detectable in numerous cells, while NS1-CFP expression could only be detected in a small subset of cells, and the intensity of eCFP fluorescence appeared to be much less than that of eYFP (Figure 18). The NS1 domain of the fluorescent fusion protein was verified to be functional, because even in the absence of extraneous NS1 from a helper virus some fluorescent cells could be detected. Additionally, when the lysate of cells transfected with NS1-CFP construct was analyzed using qPCR, the viral DNA was detected at a high concentration (4.62 E+06 copies per μL) indicating that NS1-mediated viral DNA replication had occurred

in these cells. Therefore, the problem with NS1-CFP fusion must be rooted in the eCFP domain (perhaps, it has problems folding correctly under the conditions of my experiments). It was then decided to replace NS1-CFP fusion with NS1-GFP (Afanasiev et al., 1999) that has been used successfully in our lab for years. While it is not generally advised to use GFP and YFP as a donor-acceptor pair for FRET experiments because of too much spectral overlap, the possibility of GFP/YFP signal separation has been demonstrated before. Baumann et al. (1998) showed that a good signal separation can be achieved by utilizing the blue tail of the GFP emission spectrum and the red tail of the YFP emission spectrum.

Figure 18. Testing NS1 and NS2 fluorescent protein fusions.

A – NS2-YFP fusion. Most fields contain positive cells and look similar to the one shown.
B – YFP-NS2 fusion. Most fields contain positive cells and look similar to the one shown.
C – NS1-CFP fusion. Only few weakly-positive cells found in the entire cell culture flask.

The two FRET methods were considered: acceptor photobleaching and sensitized emission of acceptor. Acceptor photobleaching method is based on increased fluorescence of the donor after the acceptor is destroyed by photobleaching and the FRET no longer occurs. The FRET efficiency determined in this method is a direct

measurement of transferred fluorescent energy, which can be compared with other FRET efficiency values within and between FRET experiments. It is calculated by the formula $\mathbf{E = (1 - I_{before} / I_{after})*100\%}$ where E = FRET efficiency; I_{before} and I_{after} = fluorescence intensity of the donor before and after acceptor photobleaching, respectively. The main requirement for this method to work is selectivity of photobleaching, so that a near-100% reduction in acceptor fluorescence can be achieved with no significant photobleaching of donor. Unfortunately, this requirement could not be satisfied for a GFP/YFP FRET pair. As evident from Figure 19, exposing cells to high intensity laser beam at 514 nm results in simultaneous photobleaching of donor and acceptor.

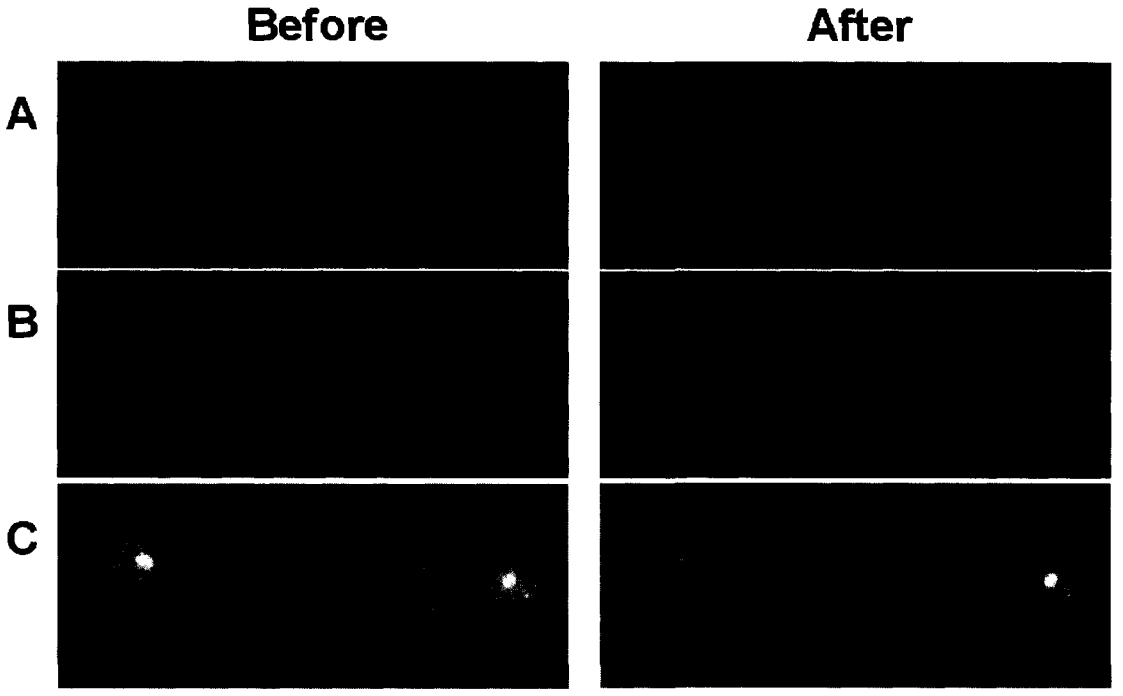

Figure 19. FRET analysis of NS1-NS2 interactions by acceptor photobleaching method.

A – GFP channel; B – YFP channel; C – composite of GFP, YFP, and brightfield channel images. Before – images taken before photobleaching; after – images taken after 10 cycles of photobleaching.

Sensitized emission FRET method, the other option considered for use in my experiments, is also known as a three-sample / three-channel method. The samples are expressing donor only, acceptor only, or both. The channels are set for donor fluorescence, acceptor fluorescence, or FRET (donor excitation with acceptor emission settings). Occurrence of FRET is evaluated by calculating the FRET index in the process that can be described with the following formulas:

(1) Donor-only sample. $\alpha_d = I_{fret} / I_d$

Donor bleed-through coefficient is calculated as a ratio of fluorescent intensity in FRET channel to that in donor channel.

(2) Acceptor-only sample. $\alpha_a = I_{fret} / I_a$

Acceptor bleed-through co-efficient is calculated as a ratio of fluorescent intensity in FRET channel to that in donor channel.

(3) Sample co-expressing donor and acceptor. $FRET = I_{fret} - I_d*\alpha_d - I_a*\alpha_a$

FRET index is calculated as fluorescent intensity in FRET channel adjusted for donor and acceptor bleed-through by subtracting the products of intensities in donor and acceptor channels and the corresponding bleed-through coefficients.

ImageJ, a freeware distributed by NIH and downloadable from http://rsb.info.nih.gov/ij/download.html was used to process and analyze image data collected in the course of FRET experiments. This freeware is modular, with components or plug-ins that can be added or removed depending on the researcher's needs. The two plug-ins used to calculate FRET indices in my experiments were **FRET and Colocalization Analyzer** (Hachet-Haas et al., 2006) and **PixFRET** (Feige et al.,

2005). The main difference between the two programs is in the way in which the bleed-through coefficients are calculated and applied. The former plug-in calculates bleed-through coefficients strictly in accordance with the formulas 1 and 2, and applies them as constants in the formula 3. The authors of the latter plug-in argue that, while this approach is generally valid, sometimes the bleed-through coefficients behave as functions rather than constants – they appear to change depending on each pixel's fluorescence intensity in donor or acceptor channel. Therefore, PixFRET gives an option of representing bleed-through coefficients as functions, which can be applied pixel-by-pixel. At the same time, the FRET and Co-localization Analyzer has an advantage of refining FRET results based on the assumption that the proteins interacting with each other must necessarily co-localize. Any pixels with positive FRET index but without the evidence for fluorochrome co-localization are masked and eliminated from the final FRET image.

The two plugins also differ in the way the final FRET image is generated. In the images generated by the FRET and Co-localization Analyzer, each pixel's value is numerically equal to that of the calculated FRET index. The lookup table (LUT) used by this program highlights in red, yellow, and white the pixel values that are indicative of FRET, while the lower, unreliable values of FRET index appear in various shades of blue. Therefore, the output is in qualitative rather than quantitative form. Unlike FRET efficiency calculated in acceptor photobleaching experiments, FRET index is not used to compare the results from different experiments; it simply answers the question of FRET-or-NO FRET.

In the images generated by PixFRET, all FRET index values are scaled so that the lowest intensity pixels are assigned the value of 0, the highest intensity pixels are assigned the value of 255, and the intermediate intensity pixels are assigned values relative to these extremes. For example if the lowest calculated FRET index had a value of 8, the highest had a value of 40, and the intermediate had a value of 16, then the corresponding pixels in the output will have the values of 0, 255, and 63, respectively.

In my experiments, Aag2 cells were transfected with fluorescent constructs to provide 5 samples: NS1-GFP-only, NS2-YFP-only, YFP-NS2-only, NS1-GFP/NS2-YFP-cotransfected, and NS1-GFP/YFP-NS2-cotransfected. The cells were fixed 20-24 hr post-transfection, and 8-bit TIFF images were collected using Zeiss LSM-510 confocal microscope in accordance with the plug-in authors' recommendations (see Materials and Methods section for details). Analysis of images was also conducted as recommended by the authors of the corresponding plug-in, but with several modifications. Firstly, images from each sample were cropped from original 512 x 512 pix size to 85 x 85 pix size and combined into montages. This modification resulted in improved signal-to-noise ratio and allowed analyzing multiple cell images at once. Secondly, I modified LUTs applied to the final output images (note that changing a LUT does not alter the numeric values of pixels, it only affects the colors assigned to them). For the FRET and Co-localization Analyzer output, all pixels with the FRET index values below 16 were assigned the same shade of grey color. These values are considered negative for FRET, appearing in various shades of blue in the original program. For the PixFRET output that is in grayscale in the original program, the "smart" LUT was applied, which highlighted in

red, yellow, and white the pixels with the values of about 160 and higher. The pixels with the values below 160 appeared in various shades of grey and brown. Finally, to validate the bleed-through coefficients, the bleed-through samples were analyzed as though they were FRET samples.

The bleed-through evaluation results are summarized in Table 12. Note that in the case of PixFRET, three bleed-through models (constant, linear, and exponential) are constructed by the program for each set of singly-transfected cells (Figure 20). PixFRET does not perform a statistical analysis to determine which of the three models represents the best fit. Instead, the decision is left up to the researcher's discretion. The bleed-through models that I chose in the course of PixFRET calculations are shown in Table 12.

Based on the bleed-through data, the FRET indices were calculated and represented graphically (Figure 21). As it is apparent from the Figure 21, there is evidence for FRET occurring between fluorescently labeled NS1 and NS2 proteins, and when the samples transfected with a single fluorescent protein construct were analyzed as

	NS1-GFP bleed-through coefficient	NS2-YFP bleed-through coefficient	YFP-NS2 bleed-through coefficient
FCA	$\alpha = 0.208$ (constant)	$\alpha = 0.069$ (constant)	$\alpha = 0.113$ (constant)
PixFRET	$\alpha = 0.231$ (constant)	$\alpha = 0.070 + 0.00006*I_a$ (linear function)	$\alpha = 0.115 +$ $+ 0.030*\exp[-0.00367*I_a]$ (exponential function)

Table 12. Evaluation of bleed-through coefficients.

FCA – FRET and Co-localization Analyzer.

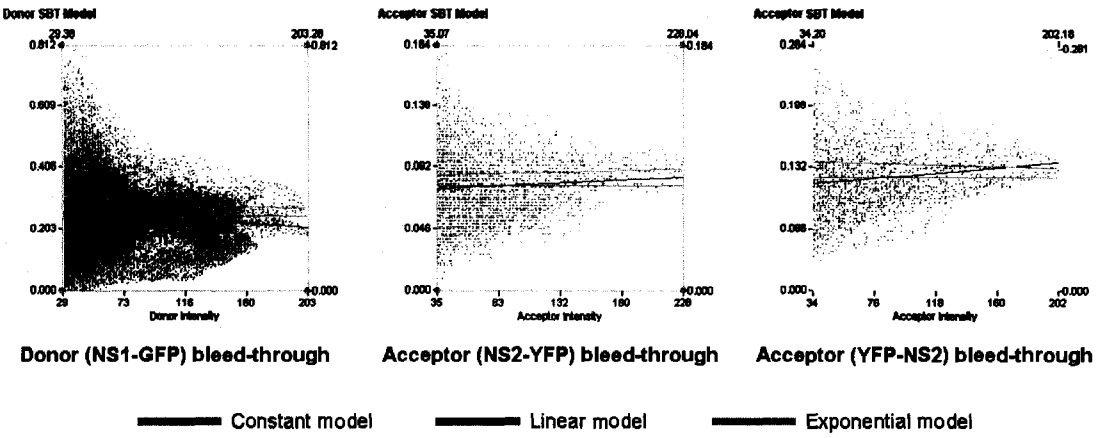

Figure 20. Bleed-through evaluation in PixFRET.

Constant model assumes that the bleed-through is independent from the fluorochrome concentration. Linear and exponential models consider possibility that the bleed-through depends on the fluorochrome concentration and that this dependency can be described through the linear or exponential relationship, respectively.

though they were co-transfected samples, no FRET was detected except in one cell analyzed by PixFRET. This artifact could be explained by scaling of the final image by PixFRET, which sometimes results in amplification of intensity of pixels that have low values on absolute scale, but high values relative to the rest of the image.

Section 2-5. In-vitro studies of recombinant NS2 expressed in E. coli

2-5-1. General considerations

I started this project with intent to over-express full or partial-length brevidensoviral NS2 proteins, which could then be studied by X-ray crystallography and pull-down assays. *E. coli* expression system was chosen because of its simplicity, versatility, and cost efficiency. Although the use of such system is associated with risks

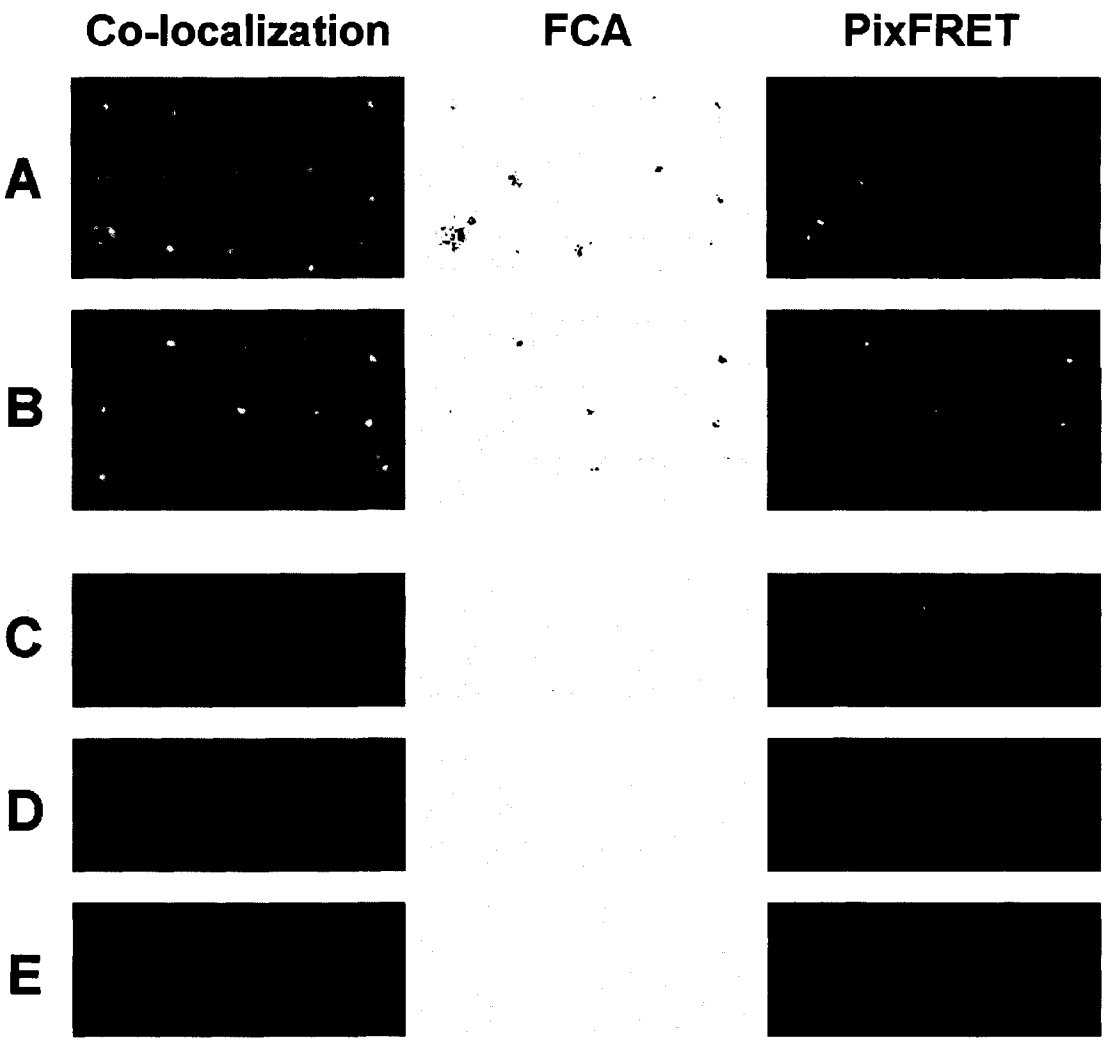

Figure 21. FRET results and controls.

Co-localization – the composite images combining the graphical output of the donor (GFP, false-colored green) and acceptor (YFP, false-colored red) channels. FCA – the graphical output of the "FRET and Co-localization Analyzer" plugin (false-colored using "coloc fret index" LUT). PixFRET – the graphical output of the PixFRET plugin (false-colored using "smart"

Panels A-B – NS1-GFP / NS2-YFP and NS1-GFP / YFP-NS2 FRET samples, respectively. Panels C-E – controls: cells transfected with individual constructs, NS1-GFP, NS2-YFP, and YFP-NS2, respectively, but analyzed as though they were co-transfected FRET samples.

of protein misfolding, aggregation, and degradation, as well as potential codon usage issues and the lack of post-translational modifications, these risks can be mitigated (for example, see Baneyx, 1999). Often the drawbacks of prokaryotic expression systems are outweighed by the benefits. In case of brevidensoviral non-structural proteins, one of such benefits is reduction of potential toxic effects. Paterson et al. (2005) have shown that expression of ANS1-GFP fusion in mosquito cells, which also resulted in ANS2 expression, caused the cell cycle arrest at G2 phase. At this time, we don't know which of the non-structural proteins altered the cell cycle or how specific this effect is, but it is highly unlikely for a similar effect to occur in a completely unrelated prokaryotic organism.

Codon usage has been shown to play a major role in successful expression of structural protein VP1 – the only mosquito densovirus protein successfully expressed in our lab prior to this work (Dr. Rachel Specht – unpublished data). To determine whether the same is true about NS2 proteins, I analyzed NS2 gene sequences from *Ae*DNV and *A*PeDNV using *E. coli* Codon Usage Analyzer 2.1, a free web-based application created by Morris Maduro and accessed at http://www.faculty.ucr.edu/~mmaduro/codonusage/usage.htm. This program analyses each codon of a given sequence and highlights those that are underrepresented in *E. coli* class II genes (the genes highly and continuously expressed during exponential growth - Hénaut and Danchin, 1996). Of all codons that occur in NS2, those listed in Table 13 were determined to be grossly underrepresented in *E. coli* (threshold = less than 1% occurrence among all synonymous codons for a given amino-acid). To overcome potential problems with translating this

protein, the decision was made to use Rosetta-2 cells (Novagen) derived from BL21(DE3) by introducing a proprietary plasmid pRARE-2. This plasmid provides *in-trans* 7 tRNA species, including those required for successful translation of rare codons listed in Table 13.

Codon	Amino-acid	Frequency in ANS2	Frequency in PNS2	Complemented by pRARE-2?
AGA	R	3	4	yes
AGG	R	2	6	yes
ATA	I	13	15	yes
CGG	R	1	2	yes
CTA	L	3	4	yes
Total		22	31	
Percent		6.08%	8.54%	

Table 13. Analysis of codon usage in mosquito densovirus NS2 genes.

2-5-2. Construction and evaluation of various pET21 and pET42 constructs

I began prokaryotic expression experiments by constructing plasmids pET21-PNS2 and pET42-PNS2. The former was designed to express full-length *A*PeDNV NS2 protein with a His_6 tag fused to the carboxy-terminus and with a native amino-terminus. The latter was designed to express the same protein, but with several domains (most notably, GST) fused to its amino-terminus. The Rosetta-2 cells were transformed with these plasmids, grown in LB medium with antibiotics, and induced with IPTG as described in the Materials and Methods section of this work. Expression of PNS2 and GST-PNS2 was clearly demonstrated by Western analyses (Figure 22), which showed the

bands of roughly expected size (theoretical MW = 42.3 kDa for recombinant PNS2 and 73.9 kDa for GST-PNS2 fusion). However, the levels of expression were low in both cases, as judged by the Coomassie-stained gels. In addition, when the cells were disrupted with lysozyme and centrifuged, most of the protein released from the cells separated into the pellets. In contrast to fluffy fragile pellets from uninduced samples, these pellets were unusually compact and impossible to resuspend by the means other than prolonged sonication. This demonstrated that NS2 proteins might have a tendency to aggregate under certain conditions.

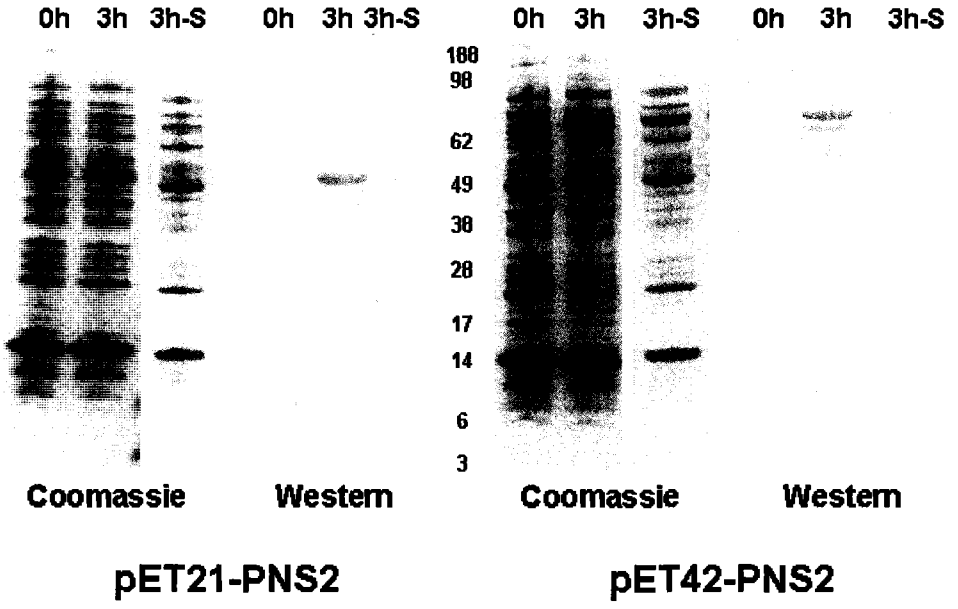

Figure 22. Expression of full-length NS2 protein from *A*PeDNV using pET21 and pET42 expression vectors.

All samples were resuspended in 20 mM Tris-HCl pH 7.4 to OD[600] = 10, disrupted with lysozyme, and analyzed by Coomassie stain and Western blot. 0h – total lysate of cells harvested immediately before induction with IPTG; 3h – total lysate of cells harvested 3 hr post-induction; 3hr-S – supernatant of 3h lysate.

As discussed in Section 2-4, brevidensoviral NS2 proteins were predicted to contain a large globular amino-terminal domain, followed by a disordered region (Figure 16). Another much smaller domain was predicted to be located at the carboxy-terminus of NS2 proteins. It has been suggested to express these domains separately in attempts to improve protein yield and solubility. Therefore, plasmids pET21-trPNS2-1 and pET21-trPNS2-2 were constructed to express residues 1-258 and 258-363 of PNS2, respectively. Surprisingly, the yields of these truncated PNS2 species were even lower than that of the full-length protein. The Western blot bands were barely visible, and the Coomassie stains of samples before and after induction were indistinguishable (data not shown).

In further search of better NS2 constructs, I turned to Instability Index (I. I.) analysis that can be performed online as part of ProtParam calculations (http://www.expasy.org/cgi-bin/protparam). The algorithm for I. I. calculation is based on the research by Guruprasad et al. (1990) who demonstrated correlation between frequency of certain dipeptides within a protein sequence and that protein's stability. The authors further proposed a way to express composition of these dipeptides in a single numerical value (I. I.) that suggests high protein stability if it is below 40 or low protein stability otherwise. The authors validated this finding by analysis of numerous proteins with known half-life, which came from various prokaryotic and eukaryotic organisms. The exact mechanism by which dipeptide composition could influence protein stability is still unknown. It is possible, however, that I. I. reveals some patterns recognized by protein degradation systems of many organisms representing different domains of life. For all species of NS2 constructed and tested up to this point, I. I. exceeded 40, and these

proteins were predicted to be unstable. To determine whether it is possible to express a species of NS2 similar to those already tested, but with a higher stability, I constructed eight additional versions of recombinant NS2 *in-silico* by varying the source of NS2 (*Ae*DNV or *A*PeDNV), the length (full-length, N-terminal domain, C-terminal domain), and the fusion (N-terminal GST or native amino-terminus). Each of these hypothetical proteins was analyzed by ProtParam, and I. I. was recorded for each protein sequence. The results are presented in Figure 23. The only species of NS2 predicted to be stable was GST-trANS2-1 fusion with I. I. = 38.0, which was selected to be constructed and expressed next.

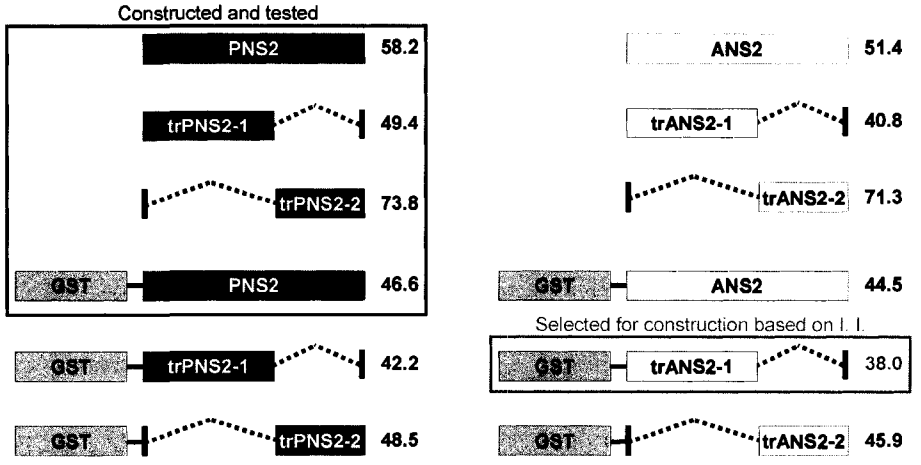

Figure 23. Analysis of instability indices (I. I.) of existing and proposed varieties of recombinant NS2 proteins.

Rosetta-2 cells were transformed with pET42-trANS2 plasmid, grown on LB medium with antibiotics, and induced with IPTG as described in the Materials and Methods section. The samples were analyzed by Coomassie stain and dotblot (Figure 24, A). GST-trANS2 fusion protein expression was evident from Coomassie-stained gel

(expected MW = 62.4 kDa), and the dotblot results confirmed the protein's identity. The protein yield appeared to be higher compared to the previously tested NS2 varieties. Initially, the recombinant NS2 protein appeared to be largely insoluble, separating mostly into compact pellets. However, optimization of the lysis protocol (most notably, addition of Triton X-100 to the lysis buffer) resulted in retention of the protein in the supernatant, as evident from Figure 24, B.

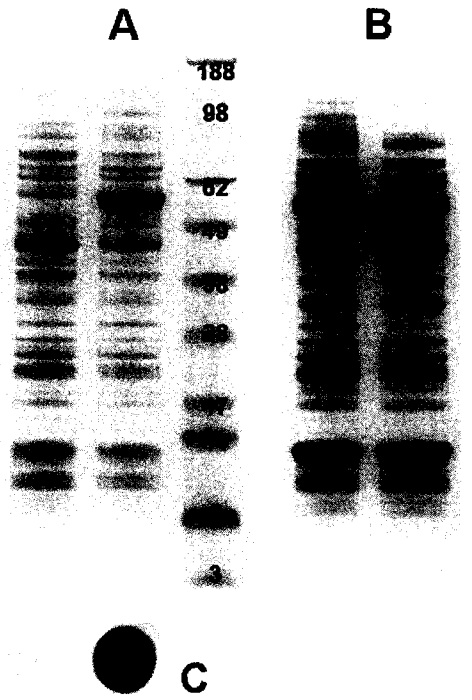

Figure 24. Expression of GST-trANS2 fusion in Rosetta-2 cells.

A – Verification of expression. Left lane – before IPTG induction. Right lane – 3 hr post-induction. Both samples were concentrated to OD[600] = 15 and lysed with 1% SDS. B – Check for solubility. 3 hr post-induction, the cells were concentrated to OD[600] = 75 and lysed as described in the Materials and Methods section. Cell debris was removed by centrifugation. Left lane – crude lysate (before centrifugation). Right lane – cleared lysate (after centrifugation) C – Verification of protein identity by dotblot. Left – uninduced; right – induced.

2-5-3. Purification and concentration of GST-trANS2 fusion protein

The presence of GST tag on trANS2 protein has benefited expression and purification of this protein in several ways. It appeared to increase protein stability during the expression stage. Since GST domain is highly soluble, its presence likely contributed to improved solubility of the entire fusion protein, which resulted in its retention in soluble form during the lysis stage. However, the main purpose of GST tag is to provide the means for rapid and specific affinity purification. GST tag is derived from *Schistosoma japonicum* Glutathione-S-Transferase. It binds the substrate (reduced glutathione) with high affinity and specificity. When glutathione is immobilized on a solid phase, the GST-tagged fusion proteins can be sequestered, washed, and subsequently eluted with excess of free glutathione. In the MagneGST protein purification system (Promega), the solid phase is represented by glutathione-coated magnetic beads, which separate rapidly from the liquid phase when placed in a magnetic field.

The results of GST-trANS2 purification and concentration are shown in Figure 25. When the default manufacturer's protocol for MagneGST purification was used, the fusion protein bound completely to the magnetic particles, as judged by its absence in the flow-through fraction (lane 3). However, only traces of the protein were found in the elution fraction (lane 4), indicating unusually tight association between the fusion protein and the magnetic particles. Manufacturer's recommendations for improving elution efficiency were then followed. High salt concentration (500 mM NaCl) and doubled amount of reduced glutathione (100 mM) contributed to increased concentration of the

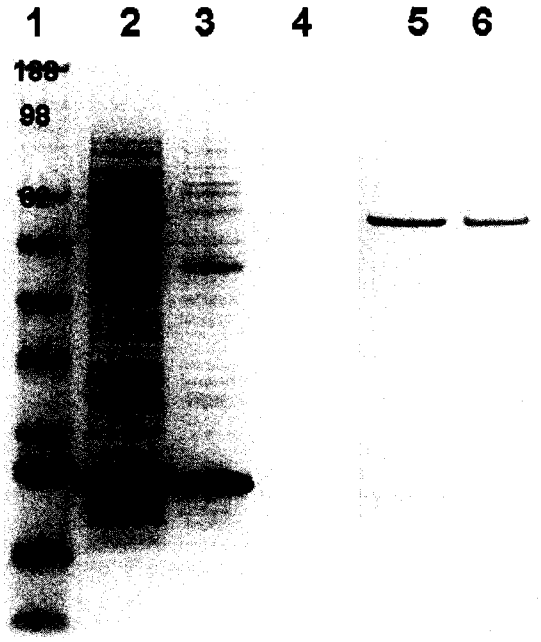

Figure 25. Purification of GST-trANS2 fusion protein.

1 – marker; 2 – protein-containing lysate; 3 – flow-through; 4 – eluate by default protocol; 5 – eluate by modified protocol; 5 – hot 8 M urea extract after modified elution.

fusion protein in the eluate (lane 5). At the same time, significant amount of the protein remained attached to the beads, and even hot 8 M urea solution did not appear to strip the beads of all protein (lane 6). Interestingly, similar observations were made on several occasions before, when the cells containing GST-PNS2 or GST-trANS2 protein were lysed without Triton X-100, and the protein separated into the pellets. These pellets were found to be partially resistant to 8 M urea treatment, with only small amount of protein detected in the liquid phase even after prolonged incubation (several hours with shaking). This can likely be explained by unusually firm consistency of the pellets, which makes their interior completely inaccessible to the denaturing agents.

While the yield and the purity of GST-trANS2 protein were satisfactory, its concentration (estimated to be between 200-400 μg/mL) was not sufficient for most *in-vitro* applications. Additionally, high salt concentration and the presence of detergent would present a serious problem for crystallization attempts. Therefore, I decided to concentrate the sample of eluted protein with simultaneous buffer exchange using ultrafiltration. iCon concentration devices (Pierce) were used for this purpose in accordance with manufacturer's recommendations, as described in the Materials and Methods section of this work. The goal was to achieve 50-fold concentration of the protein sample with simultaneous reduction of salt and detergent concentration. The construction of iCon devices assured the filtration stop after the levels of filtrate and retentate equalize, thus providing the means to control final retentate volume. Several samples were collected for SDS-PAGE analysis in the course of concentration process. These included starting eluate sample (15 μL), 5-fold and 10-fold concentrated samples (15 μL each), 25-fold and 50-fold concentrated samples (5 μL each), and the first filtrate sample (15 μL). Because the lower chamber of the device had to be filled with buffer to provide desired deadstop volume, the filtrate mixed with buffer and became too diluted to detect any protein leakage beyond the first concentration cycle (Table 14). The device was visually checked after each concentration cycle in order to detect protein precipitation in the retentate.

According to the manufacturer, the concentration process should be very rapid (on the order of several minutes). This was the case with the first concentration cycle; however, the second cycle took about 30 min to complete, and the subsequent cycles took

		Cycle 1	Cycle 2	Cycle 3	Cycle 4
Upper chamber calculations	Start volume	5.00 **15 µL sample**	1.00	0.50	0.20
	End (deadstop) volume	1.00 **15 µL sample**	0.50 **15 µL sample**	0.20 **5 µL sample**	0.10 **5 µL sample**
	Retentate conc. factor	5.00	10.00	25.00	50.00
Total amount of liquid in the device required for a desired deadstop volume		9.00	8.25	7.60	7.20
Lower chamber calculations	Start volume	4.00	7.25	7.10	7.00
	End volume	8.00 **15 µL sample**	7.75	7.40	7.10
	Filtrate volume	4.00	0.50	0.30	0.10
	Filtrate dilution factor	2.00	15.50	24.67	71.00
	Lower chamber volume adjustments	-0.75	-0.65	-0.40	

Table 14. Concentration of samples containing NS2 protein using iCon devices.

several hours each. By the end of the third cycle, the signs of protein precipitation in the retentate became evident, with even more precipitate formed during the final cycle. To determine the amount of soluble protein in the retentate at the end of the final cycle, the retentate was centrifuged, and the supernatant was separated from the pellet. Five µL of supernatant were collected for SDS-PAGE analysis. Additionally, the walls of the upper device chamber were washed with buffer. The wash was spun down in the tube that already contained the pellet from the previous centrifugation. The combined pellet was

resuspended in 8 M urea for 30 min, and 5 μL of suspension was used for SDS-PAGE analysis. The results of SDS-PAGE analysis are shown in Figure 26. As the volume of retentate decreased throughout the concentration process, the protein concentration did not appear to change (lanes 4-7). At the same time, there was no evidence of the protein leaking through the filter (lane 3 is empty). The most likely explanation is that increased protein concentration causes it to aggregate on contact with the filter and to form a firm film, thus removing the excess protein from the retentate. This film was likely responsible for the dramatic decrease in the flow rate. Eventually, most of the protein became aggregated, which resulted in visible precipitate formation. By the end of concentration process, very little protein remained in the solution (lane 8), and relatively small amount of the protein could be recovered from the pellet (lane 9) because of

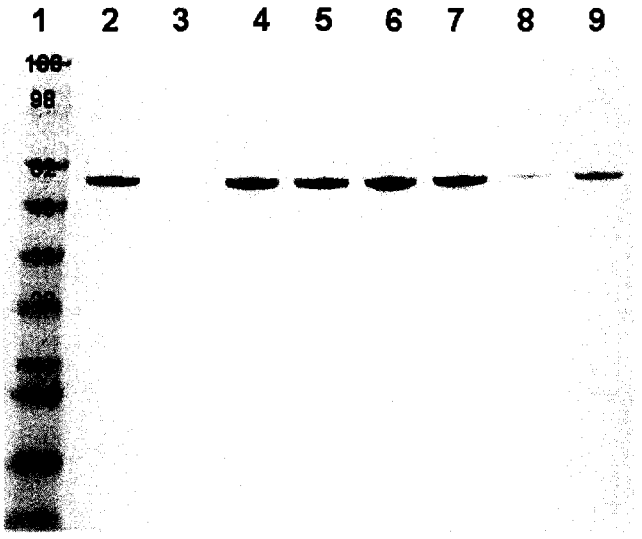

Figure 26. Concentration of GST-trANS2 fusion protein.

1 – marker; 2 – starting sample (15 μL); 3 – first filtrate (15 μL); 4 – five-fold concentrate (15 μL); 5 – 10-fold concentrate (15 μL); 6 – 25-fold concentrate (5 μL); 7 – 50-fold concentrate (5 μL); 8 – supernatant of the 50-fold concentrate; 9 – 8 M urea extract of the pellet.

previously discussed partial resistance of NS2-containing pellets to the denaturing agents. Inability to concentrate GST-trANS2 fusion protein in a low-salt detergent-free environment made it impossible to continue with X-ray crystallography studies.

2-5-4. DNA pull-down assays and investigation of putative NS2-binding region

The fact that at least some of the fusion protein could be eluted from the MagneGST beads without the use of denaturing agents indicated that not all protein was associated with the beads in an aggregated, inaccessible form. Those protein molecules that were not bound by aggregation could still interact with other protein or DNA molecules, making the pull-down assays possible. In these assays, interaction between the molecules is studied by sequestering molecules of one type (bait) and detecting the molecules of other types (prey) that became associated and sequestered with the bait. When GST-tagged proteins are used as baits, MagneGST system can be used to conduct pull-down assays.

Currently, we do not know much about brevidensoviral NS2 interactions, other than the preliminary evidence for NS1/NS2 interactions produced as a result of FRET experiments (Section 2-4 of this work). It would be interesting to look at interactions between NS2 and host cell proteins, but the tools for detecting and identification of mosquito proteins are still quite limited. So instead of protein-protein interactions, I decided to investigate possible interactions between NS2 protein and viral DNA. The nuclear localization of NS2 strongly suggested that this protein might interact with DNA, either directly or in association with other proteins. Also, the high theoretical pI values (9.55 for ANS2 and 9.47 for PNS2) hinted at these proteins' ability to interact with

negatively charged molecules, such as DNA. To conduct pull-down assays, GST-trANS2 fusion protein was immobilized on MagneGST beads, washed, and reacted with a DNA sample. After another round of washing, the beads were treated with proteinase K (Qiagen) in 1% SDS. This treatment destroyed all proteins associated with the beads (verified by SDS-PAGE) and eluted DNA into the liquid phase. The eluates were loaded on agarose gel, and electrophoresis was conducted. The gels were stained with ethidium bromide and imaged using GelDoc camera (BioRad).

Either non-specific or specific DNA samples were used as prey. Non-specific samples were produced from *E. coli* cells, fragmented by sonication, and purified by ethanol precipitation. In addition to genomic DNA fragments, these samples contained most of bacterial RNA species, represented predominantly with tRNA. The results of non-specific pull-down experiment are demonstrated in Figure 27. Interestingly, some nucleic acid was eluted from the beads treated with bait but no prey (lane 1). Initially, this nucleic acid was misidentified as RNA: this was a result of contamination with large amounts of yeast tRNA used in some early modifications of pull-down experiments. However, the nucleic acid is clearly resistant to RNaseA digestion (lane 2), so it must be residual genomic DNA, highly fragmented, but not completely degraded by DNaseI in the process of cell lysis and protein preparation. When the prey DNA was added, the residual DNA was outcompeted and replaced by the new DNA fragments, but not by RNA, despite the fact that concentration of RNA in the prey sample was higher than that of DNA (lanes 3-5 and 7-9). Replacement of some DNA fragments with others indicated

that DNA molecules could associate and dissociate freely, i.e. they were not trapped in GST-trANS2 aggregates, as one might suspect.

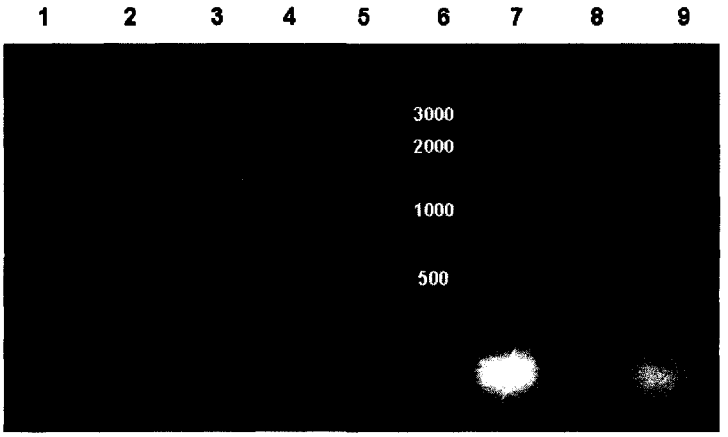

Figure 27. Pull-down experiment with non-specific DNA prey.

1 and 2 – residual DNA bound to GST-trANS2 fusion protein in the process of protein preparation (1 – no RNaseA treatment; 2 – RNaseA treatment before elution). 3-5 – pull-down experiment (3 – DNaseI treatment before elution; 4 – RNaseA treatment before elution; 5 – mock treatment before elution). 6 – markers. 7-9 – prey DNA treated with DNaseI (7), RNaseA (8), or mock-treated (9).

The non-specific DNA pull-down experiment demonstrated that brevidensoviral NS2 proteins have some affinity for DNA, but because this DNA came from a species completely unrelated to the virus or to its host, no specific interactions could be observed or expected to occur. In contrast, the specific prey DNA samples contained fragments of viral DNA in its double-stranded form (generated from pUCA plasmid by restriction digests), so that specific NS2-DNA interactions could be studied. DNA samples discussed in this work were designed to generate pairs of fragments with a similar yet distinguishable size. *Ale*I x *Blp*I x *Bst*BI (digest A) produced a pair with fragment sizes of 592 bp and 706 bp, while *Bst*BI x *Hpa*I x *Nco*I (digest B) produced a pair with fragment sizes of 908 bp and 1115 bp. Because of similar sizes, the starting amounts of

DNA in the two fragments of each pair were also similar. However, if NS2 preferentially interacted with one fragment, it would be enriched relative to other fragments in the eluate fraction. This enrichment could be easily detected on the gel.

I conducted pull-down experiments using each digest, and then repeated these experiments several months later. The first time, the 592-bp digest A fragment and 908-bp digest B fragment produced the bands that were clearly brighter than their counterparts, although this effect was observed only when higher DNA concentration was used (Figure 28, A). Presumably, these fragments became enriched because they were preferentially bound by NS2 under conditions when the binding capacity of the bait was exceeded and the DNA molecules had to compete for the binding sites. Since the locations of these fragments within the viral genomes overlap, it was hypothesized that they both contain the same putative NS2-binding region located upstream from the structural gene promoter P(VP) (Figure 28, C). When this experiment was repeated, the same protocol was followed, but some modifications were made. One such modification was inclusion of samples in which separately expressed GST domain was used as a bait in place of GST-trANS2 fusion. Another modification was ethanol precipitation of eluates before loading them on the gel (this removed SDS from the gel). The use of GST-only control confirmed that association of DNA with the beads was primarily NS2-mediated, as the amount of DNA eluted in GST-only control was significantly lower. Unfortunately, the other results of the repeated experiments created significant amount of uncertainty regarding specific DNA-binding properties of NS2. This time, 706-bp digest A fragment and 1115-bp digest B fragment became enriched, and these fragments do not

share any sequence (Figure 28, B). While there is no question that NS2 can preferentially bind certain DNA fragments, the conditions that determine the preference have remained unknown to date.

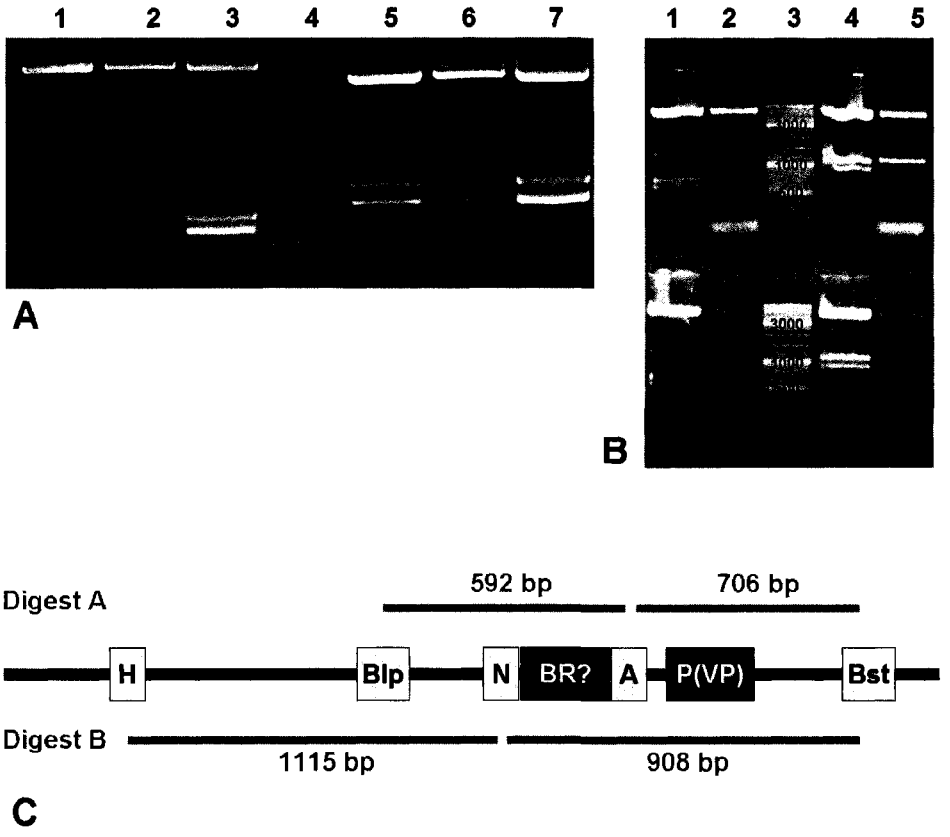

Figure 28. Pull-down experiments with specific DNA prey.

A – initial experiment. 1 – digest A prey DNA sample; 2 – digest A eluate (1 ug of prey DNA per reaction); 3 – digest A eluate (10 ug of prey DNA per reaction); 4 – marker; 5- digest B prey DNA sample; 6 – digest B eluate (1 ug of prey DNA per reaction); 7 – digest B eluate (10 ug of prey DNA per reaction).

B – repeated experiment. Top lanes – GST-trANS2 fusion as a bait; bottom lanes – GST domain as a bait. 1 – digest A prey DNA sample; 2 – digest A eluate (10 ug of prey DNA per reaction); 3 – marker; 4 – digest B prey DNA sample; 5 – digest B eluate (10 ug of prey DNA per reaction).

C – location of prey DNA fragments within the viral genome. H – *Hpa*I site; Blp – *Blp*I site; N – *Nco*I site; BR? – putative NS2-binding region; A – *Ale*I site; P(VP) – structural gene promoter; Bst – *Bst*BI site

Interestingly, the possibility that NS2-binding region might exist just upstream from the structural gene promoter stimulated other directions of my research. Most notably, it led to the study of the role played by NS2 in P(VP) trans-activation, which has been described earlier in this work (Section 2-3). The finding that NS2 was necessary for achieving maximum activity of this promoter was thought for some time to have corroborated the existence of NS2-binding region. However, repeated pull-down experiments that put specificity of NS2-DNA interactions under question prompted me to re-evaluate connections between the two studies. If the NS2-binding region truly existed and if this region played any role in P(VP) trans-activation, then deleting this region should result in the loss of effects described in Section 2-3. To check this, p61-ΔPBR plasmid was constructed that was similar to p61-NcoRE, except for the deletion of *Nco*I x *Ale*I region (Figure 29). The P(VP) promoter and the VP-β-Gal fusion gene under control of this promoter remained intact. Effects of NS2 on P(VP) activity were then studied as described in Section 2-3, except p61-ΔPBR was used as a reporter construct. The results clearly demonstrated that NS2 was still required for attaining maximum level of promoter activity (Figure 30). The fact that deletion of putative NS2-binding region had no effect on NS2-mediated enhancement of P(VP) activity made existence of such region even less likely.

2-5-5. Alternative pull-down assay using ReactiBind strips

Another issue with pull-down assays described above is relatively high concentration of protein and DNA, which could contribute to various *in-vitro* artifacts. To address this issue, the pull-down assays were modified as follows. The MagneGST

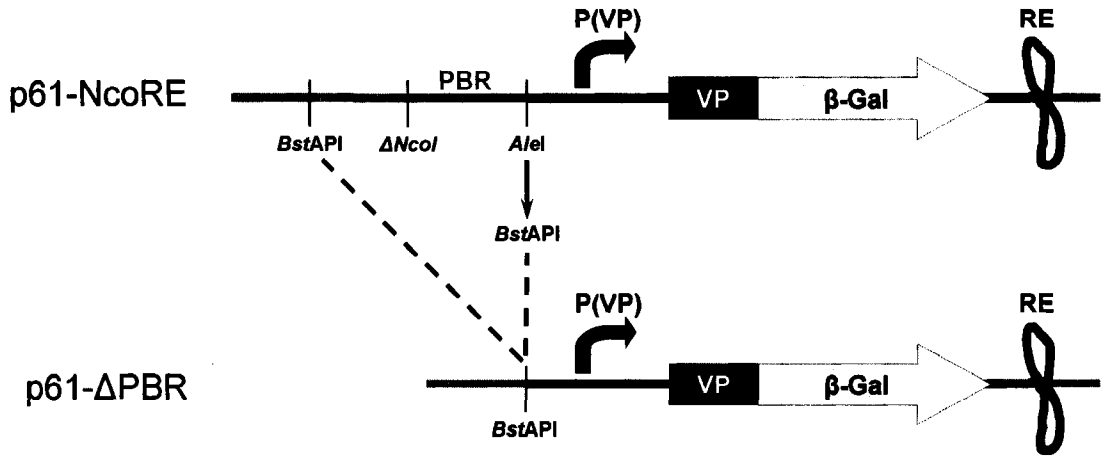

Figure 29. Construction of p61-ΔPBR plasmid.

*Ale*I site was changed to *Bst*API site by site-specific mutagenesis, and the region between the two *Bst*API sites was deleted. Δ*Nco*I – *Nco*I site present in pUCA, but destroyed as a result of blunt-end ligation in the process of p61-NcoRE cloning. PBR – putative NS2-binding region. RE – right end of the viral genome.

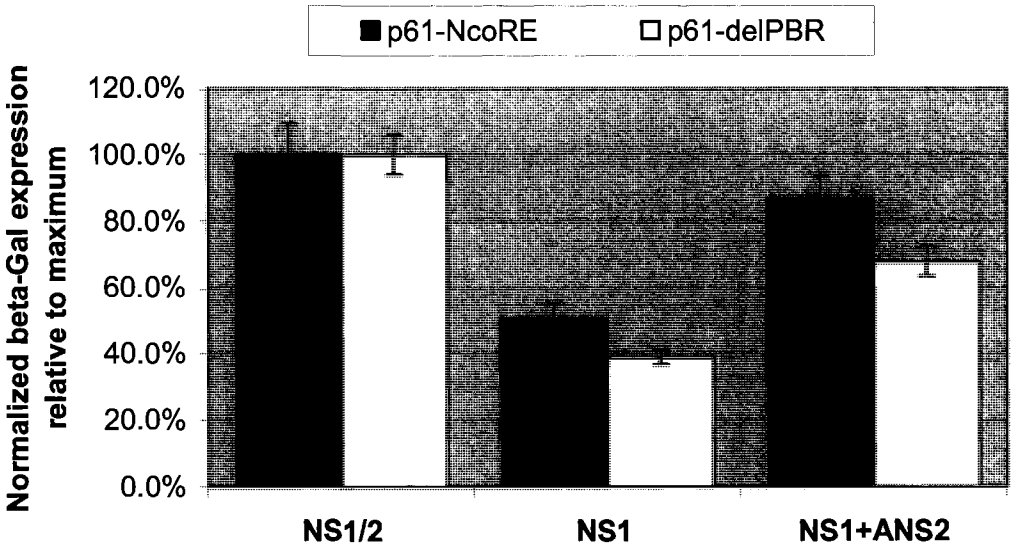

Figure 30. NS2 trans-activation and complementation studies using p61-NcoRE and p61-ΔPBR as reporter constructs for P(VP) promoter activity.

NS1/2 – NS1 and NS2 supplied by pUCA-INV; NS1 – NS1 is supplied by pUCA-IM, no NS2 supplied; NS1+ANS2 – NS21 supplied by pUCA-IM, NS2 supplied by Hsp-ANS2.

system was replaced with ReactiBind glutathione-coated 8-well strips (Pierce) that, according to the manufacturer, could bind up to 10 ng of GST-tagged protein per well. Six wells were filled with the bait samples containing the excess (approx. 1 ug) of GST-trANS2 fusion protein or GST control protein (3 wells of each). Two wells were filled with negative bait control (buffer with no protein). The protein was bound to the wells according to the manufacturer's requirements and as described in the Materials and Methods section. The wells were washed and filled with diluted prey samples containing 6 ng of DNA each. The prey samples were generated by *Bst*API x *Sal*I restriction digest of pUCA, followed by isolation of the 250-bp fragment and diluting it 100-fold with PBS. This fragment contains the 181-bp region of NS1/NS2 genes, which is targeted by TaqMan qPCR assay described earlier in this work (Figure 31). After the prey was bound and washed, elution step was carried out using modified elution buffer with decreased SDS concentration (0.1% instead of 1%). The eluates and the original prey sample serially (3-fold) diluted in water. 81-fold diluted eluates and 6561-fold diluted original prey sample were tested using qPCR assay. Under conditions of this experiment, only small fraction of total prey DNA was bound to the wells, with only slight increase (1 log or less) in the wells containing GST-trANS2 fusion protein compared to the control wells (Figure 32).

These results confirm that NS2 has some affinity for DNA, but this affinity is so weak that it is unlikely to play any role *in vivo*. At the same time, it is important to remember that, under physiological conditions, NS2 protein is not attached to flat surfaces in a thin layer, and viral DNA is not likely to be evenly distributed throughout

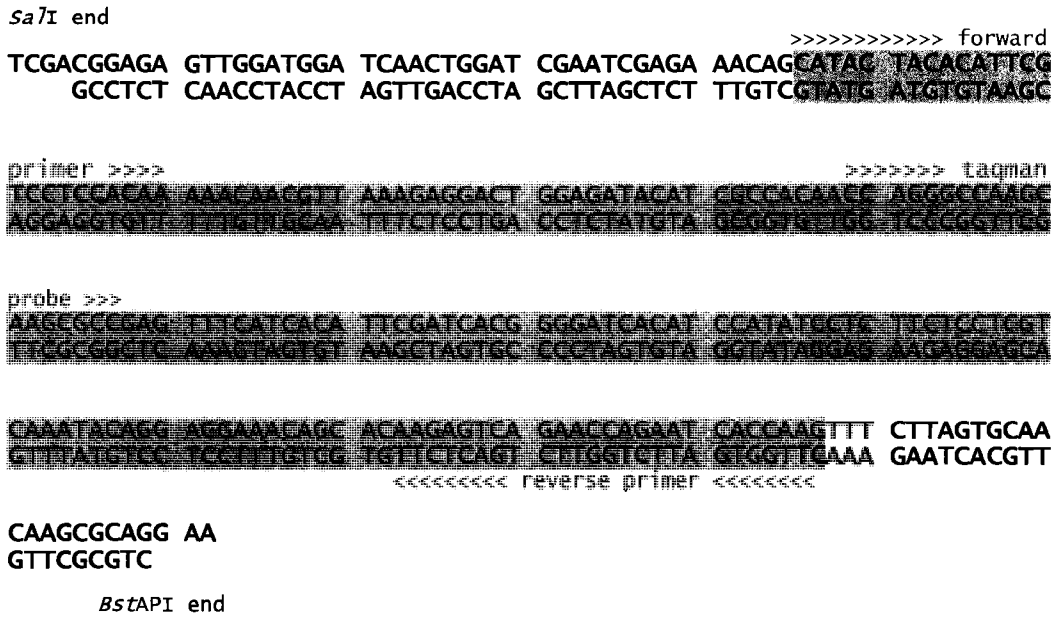

Figure 31. 250-bp *Bst*API x *Sal*I fragment of pUCA contains sequence recognized by TaqMan assay

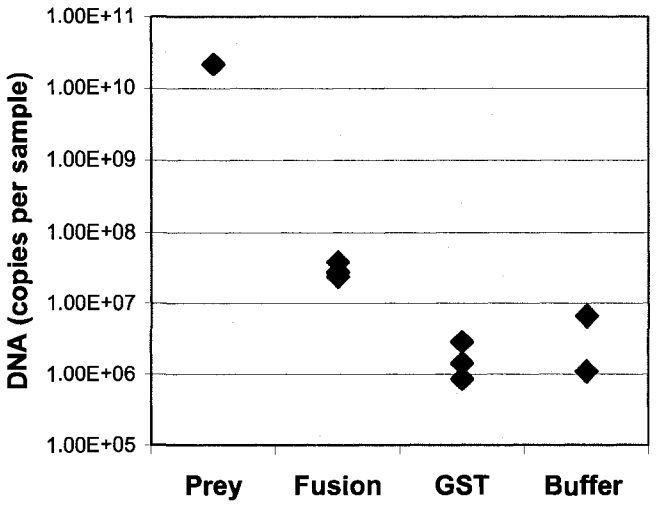

Figure 32. Alternative pull-down assay using ReactiBind strips.

Prey – original DNA prey. Fusion – eluates from wells containing GST-trANS2 fusion protein as a bait. GST – eluates from the wells containing GST control protein as a bait. Buffer – eluate from the wells containing no protein (treated with buffer only).

the nucleoplasm. Therefore, *in-vitro* binding assays might not adequately reflect the properties of this protein. In the following chapter, I will attempt to analyze the findings described above and offer my view on the research that could be done to further understand the properties of brevidensoviral NS2 proteins.

Chapter 3. Discussion, conclusions, and prospects

Section 3-1. Mutations in brevidensoviral NS2 genes have different phenotypic manifestations depending on the type of mutation and the route of infection

The results of experiments described in the Section 2-2 of this work prove the importance of NS2 in mosquito densovirus life cycle, both during cell culture propagation and in mosquito host infections. All NS2 mutants tested for their ability to infect *Aedes aegypti* mosquito larvae failed to amplify in the mosquito host and did not accumulate in the rearing water samples. Surprisingly, hybrid 13, a chimeric construct that was indistinguishable from the wild type mosquito densoviruses when propagated in cell culture, was among the mutants that failed the mosquito infectivity test. A detailed analysis of experimental data reveals that there is no single "mutant NS2 phenotype." Instead, the nature and the extent of observed defects (if any) depend on the type of mutation and on the system used to assay the mutant phenotype (Table 15).

When transfection is used to initiate viral propagation in cell culture, NS2-null mutant of *Ae*DNV is the only strain that displays an abnormal phenotype. As reported in the Section 2-2, the ability of this mutant to synthesize viral DNA and to propagate in cell culture is markedly decreased. This makes NS2-null mutant of *Ae*DNV similar to MVM NS2 mutants grown in murine cells, as described in Naeger et al (1990). However, important differences exist between NS2-deficient mutants of the two viruses. In MVM,

Test system / Mutant type	C6/36 cell cultures					*Ae. aegypti* lavae
	Transfected Tested for:			Infected Tested for:		Infected Tested for:
	DNA SYN	CAPS SYN	EE	POS	DNA ACC	DNA ACC
NS2-null	↓↓↓	↓	Comp	Absent	-	Not accum
G172 point mutants	Comp (G172E)	Comp	-	Absent	Not accum (G172E)	Not accum (G172E)
Non-viable hybrids 5, 8, 11, 12	Comp (Hybr. 5, 8, 12)	Comp	Comp (Hybr. 12)	Absent	-	Not accum (Hybr. 12)
Viable hybrids 4, 6, 9, 10, 13	Comp (Hybr. 4, 6, 13)	Comp	Comp (Hybr. 13)	Present	-	Not accum (Hybr. 13)

Table 15. Summary of experiments conducted to characterize various NS2 mutants.

DNA SYN – synthesis of viral DNA assessed by qPCR; CAPS SYN – synthesis of capsids estimated by IFA; EE – efficiency of encapsidation; POS – cells positive for capsid antigen, accessed by IFA; DNA ACC – accumulation of viral DNA in the culture medium or the rearing water samples; ↓↓↓ – markedly decreased; ↓ – somewhat decreased; comp – comparable to the wild type; (-) – not performed. If only selected mutants were tested, these are indicated in parentheses.

a failure to process and assemble VP2 subunits that accumulate in the nucleus results in negative feedback mechanisms, which shut down further synthesis of viral DNA and down-regulate translation of VP messages (Cotmore et al., 1997). Moreover, the synthesis of single-stranded viral genomes is affected the most, as it becomes undetectable. Meanwhile, the synthesis of the double-stranded RF continues at the low but detectable level (5% of that in the wild type). In contrast, the synthesis and packaging of genomic DNA does not seem to be specifically affected in the case of *Ae*DNV NS2-null mutant, as the proportion of encapsidated DNA in total viral DNA pool is comparable to the wild type. While the synthesis of viral capsids appears to be

somewhat decreased based on immuno-fluorescence intensity, there is no sign of significant down-regulation similar to that observed in MVM. It appears, therefore, that the decrease in overall efficiency of viral DNA replication is a primary defect in *Ae*DNV NS2-null mutant phenotype, while the decrease in capsid synthesis results from the lesser number of DNA templates available for transcription. Additionally, the decrease in capsid synthesis could be a consequence of incomplete trans-activation of P(VP) promoter in the absence of NS2, as discussed in the Section 2-3. Importantly, the defects observed in the brevidensoviral NS2-null phenotype are quantitative, not qualitative. This is a strong indication that, similarly to MVM, brevidensoviral NS2 proteins regulate the viral reproduction by modulating the environment of the host cell, which may require NS2 to interact with both viral and cellular constituents.

All other NS2 mutants described in this work reproduced remarkably well following the transfection of infectious clones into C6/36 cells. No defects in synthesis or encapsidation of viral DNA could be detected. The synthesis of viral capsids was comparable to the wild type. On multiple occasions, the cells transfected with the mutant constructs and assayed by IFA appeared even brighter then the wild type, although this observation was largely subjective. Surprisingly, this apparently normal phenotype displayed post-transfection by all mutants except NS2-null did not always correlate with the phenotype observed upon infection of the new C6/36 cells. As reported earlier in this work, an unknown defect in *A*PeDNV NS2 protein caused by G172 mutations introduced through recombination or a base substitution made the mutants non-infective.

Standardizing of infectious dose by the viral DNA content had no effect on the outcome of infection.

Since this defect was not observed upon transfection of the double-stranded DNA constructs, it must have been associated with the steps bypassed by this route of viral infection initiation. These steps include attachment, penetration, uncoating, and so-called conversion – synthesis of covalently closed double-stranded monomeric DNA molecules from the single-stranded genomes following the uncoating step (Bashir et al., 2000). Success of these steps depends largely on the virion integrity, so it was proposed that G172 mutations of *A*PeDNV NS2 result in incorrect capsid assembly and/or incomplete packaging of genomic DNA. For this hypothesis to be true, the capsid assembly defects must be serious enough to eliminate infectivity of the progeny virions, but too mild to activate negative feedback mechanisms described earlier. This combination of conditions seems unlikely, although we have no experimental evidence for or against this hypothesis.

An alternative hypothesis (also purely theoretical) focuses on the conversion step. As described in Bashir et al. (2000), this step can be completed by cellular DNA replication machinery alone. The participation of viral non-structural proteins in the first rounds of conversion is unlikely, as they have not been shown to incorporate into the virions except for a single copy of NS1 covalently linked to the 5'-end of the genome and usually cleaved off by the time the conversion starts. However, after the first few rounds of conversion, the newly-synthesized non-structural proteins could modify the host cell environment in a way that greatly increases efficiency of conversion for the remaining

copies of genomic DNA. If brevidensoviral NS2 proteins participate in this process, the mutations could result in a conversion slowdown to the point that would make accumulation of viral DNA and proteins undetectable by our methods. This hypothesis seems to be more plausible than the previous one because it is consistent with involvement of brevidensoviral NS2 in viral DNA replication, as proposed earlier in this section. At the same time, the lack of experimental data addressing either hypothesis makes it impossible to come to definitive conclusion at this time.

As it is apparent from the working hypothesis formulated at the end of Chapter 1, in my research I focused primarily on possible interactions between brevidensoviral NS2 and other viral constituents. However, the data presented in this work suggest that the host cell constituents and their interactions with NS2 proteins may also be important in brevidensoviral life cycle. The best illustration of this comes from an observation that a "viable" hybrid 13 failed to accumulate following the mosquito larvae infection. This hybrid does not carry the G172E mutation, but being a chimeric construct, it expresses non-structural proteins that may differ from the wild type in some way. These differences are not apparent when the virus is propagated in C6/36 cell cultures; therefore, any defect that manifests in mosquito larvae infection must be cell-type-dependent, akin to NS2 mutations in MVM (Naeger et al., 1990). When a mutant displays the cell-type-dependent phenotype, it is very likely that the mutated protein interacts with cellular constituents.

Section 3-2. Brevidensoviral NS2 enhances, but is not required for NS1-mediated activation of the structural gene promoter

It is known that the non-structural protein NS1 is required for efficient expression of parvoviral genes (Doerig et al., 1988; Hanson and Rhode, 1991), but the role of NS2 proteins in this process is unclear. In the case of mosquito densoviruses, NS2 does not appear to be essential for *Ae*DNV structural gene promoter P(VP) activation. This conclusion can be made from two observations: that NS2 alone has no effect on viral promoter activity (Afanasiev et al., 1994) and that the mutant incapable of NS2 synthesis still expresses capsid proteins, albeit at somewhat decreased levels (this work). However, these observations do not exclude possibility that NS2 modulates trans-activation effect of NS1, so I decided to determine the role of NS2 in trans-activation of P(VP) using modification of procedure described by Ward et al. (2001).

As a result, it was shown that NS1 can trans-activate the structural gene promoter with and without NS2. However, the effect exerted by NS1 expressed alone was lower than that in the presence of NS2. In other words, the hypothesized role of NS2 as an enhancer of NS1-mediated P(VP) activation has been confirmed in the course of these experiments. Importantly, the functional co-operation between NS1 and NS2 was consistent with co-localization and direct interaction between the two non-structural proteins demonstrated in Section 2-4 of this work.

Section 3-3. Brevidensoviral NS2 is specifically targeted to the nucleus where it co-localizes and interacts with NS1

NS2 proteins of *Ae*DNV and MVM are characterized by strikingly different subcellular localization patterns. As reviewed in Cotmore and Tattersall (1990), the phosphorylated form of MVM NS2 is excluded from the nucleus either through oligomerization or because it interacts with cytoplasmic constituents. The non-phosphorylated form of MVM NS2 can be detected in the nucleus, but it is thought to passively diffuse into the nucleus from the cytoplasm. Since the size of MVM NS2 is only 25 kDa, this scenario is certainly possible: the protein size cutoff for passive diffusion through the nuclear pore complexes has been estimated at about 40 kDa (Lange et al., 2007). In contrast, brevidensoviral NS2 proteins are larger (41 kDa) and should not be able to passively diffuse in and out of the nucleus. According to Erin Robinson (Azarkh, Robinson, et al., 2008), expression of *Ae*DNV NS2 is first detected in the nucleus, and the protein retains its strictly nuclear localization until the later stages of viral infection.

Interestingly, no diffuse or cytoplasmic localization of the full-length NS2 was ever observed in the course of experiments described in the Section 2-4, regardless of the duration of infection. This apparent discrepancy is likely explained by the differences in the experimental setup. In the former group of experiments, the cells were infected with the wild-type viruses or with the mixture of wild-type and recombinant (NS1-GFP) viruses. Therefore, expression of viral non-structural proteins was observed in a context of ongoing reproduction of the virus. In the later group of experiments, the cells were

transfected with infectious clones of interest. Expression of NS2 occurred either in the absence of other viral proteins (Hsp-NS2 constructs) or in the presence of viral proteins provided by replication-deficient NS2-null mutant of *Ae*DNV. Under these conditions, virus propagation was nonexistent or diminished. The observation that the change in NS2 localization during the late stages of viral infection likely depends on concomitant viral reproduction is important, as it suggests the protein's involvement in the processes occurring during these stages. It is possible, for example, that brevidensoviral NS2 proteins participate in nuclear egress of the progeny virions, as it is the case with MVM (Miller and Pintel, 2002).

Since there is no evidence for passive diffusion of brevidensoviral NS2 proteins into the nucleus, appearance of these proteins in the nucleus must be a result of targeted event. As described in the Section 2-4, *Ae*DNV NS2 protein did not require other viral proteins for its transport into the nucleus, but the presence of intact carboxy-terminus that contains putative bi-partate NLS was essential. Unfortunately, the size of truncated NS2 protein used to determine importance of C-terminal region for the protein's nuclear localization was small enough to allow passive diffusion through the nuclear pore complexes. While this can be viewed as a flaw in experimental setup, a large proportion of cells transfected with the truncated NS2 construct displayed the protein's exclusion from the nucleus. This is consistent with the loss of NLS, but not with passive diffusion, which should result in a diffuse intracellular location of the protein. It is also important to note, that the putative bi-partite NLS were found to be highly conserved in all brevidensoviruses, and they could also be found in NS2 proteins of other members of

Densovirinae subfamily (see Table 11). This is evidence, though indirect that the putative bi-partite NLS are functional in insect parvoviruses.

Co-expression of fluorescently labeled *Ae*DNV NS1 and NS2 proteins in Aag2 cells revealed that the two proteins co-localize in punctate regions of the nucleus. This observation is in agreement with numerous similar observations made by Joe Corsini, Erin Robinson, and other members of our lab (Azarkh, Robinson, et al., 2008). Visualization of NS2 using YFP fluorescent tags added confidence to these observations, as it no longer depended on permeabilization of the cell and the quality of primary and secondary antibodies. However, the main purpose of visualizing fluorescently-labeled NS1 and NS2 proteins in the same cell was to determine if their co-localization is accompanied by direct interaction. As described in the Section 2-4, FRET analysis demonstrated existence of such interaction. The significance of this interaction for the function of either non-structural protein is unclear. Certainly, NS1-NS2 interaction is not essential for the function of the NS1 protein, as the NS2-null mutant still synthesizes viral DNA and proteins, albeit at the decreased levels. This does not exclude the possibility that binding of NS2 somehow stabilizes the structure of NS1 or enhances its performance. Conversely, it could be that NS2 structure is altered or stabilized by NS1 binding, and this might be important for NS2 function. Some observations described next suggest that the latter scenario is likely.

Section 3-4. Problems with prokaryotic expression and in-vitro testing of recombinant brevidensoviral NS2 proteins may help us understand the behavior of these proteins in vivo

Experimental results presented in Section 2-5 of this work indicate that NS2 can bind DNA. Under conditions of these experiments, interaction between NS2 and DNA was largely non-specific, and was observed only at high concentrations of recombinant NS2 and prey DNA samples. Studies conducted to determine specificity of NS2 interactions with certain viral DNA sequences were inconclusive, as different, mutually exclusive fragments of viral DNA became enriched upon repeated experiments.

In general, working with recombinant NS2 was associated with the number of difficulties, which, depending on the researcher's attitude, could either be viewed as major nuisances or as the valuable hints about brevidensoviral NS2 properties. The latter view warrants a closer look at these difficulties, some of which are listed below.

- The yield of recombinant protein was quite low, even for the best-expressing construct pET42-trANS2.
- The protein could not be extracted from the cells using B-Per extraction reagent (Pierce). When the cells were lysed, the protein would segregate into the pellets unless 1% Triton X-100 was added to the lysis buffer. These pellets were unusually compact, sturdy, and only partially soluble in the presence of denaturing agents.
- Any attempt to purify or concentrate the protein contained in a soluble fraction resulted in "disappearance" of the protein, which was not detected in any flow-through, filtrate, wash, retentate, or eluate fractions, indicating that it likely precipitated on a solid phase involved in purification procedure. Treatments of that

solid phase with denaturing agents usually resulted in only partial recovery of the protein.

These and many other problems encountered with expression of recombinant NS2 in prokaryotic system are likely to be the many sides of the same phenomenon – the propensity of brevidensoviral NS2 proteins to aggregate. Though superficially similar, aggregation of NS2 must be distinguished from the inclusion body formation – a common side effect of over-expressing heterologous proteins in prokaryotic systems. Inclusion bodies form *in vivo* when a heterologous protein accumulates at high concentration in the bacterial cytoplasm. Under these conditions, the nascent protein often undertakes a deviant folding pathway, which results in exposure of hydrophobic residues leading to protein aggregation (reviewed in Idicula-Thomas and Balaji, 2005). In contrast, GST-trANS2 aggregates did not form *in vivo* since the soluble protein could be recovered when the cells were lysed in the presence of a mild non-ionic detergent. Instead, the protein aggregation occurred *in vitro* when high local concentration of this recombinant NS2 protein was created by various purification and concentration procedures. These included the MagneGST (Promega) pull-down assays used to study interactions between the recombinant NS2 protein and the fragments of viral DNA. Aggregation of NS2 on the surface of glutathione-coated magnetic beads could certainly affect the DNA binding patterns and contribute to somewhat erratic results described above.

In vivo accumulation of NS2 in small nuclear compartments (the punctate nuclear bodies described earlier in this work) likely results in high local concentrations of the

protein, comparable to those observed during *in vitro* manipulations with recombinant NS2, yet it does not cause uncontrollable aggregation and precipitation of the protein. This discrepancy between *in-vivo* and *in-vitro* observations can be explained by the differences in the protein environment, and protein-protein interactions are likely to play an important role in stabilization of NS2 structure *in vivo*. As discussed in Section 2-4 of this work, the carboxy-terminal region of NS2 was predicted to be largely disordered. The growing body of evidence indicates that the so-called intrinsically unstructured proteins and protein regions efficiently interact with their targets (Dyson and Wright, 2005). These interactions often induce the folding of previously unstructured regions in the ways impossible when the protein is expressed alone. It is, therefore, likely that the C-terminal region of brevidensoviral NS2 proteins plays a role in protein-protein interactions that stabilize its structure and render it physiologically active. Interestingly, the last 63 C-terminal residues of brevidensoviral NS2 proteins are nearly 100% conserved (a single amino-acid substitution is found in some strains), which cannot be explained by conservation of overlapping NS1 gene based on chi-square analysis (my unpublished observations). A likely candidate target for NS2 binding is NS1, whose interaction with NS2 has been demonstrated by FRET microscopy analysis, as described earlier in this work. A circumstantial evidence for importance of NS1-NS2 interaction comes from the fact that all densoviruses use "leaky scanning" strategy to express these proteins. This strategy insures that the relative amounts of NS1 and NS2 synthesized at any given point of the viral life cycle are constant, which may be especially important for the direct interactions between these non-structural proteins. Therefore, expression of

NS2 protein alone likely puts it in physiologically irrelevant context, which causes multiple problems. On the other hand, co-expression of NS1 and NS2 in a system that supports native folding and post-translational modification processes (such as baculovirus or *Drosophila* expression systems) could result in structured, functional protein complexes. These complexes could be further purified, concentrated, and used for various *in-vitro* studies, including the DNA binding assays.

Section 3-5. Brevidensoviral NS2 proteins deserve further attention of parvovirologists

The research presented in this work indicates that NS2 proteins of mosquito densonucleosis viruses play important roles in the life cycle of these viruses. NS2 proteins are targeted to the nucleus were they interact with NS1 and likely with some cellular proteins to form distinct nuclear bodies. Through these interactions, NS2 improves efficiency of viral DNA replication and, to a lesser extent, of viral protein expression. Participation of NS2 in these processes appears to be especially important during the early stages of viral reproduction.

The research presented in this work increased our understanding of brevidensoviral NS2 proteins, but the number of questions that arose in the course of the research has yet to be answered. What are the host cell proteins that interact with NS1 and NS2 and participate in the formation of nuclear bodies? What role do these proteins play in the viral life cycle? What stages of viral reproduction can be mapped to the nuclear bodies? Does NS2 interact with DNA *in vivo*? If so, are those interactions

sequence-specific? These questions will have to be answered before we gain more-or-less complete understanding of the properties and functions of brevidensoviral NS2 proteins. When we do, we will be better equipped for manipulating mosquito densoviruses on genetic level, which in turn could lead to more efficient use of these viruses as biologic mosquito control agents.

References

1. Afanasiev B. N., Galyov E. E., Buchatsky L. P., and Kozlov Y. V. 1991. Nucleotide sequence and genomic organization of *Aedes* densonucleosis virus. Virology. 185:323-336

2. Afanasiev B. N., Kozlov Y. V., Carlson J. O., and Beaty B. J. 1994. Densovirus of *Aedes aegypti* as an expression vector in mosquito cells. Experimental parasitology. 79:322-339

3. Afanasiev B. N., Ward T. W., Beaty B. J., and Carlson J. O. 1999. Transduction of Aedes aegypti mosquitoes with vectors derived from Aedes densovirus. Virology. 257: 62-72

4. Astell C. R., Thomson M., Merchilinsky M., and Ward D. C. 1983. The complete DNA sequence of minute virus of mice, an autonomous parvovirus. Nucleic Acid Res. 11:999-1018

5. Azarkh E., Robinson E., Hirunkanokpun S., Afanasiev B., Kittayapong P., Carlson J., and Corsini J. 2008. Mosquito densonucleosis virus non-structural protein NS2 is necessary for a productive infection. Virology. 374:128-137

6. Baneyx F. 1999. Recombinant protein expression in *Escherichia coli*. Curr Opinion Biotech. 10:411-421

7. Bashir T., Hörlein R., Rommelaere J., and Willwand K. 2000. Cyclin A activates the DNA polymerase δ-dependent elongation machinery *in vitro*: a parvovirus DNA replication model. Pros Natl Acad Sci. 97:5522-5527

8. Baumann C. T., Lim C. S., and Hager G. L. 1998. Simultaneous visualization of the yellow and green forms of the Green Fluorescent Protein in living cells. J Histochem Cytochem. 46:1073-1076

9. Bodendorf U., Cziepluch C., Jauniaux J.-C., Rommelaere J., and Salomé N. 1999. Nuclear export factor CRM1 interacts with non-structural proteins NS2 from parvovirus minute virus of mice. J Virol. 73:7769-7779

10. Bonami J. R., Trumper B., Mari J., Brehelin M., and Lightner D. V. 1990. Purification and characterization of the infectious hypodermal and haematopoietic necrosis virus of penaeid shrimps. J Gen Virol. 71:2657-2664

11. Brockhaus K., Plaza S., Pintel D. J., Rommelaere J., and Salome N. 1996. Nonstructural proteins NS2 of minute virus of mice associate in vivo with 14-3-3 protein family members. J Virol. 70:7527-7534

12. Buchatsky L. P. 1989. Densonucleosis of bloodsucking mosquitoes. Dis Aquat Org. 6:145-150

13. Buchatsky L. P., Bogdanova E. N., Kuznetsova M. A., Lebedinets N. N., Kononko A. G., Chabanenko A. A., and Podrezova L. M. 1988. [Field trials of viral preparation viroden on preimago stages of bloodsucking mosquitoes]. Med Parasitol I Parasit Bolezni. 3:69-71 (Russian)

14. Buchatsky L. P., Kuznetsova M. A., Lebedinets N. N., and Kononko A. G.. 1987. [Development and basic properties of a virus preparation viroden]. Vopr Virusol. 6:729-733 (Russian; English abstract)

15. Buchatsky L. P., Lebedinets N. M., and Kononko G. G. 1997. [Densonucleosis of bloodsucking mosquitoes (the student handbook for biology majors)]. Taras Shevchenko University, Kiev, Ukraine. (Ukrainian)

16. Carlson J., Suchman E., and Buchatsky L. 2006. Densoviruses for control and genetic manipulation of mosquitoes. Adv Virus Res. 68:361-392

17. Cavalier-Smith T. 1974. Palindromic base sequences and replication of eukaryote chromosome ends. Nature. 250:467-469

18. Chen K. C., Tyson J. J., Lederman M., Stout E. R., and Bates R. C. 1989. A kinetic hairpin transfer model for parvoviral DNA replication.

19. Chen S., Cheng L., Zhang Q., Lin W., Lu X., Brannan J., Zhou Z. H., and Zhang J. 2004. Genetic, biochemical, and structural characterization of a new densovirus isolated from a chronically infected Aedes albopictus C6/36 cell line. Virology. 318:123-133

20. Cheng LP., Chen SX., Zhou Z. H., and Zhang JQ. 2007. Structure comparisons of *Aedes albopictus* densovirus with other parvoviruses. Sci China Ser C-Life Sci. 50:70-74

21. Clemens K. E. and Pintel D. J. 1988. The two transcription units of the autonomous parvovirus minute virus of mice are transcribed in a temporal order. J Virol. 62:1448-1451

22. Corsini J., Carlson J. O., Maxwell F., and Maxwell I. H. 1995. Symmetric-strand packaging of recombinant parvovirus LuIII genomes that retain only the terminal regions. J Virol. 69:2692-2696

23. Cotmore S. F., D'Abramo Jr. A. M., Carbonell L. F., Bratton J., and Tattersall P. 1997. The NS2 plypeptide of parvovirus MVM is required for capsid assembly in murine cells.

24. Cotmore S. F. and Tattersall P. 1989. A genome-linked copy of the NS-1 polypeptide is located on the outside of infectious parvovirus particles. J Virol. 63:3902-3911

25. Cotmore S. F. and Tattersall P. 1990. Alternate splicing in a parvoviral nonstructural gene links a common amino-terminal sequence to downstream domains which confer radically different localization and turnover characteristics. Virology. 177:477-487

26. Cotmore S. F. and Tattersall P. 1995. DNA replication in the autonomous parvoviruses. Sem Virol. 6:271-281

27. Cotmore S. F. and Tattersall P. 2005. Genome packaging sense is controlled by the efficiency of the nick site in the right-end replication origin of parvoviruses minute virus of mice and LuIII. J Virol. 79:2287-2300

28. Cziepluch C., Lampel S., Grewenig A., Grund C., Lichter P., and Rommelaere J. 2000. H-1 parvovirus-associated replication bodies: a distinct virus-induced nuclear structure. J Virol. 74:4807-4815

29. Diffoot-Carlo N., Vélez-Pérez L., and de Jesús-Maldonado I. 2005. Possible active origin of replication in the double stranded extended form of the left terminus of LuIII and its implications on the replication model of the parvoviruses. Virol J. 2:47

30. Dingwall C. and Laskey R. A. 1991. Nuclear targeting sequences – a consensus? Trends in Biochem Sciences 16:478-481

31. Doerig C., Hirt B., Beard P., and Antonietti J.-P. 1988. Minute virus of mice non-structural protein NS1 is necessary and sufficient for trans-activation of the viral P39 promoter. J Gen Virol. 69:2563-2573

32. Dyson H. J. and Wright P. E. 2005. Intrinsically unstructured proteins and their functions. Nat Rev Mol Cell Biol. 6:197-208

33. Feige J. N., Sage D., Wahli W., Desvergne B., and Gelman L. 2005. PixFRET, and ImageJ plug-in for FRET calculation that can accommodate variations in spectral bleed-throughs. Microscopy Res Tech. 68:51-58

34. Greider C. W. and Blackburn E. H. 1985. Identification of a specific telomere terminal transferase activity in *Tetrahymena* extracts. Cell. 43:405-413

35. Gubitz A. K., Feng W., and Dreyfuss G. 2004. The SMN complex. Exp Cell Res. 296:51-56

36. Gunther M. and Tattersall P. 1988. The terminal protein of minute virus of mice is an 83 kilodalton polypeptide linked to specific forms of double-stranded and single-stranded viral DNA. FEBS Letters. 242:22-26

37. Guruprasad K., Reddy B. V., Pandit M. W. 1990. Correlation between stability of a protein and its dipeptide composition: a novel approach for predicting *in vivo* stability of a protein from its primary sequence. Protein engineering. 4:155-161

38. Hachet-Haas M., Converset N., Marchal O., Matthes H., Gioria S., Galzi J.-L., and Lecat S. 2006. FRET and Colocalization Analyzer – a method to validate measurements of sensitized emission FRET acquired by confocal microscopy and available as an ImageJ plug-in. Microscopy Res Tech 69:941-956

39. Hanson N. D. and Rhode III S. L. 1991. Parvovirus NS1 stimulates P4 expression by interaction with the terminal repeats and through DNA amplification. J Virol. 65:4325-4333

40. Hellen C. U. T. and Sarnow P. 2001. Internal ribosome entry sites in eukaryotic mRNA molecules. Genes and Development. 15:1593-1612

41. Hénaut A. and Danchin A. 1996. Analysis and Predictions from *Escherichia coli* sequences. In *Escherichia coli and Salmonella*, Neidhardt F. C. ed., Vol. 2, Ch. 114:2047-2066, 1996, ASM press, Washington, D.C.

42. Hueffer K. and Parrish C. R. 2003. Parvovirus host range, cell tropism, and evolution. Current Opinion Microbiol. 6:392-398.

43. ICTVdB Management, 2006. 00.050.2.03. Brevidensovirus. In: *ICTVdB - The Universal Virus Database*, version 4. Büchen-Osmond, C. (Ed), Columbia U., New York

44. Idicula-Thomas S. and Balaji P. V. 2005. Understanding the relationship between the primary structure of proteins and its propensity to be soluble on overexpression in *Escherichia coli*. Protein Science. 14:582-592

45. Johnson A. and O'Donnel M. 2005. Cellular DNA Replicases: components and dynamics at the replication fork. Annu Rev Biochem. 74:283-315

46. Jousset F. X., Baquerizo E., and Bergoin M. 2000. A new densovirus isolated from the mosquito *Culex pipiens* (Diptera: Culicidae). Virus Res. 67:11-16

47. Jousset F. X., Barreau C., Boublik Y., and Cornet M. 1993. A parvo-like virus persistently infecting a C6/36 clone of Aedes albopictus mosquito cell line and pathogenic for Aedes aegypti larvae. Virus Res. 29:99-114

48. Kimmick M. W., Afanasiev B. N., Beaty B. J., and Carlson J. O. 1998. Gene expression and regulation from the p7 promoter of *Aedes densonucleosis* virus. J.Virol. 72, 4364-4370

49. King J. A., Dubielzig R., Grimm D., and Kleinschmidt J. A. 2001. DNA helicase-mediated packaging of adeno-associated virus type 2 genomes into preformed capsids. EMBO J. 20:3282-3291

50. Kittayapong P., Baisley K. J., and O'Neill S. L. 1999. A mosquito densovirus infecting *Aedes aegypti* and *Aedes albopictus* from Thailand. Am J Trop Med Hyg. 64:612-617

51. Konet D. S., Anderson J., Piper J., Akkina R., Suchman E., and Carlson J. 2007. Short-hairpin RNA expressed from polymerase III promoters mediates RNA interference in mosquito cells. Insect Molecular Biology 16:199–206

52. Kozak M. 1989. The scanning model for translation: an update. J Cell Biol. 108:229-241

53. Lange A., Mills R. E., Lange C. J., Stewart M., Devine S. E., and Corbett A. H. 2007. Classical nuclear localization signals: definition, function, and interaction with importin α. J Biol Chem. 282, 5101-5105.

54. Lebedeva O. P., Kuznetsova M. A., Zelenko A. P., and Gudz-Gorban A. P. 1973. Investigation of a virus disease of the densonucleosis type in a laboratory culture of Aedes aegypti. Acta virol. 17:253-256

55. Ledermann J. P., Suchman E. L., Black W. C. 4th, and Carlson J. O. 2004. Infection and pathogenicity of the mosquito densoviruses AeDNV, HeDNV, and APeDNV in Aedes aegypti mosquitoes (Diptera: Culicidae). J Econ Entomol. 97:1828-1835

56. Legendre D. and Rommelaere J. 1992. Terminal regions of the NS-1 protein of the parvovirus minute virus of mice are involved in cytotoxicity and promoter *trans* inhibition. J Virol. 66:5705-5713

57. Li Y., Zádori Z., Bando H., Dubuc R., Fédière G., Szelei J., and Tijssen P. 2001. Genome organization of the densovirus from *Bombyx mori* (*Bm*DNV-1) and enzyme activity of its capsid. Virology. 82:2821-2825

58. Maroto B., Valle N., Saffrich R., and Almendral J. M. 2004. Nuclear export of the nonenveloped parvovirus virion is directed by an unordered protein signal exposed on the capsid surface. J Virol. 78:10685-10694

59. McGuffin L. J., Bryson K., and Jones D. T. 2000. The PSIPRED protein structure prediction server. Bioinformatics. 16:404-405

60. Mhawech P. 14-3-3 proteins – an update. Cell Res. 15:228-236

61. Miller C. L. and Pintel D. J. 2002. Interaction between parvovirus NS2 protein and nuclear export factor Crm1 is important for viral egress from the nucleus of murine cells. J Virol. 76:3257-3266

62. Muramatsu S.-I., Mizukami H., Young N. S., and Brown K. E. 1996. Nucleotide sequencing and generation of an infectious clone of adeno-associated virus 3. Virology. 221:208-217

63. Naeger L. K., Cater J., and Pintel D. J. 1990. The small nonstructural protein (NS2) of the parvovirus minute virus of mice is required for efficient DNA replication and infectious virus production in a cell-type-specific manner. J Virol. 64:6166-6175

64. Naeger L. K., Salomé N., and Pintel D. J. 1993. NS2 is required for efficient translation of viral mRNA in minute virus of mice-infected murine cells. J Virol. 64:1034-1043

65. Nuesh J. P. and Tattersall P. 1993. Nuclear targeting of the parvoviral replicator molecule NS1: evidence for self-association prior to nuclear transport. Virology. 196:637-651

66. O'Neill S. L., Kittayapong P., Braig H. R., Andreadis T. G., Gonzalez J. P., and Tesh R. B.. 1995. Insect densoviruses may be widespread in mosquito cell lines. J Gen Virol. 76:2067-2075

67. Parker J. S. and Parrish C. R. 2000. Cellular uptake and infection by canine parvovirus involves rapid dynamin-regulated clathrin-mediated endocytosis, followed by slower intracellular trafficking. J Virol. 74:1919-1930.

68. Paterson A., Robinson E., Suchman E., Afanasiev B., and Carlson J. 2005. Mosquito densonucleosis viruses cause dramatically different infection phenotypes in the C6/36 *Aedes albopictus* cell line. Virology. 337:253-261

69. Pattanakitsakul S. N., Boonnak K., Auethavornanan K., Jairungsri A., Duangjinda T., Puttatesk P., Thongrungkiat S., and Malasit P. 2007. A new densovirus isolated from the mosquito Toxorhynchites splendens (Wiedemann) (Diptera: Culicidae). Southeast Asian J Trop Med Public Health. 38:283-93

70. Prilusky J., Felder C. E., Zeev-Ben-Mordehai T., Rydberg E. H., Man O., Beckmann J. S., Silman I., and Sussman J. L. 2005. FoldIndex©: a simple tool to predict whether a given protein sequence is intrinsically unfolded. Bioinformatics. 21:3435-3438

71. Rasgon J. L. 2007. Using viruses to manipulate *Anopheles gambiae.* In *Insects as vectors: immunity and olfaction.* Entomol Res. 37 (supppl. 1):A23-A28

72. Ros C., Baltzer C., Mani B., and Kempf C. 2006. Parvovirus uncoating *in vitro* reveals a mechanism of DNA release without capsid disassembly and striking differences in encapsidated DNA stability. Virology. 345:137-147

73. Shade R. O., Matthew C. B., Cotmore S. F., Tattersall P., and Astel C. R. 1986. Nucleotide sequence and genome organization of human parvovirus B19 isolated from the serum of a child during aplastic crisis. J Virol. 58:921-936

74. Shike H., Dhar A. K., Burns J. C., Shimizu C., Jousset F. X., Klimpel K., and Bergoin M. 2000. Infectious hypodermal and hematopoietic necrosis virus of shrimp is related to mosquito brevidensoviruses. Virology. 277:167-177

75. Suchman E. and Carlson J. 2004. Production of mosquito densonucleosis viruses by *Aedes albopictus* C6/36 cells adapted to suspension culture in serum-free protein-free media. In Vitro Cell Dev Biol Anim. 40:74-75

76. Tattersall P. 1972. Replication of the parvovirus MVM. I. Dependence of virus multiplication and plaque formation on cell growth. J Virol. 10:586-590

77. Tattersall P. 1976. Rolling hairpin model for replication of parvovirus and linear chromosomal DNA. Nature. 263:106-

78. Tijseen P., Li Y., El-Far M., Szelei J., Letarte M., and Zádori Z. 2003. Organization and expression strategy of the ambisense genome of densonucleosis virus of *Galleria mellonella.* J Virol. 77:10357-10365

79. Vihinen-Ranta M., Yuan W., and Parrish C. R. 2000. Cytoplasmic trafficking of the canine parvovirus capsid and its role in infection and nuclear transport. J Virol. 74:4853-4859

80. Vihinen-Ranta M, Suikkanen S., and Parrish C. R. 2004. Pathways of cell infection by parvoviruses and adeno-associated viruses. J Virol. 78:6709-6714

81. Wang D., Yuan W., Davis I., and Parrish C. R. 1998. Nonstructural protein-2 and the replication of canine parvovirus. Virology. 240:273-281

82. Ward T. W., Kimmick M. W., Afanasiev B. N., Carlson, J. O. 2001. Characterization of the structural gene promoter of *Aedes aegypti* densovirus. J.Virol. 75:1325-1331

83. Young P. J., Newman A., Jensen K. T., Burger L. R., Pintel D. J., and Lorson C. L. 2005. Minute virus of mice small non-structural protein NS2 localizes within, but is not required for the formation of, Smn-associated autonomous parvovirus-associated bodies. J Gen Virol. 86:1009-1014

84. Zádori Z., Szelei J., Lacoste M.-C., Li Y., Gariépy S., Raymond Ph., Allaire M., Nabi I. R., and Tijssen P. 2001. A viral phospholipase A_2 is required for parvovirus infectivity. Developmental Cell. 1:291-302

85. Zhai Y., Lu X., Sun X., Fu S., Gong Z., Fen Y., Tong S., Wang Z., Tang Q., Attoui H., and Liang G. 2008. Isolation and characterization of the full coding sequence of a novel densovirus from the mosquito *Culex pipiens pallens*. J Gen Virol. 89:195-199

86. Zhang L., Foxman B., Gilsdorf J. R., and Marrs C. F. 2005. Bacterial genomic DNA isolation using sonication for microarray analysis. BioTechniques. 36:640-644